

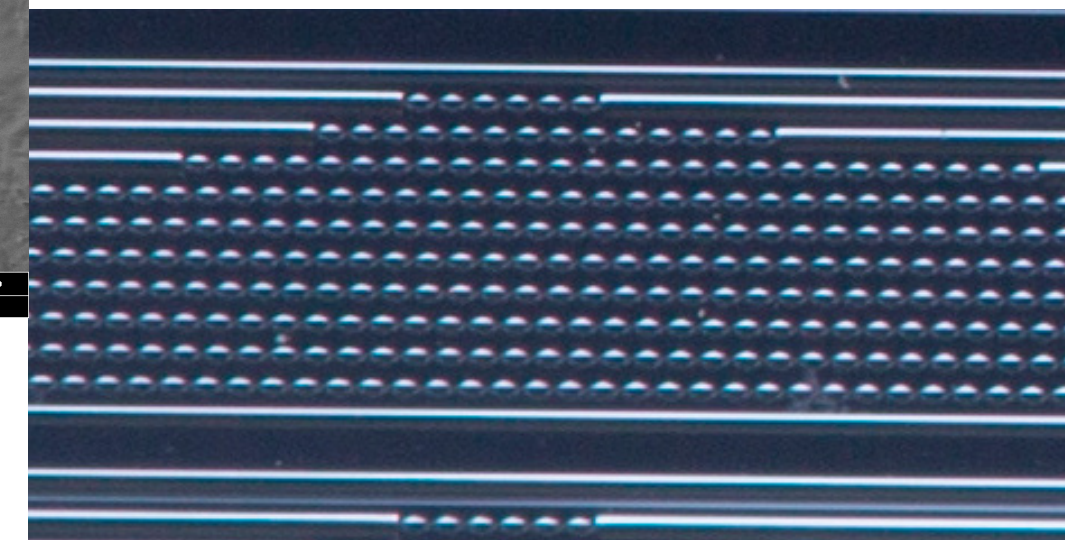
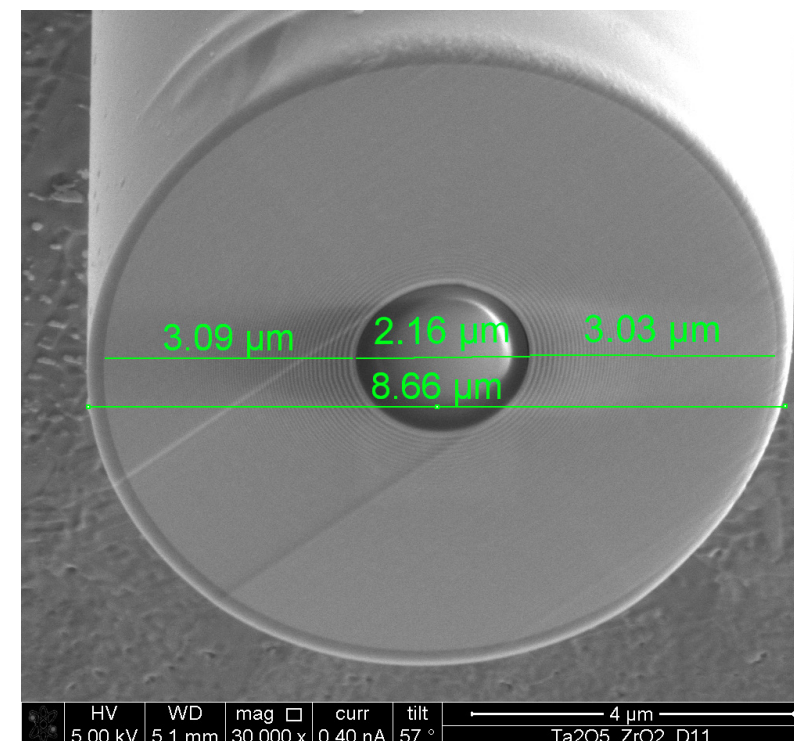
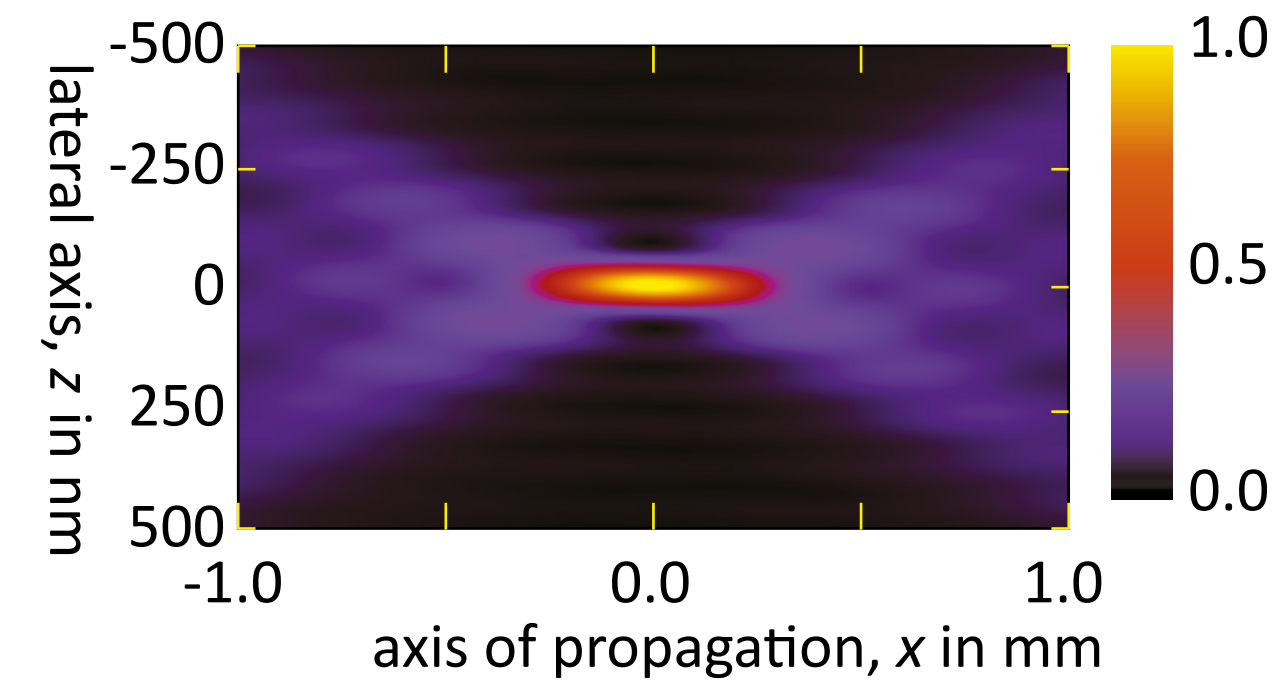
X-Ray Optics for Imaging

Hercules Specialised Course 19

Markus Osterhoff
University of Göttingen
Grenoble, May 2017

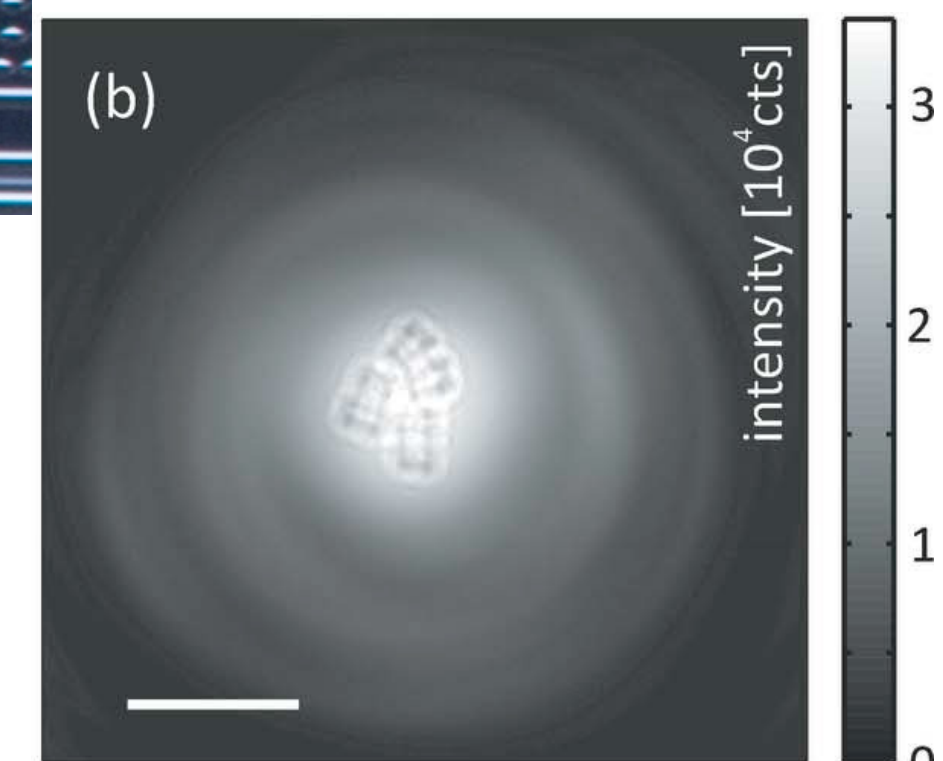
ideal mirror

(a) Intensity distribution



Outline

- ▶ Introduction + History
- ▶ Reflective Optics
- ▶ Diffractive Optics
- ▶ Refractive Optics
- ▶ Waveguides
- ▶ Discussion



Introduction and History



Advantages of Hard X-Rays

- ▶ high penetration length
looking into the volume,
3D tomography
- ▶ element specific
access to ionisation state
absorption, fluorescence, Auger
- ▶ short wavelength
matching length scales in crystals, glasses
- ▶ scattering from electron density

Disadvantages

- ▶ beam damage
- ▶ weak interaction with optics
- ▶ expensive

Outline

- ▶ *Introduction + History*
- ▶ Reflective Optics
- ▶ Diffractive Optics
- ▶ Refractive Optics
- ▶ Waveguides
- ▶ Discussion

What we want

- ▶ small focus,
i.e. high numerical aperture
- ▶ high efficiency
- ▶ long working distance,
i.e. high angles of convergence
- ▶ multiple contrasts
- ▶ weak interaction with sample;
low dose, but strong signal?

What we want

- ▶ small focus,
i.e. high numerical aperture
- ▶ high efficiency
- ▶ long working distance,
i.e. high angles of convergence
- ▶ multiple contrasts
- ▶ weak interaction with sample;
low dose, but strong signal?

What we have

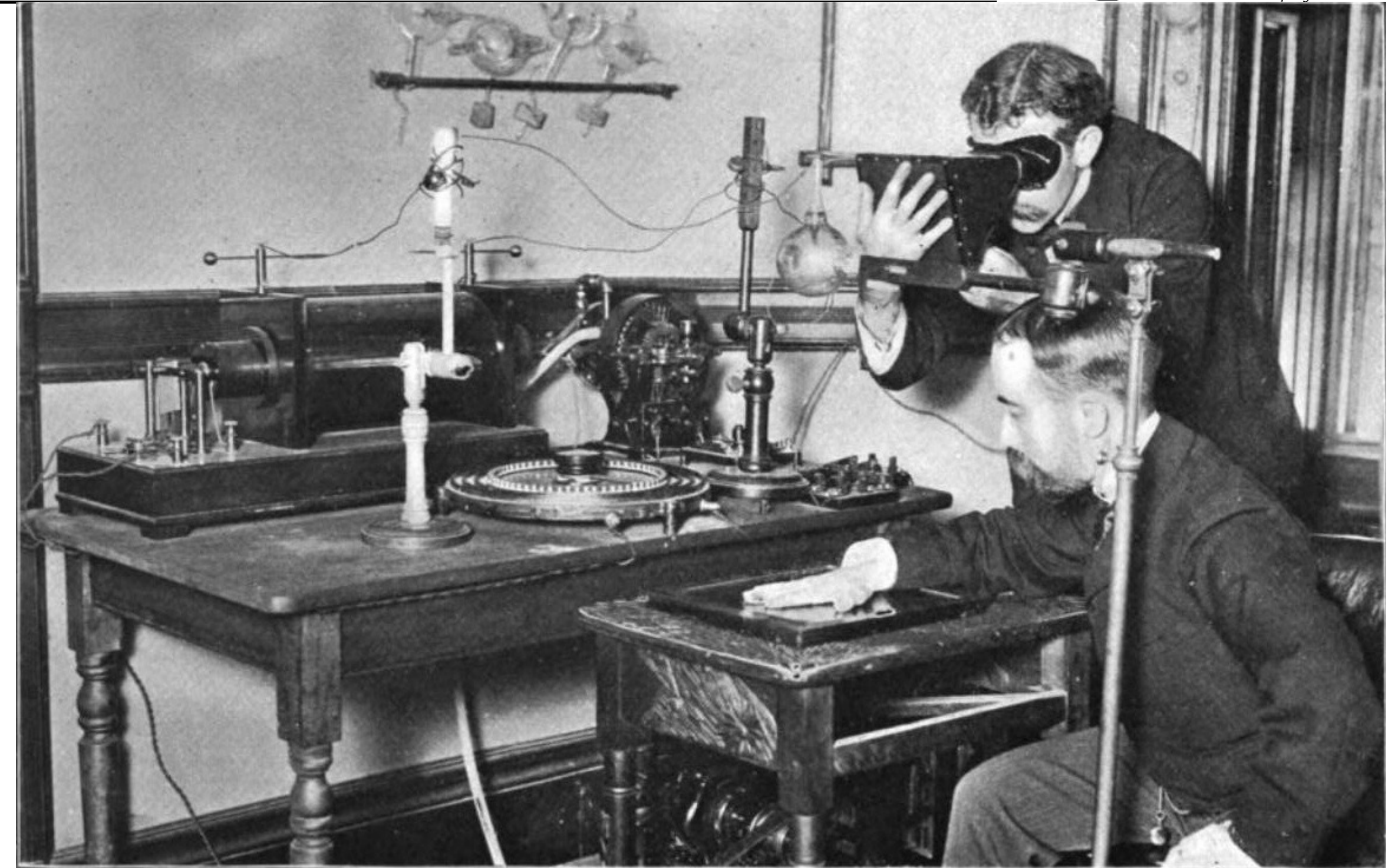
- ▶ index of refraction
 $n = 1 - \delta + i\beta$
- ▶ δ : dispersive part,
yields phase shift
- ▶ β : absorption
- ▶ typically: $\delta \sim 10^{-5}$, $\beta \sim 10^{-7}$ (hard x-rays)
- ▶ weak interaction with optics,
x-rays cannot be bent so easily ...

X-Rays and Optics - the First 50 Years



Not so much has happened ...

- ▶ discovery of X-Rays by C.W. Röntgen in 1895
- ▶ no interaction with lenses found
- ▶ particles? waves? something else?
- ▶ what are crystals? arrays of atoms?
- ▶ lattice spacing + wavelength agree



Not so much has happened ...

- ▶ discovery of X-Rays by C.W. Röntgen in 1895
- ▶ no interaction with lenses found
- ▶ particles? waves? something else?
- ▶ what are crystals? arrays of atoms?
- ▶ lattice spacing + wavelength agree

Generation of X-rays ...

- ▶ only by traditional X-ray tubes
- ▶ parasitic use of synchrotron radiation
- ▶ dedicated synchrotron radiation sources
- ▶ ESRF as 3rd generation source
- ▶ 4th generation to come, x-ray free electron lasers
- ▶ brilliance increase

Optics for (hard) X-rays:

- ▶ started about 50 years after Röntgen's discovery

Pioneers of X-Ray Optics

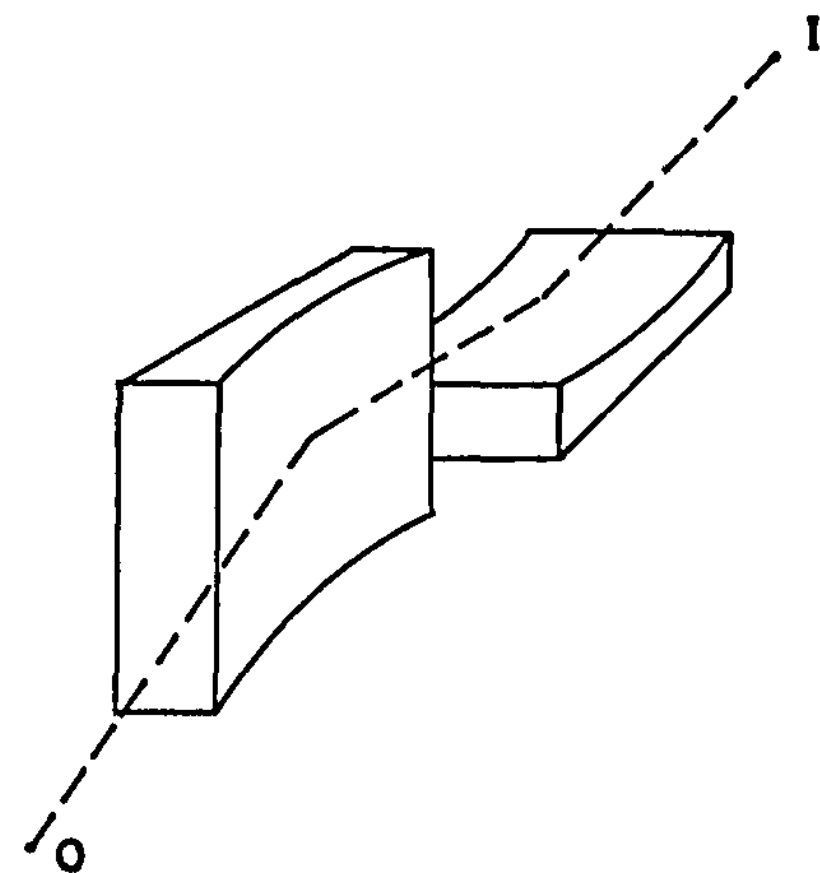
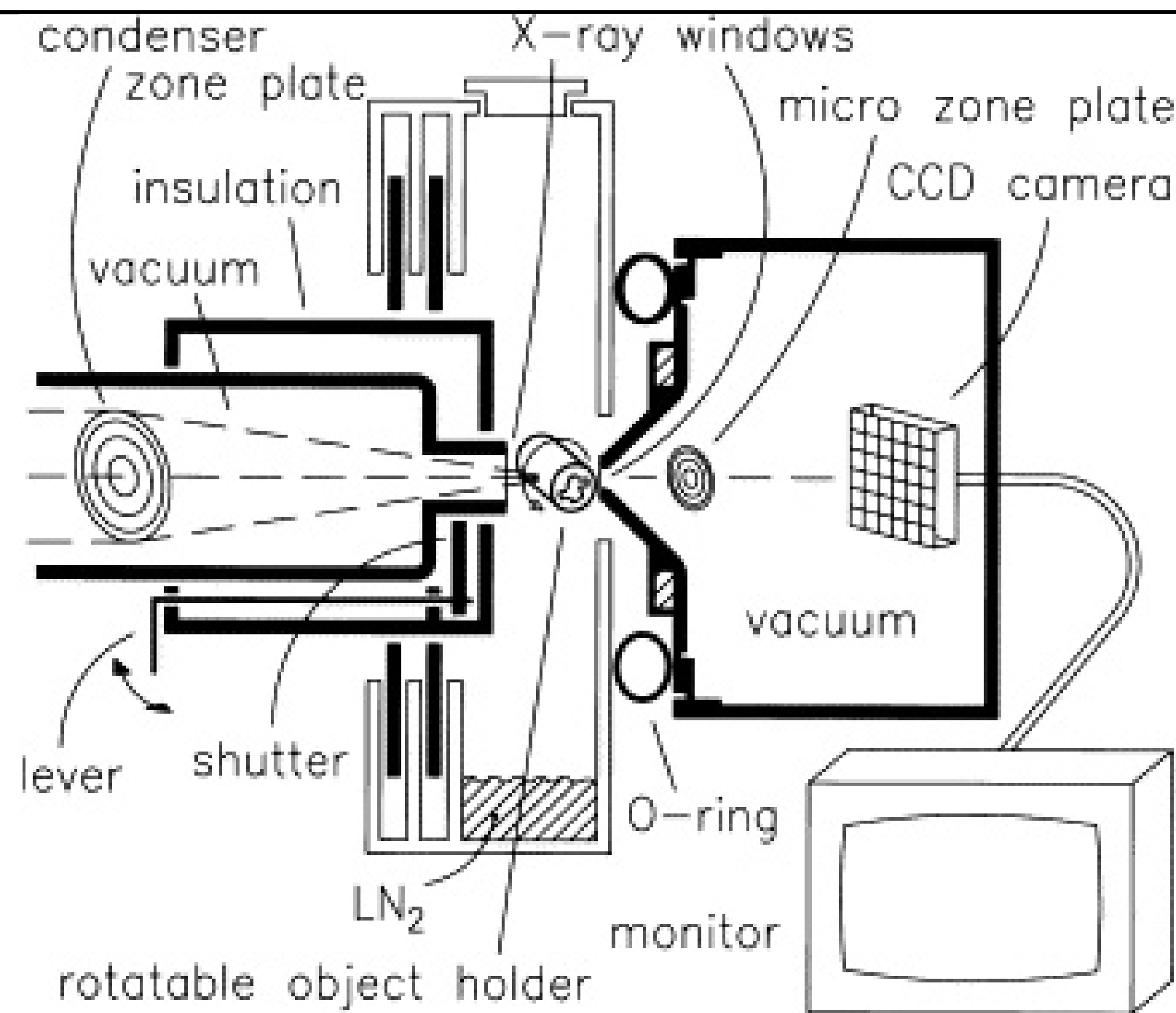


FIG. 11. Arrangement of concave mirrors to produce real images of extended objects with incidence at small grazing angles.

Kirkpatrick and Baez
1950ies: reflecting mirrors



G. Schmahl and coworkers
1980ies: Fresnel Zone Plates

A compound refractive lens for focusing high-energy X-rays

A. Snigirev*, V. Kohn†, I. Snigireva* & B. Lengeler*‡

* European Synchrotron Radiation Facility, BP220, F-38043 Grenoble Cedex, France
† Kurchatov, I. V., Institute of Atomic Energy, 123182 Moscow, Russia

The development of techniques for focusing X-rays has occupied physicists for more than a century. Refractive lenses, which are used extensively in visible-light optics, are generally considered inappropriate for focusing X-rays, because refraction effects are extremely small and absorption is strong. This has led to the development of alternative approaches^{1,2} based on bent crystals and X-ray mirrors, Fresnel and Bragg-Fresnel zone plates, and capillary optics (Kumakhov lenses). Here we describe a simple procedure for fabricating refractive lenses that are effective for focusing of X-rays in the energy range 5–40 keV. The problems associated with absorption are minimized by fabricating the lenses from low-atomic-weight materials. Refraction of X-rays by one such lens is still extremely small, but a compound lens (consisting of tens or hundreds of individual lenses arranged in a linear array) can readily focus X-rays in one or two dimensions. We have fabricated a compound lens by drilling 30 closely spaced holes (each having a radius of 0.3 mm) in an aluminium block, and we demonstrate its effectiveness by focusing a 14-keV X-ray beam to a spot size of 8 μm.

The index of refraction for X-rays in matter can be written as $n = 1 - \delta + i\beta$, where β is the absorption index and δ is the

‡ Present address: Physikalisches Institut, RWTH Aachen, 52056 Aachen, Germany.

NATURE · VOL 384 · 7 NOVEMBER 1996

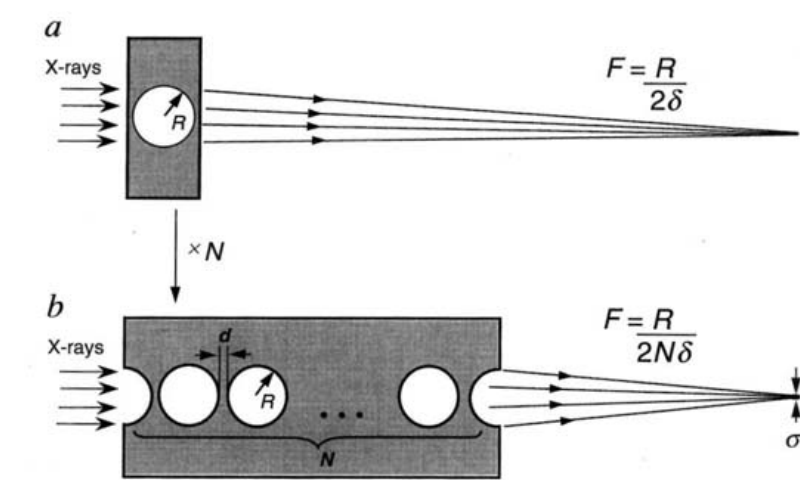


FIG. 1 Schematic diagram showing the principles of X-ray focusing by a compound refractive lens (CRL). As $(1 - \delta)$ is smaller than 1 (where δ is the decrement of the refractive index), a collecting lens for X-rays must have a concave shape. a, A simple concave lens fabricated as a cylindrical hole in the material. b, A CRL consisting of a number (N) of cylindrical holes placed close together in a row along the optical axis, focuses the X-rays at a distance that is N times shorter compared to a single lens. R is the radius of the holes, d is the spacing between the holes, λ is the X-ray wavelength, and F is the focal distance for a parallel input beam.

refractive index decrement. Refraction being very small (δ is typically between 10^{-5} and 10^{-7}), all attempts to date to build refractive lenses for X-rays have been unsuccessful. Recently, the discussion about refractive lenses has been revived. Suehiro, Miyaji and Hayashi³ have proposed a refractive lens of high-atomic-number (high-Z) material for focusing X-rays. Michette⁴

A. Snigirev and his team
1990ies: Refractive Lenses

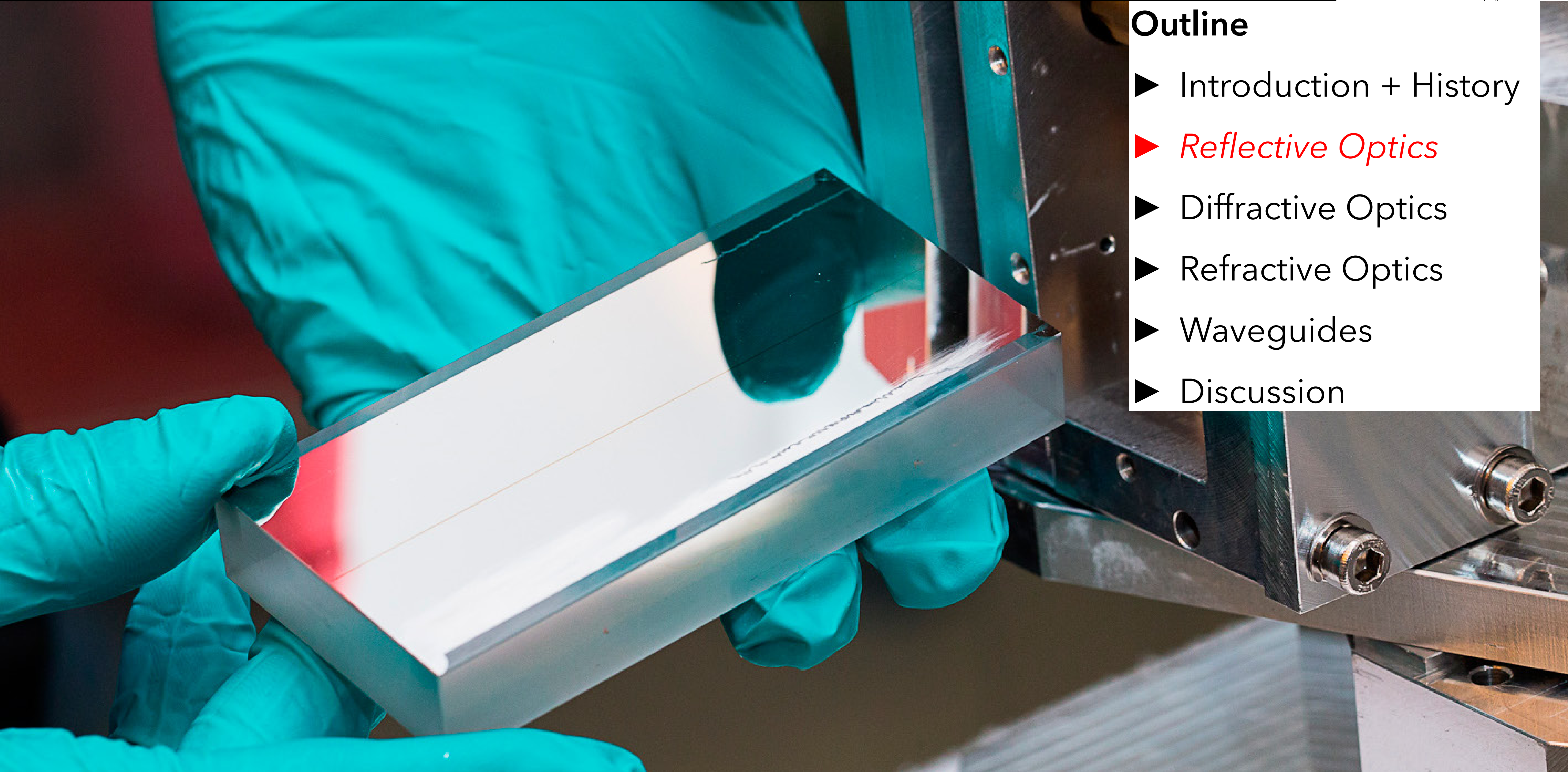
Kirkpatrick, Baez, JOSA 1948
Schmahl et al, Ultramicroscopy, 2000
Snigirev, Lengeler et al, Nature, 1996

Mirrors and Multilayer Mirrors

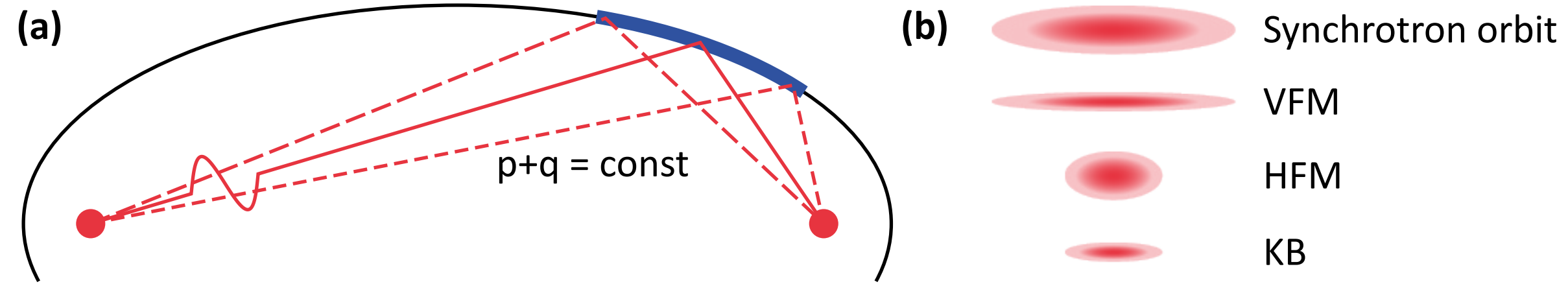


Outline

- ▶ Introduction + History
- ▶ *Reflective Optics*
- ▶ Diffractive Optics
- ▶ Refractive Optics
- ▶ Waveguides
- ▶ Discussion



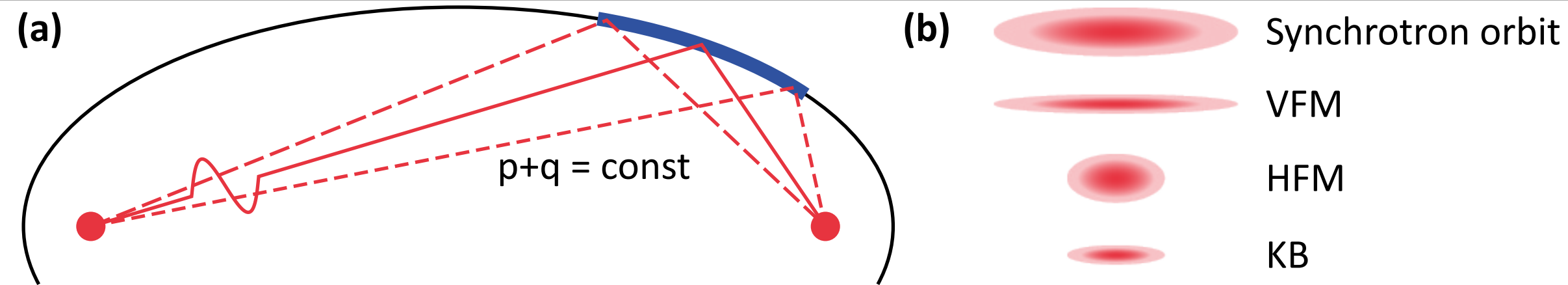
Principle and Geometry



Ellipse:

- ▶ the distance from S to F via any point on the ellipse is constant
- ▶ constant distance = constant phase
- ▶ waves interfere constructively, leading to a focus

Principle and Geometry



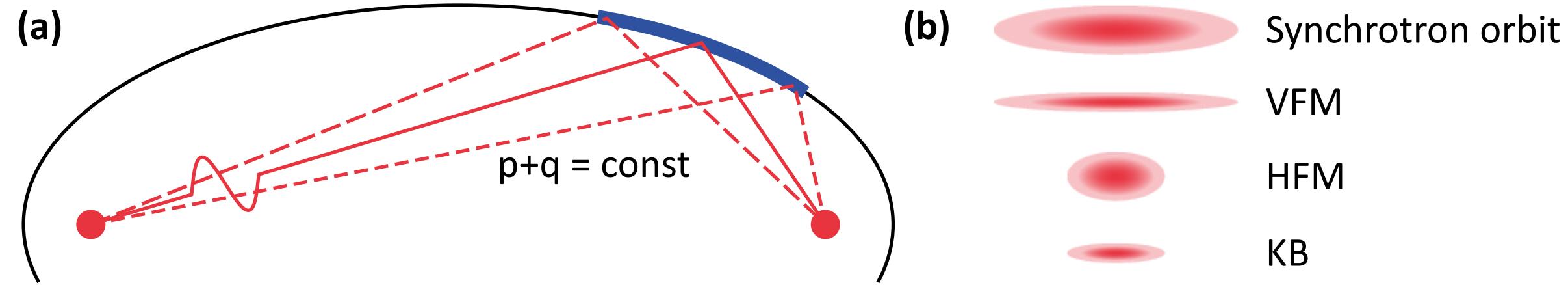
Ellipse:

- ▶ the distance from S to F via any point on the ellipse is constant
- ▶ constant distance = constant phase
- ▶ waves interfere constructively, leading to a focus

Requirements:

- ▶ high reflectivity of the surface
- ▶ good surface quality
- ▶ 3D shape or 2 crossed 2D shapes

Principle and Geometry

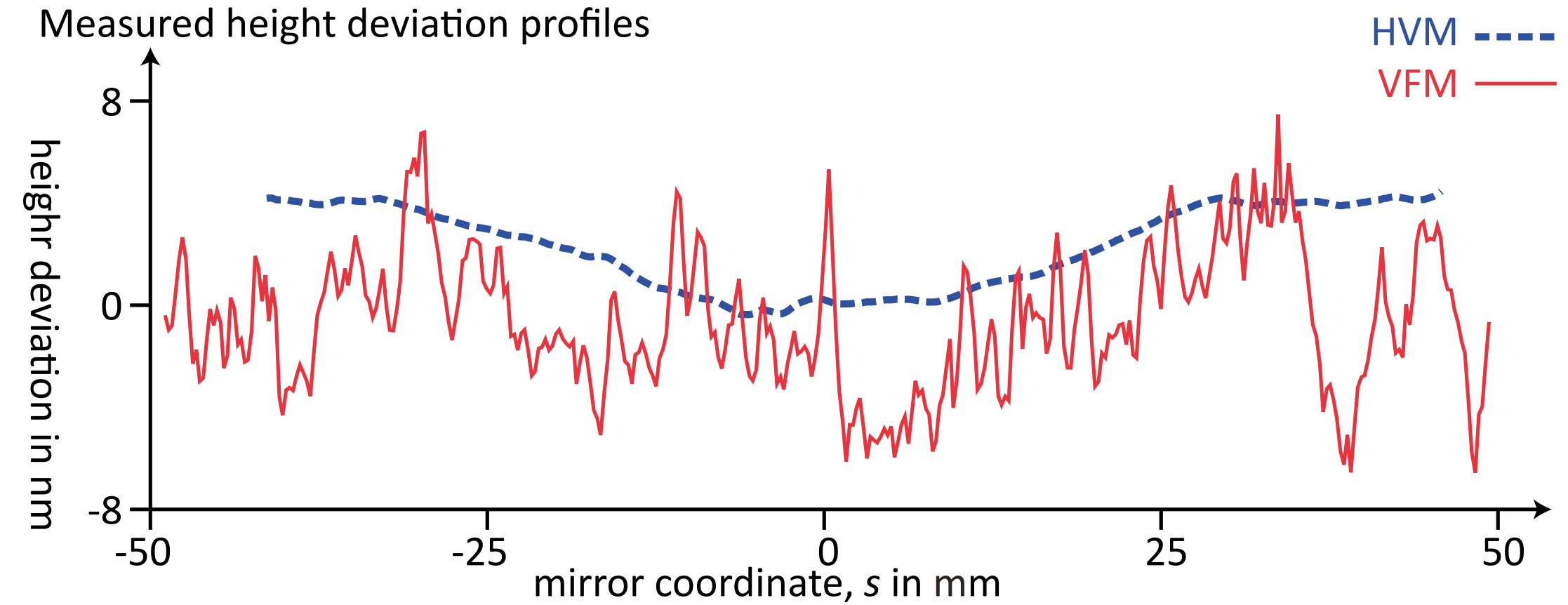


Ellipse:

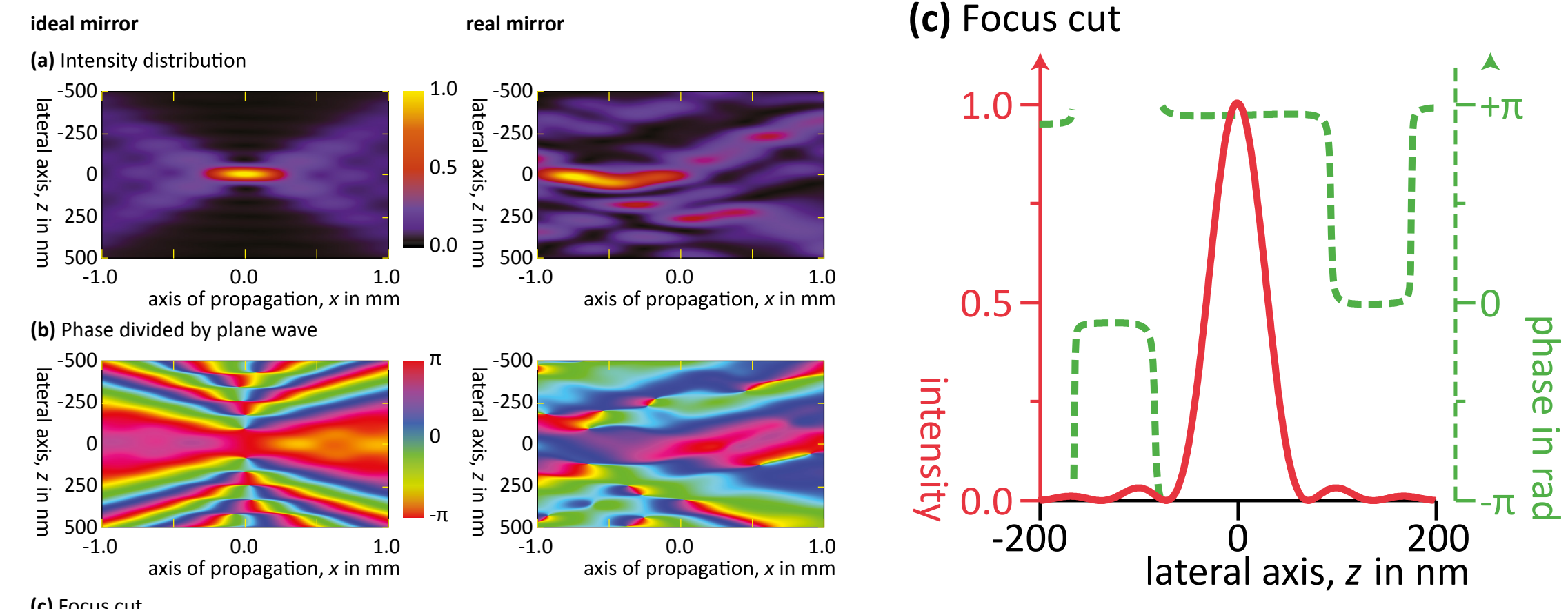
- ▶ the distance from S to F via any point on the ellipse is constant
- ▶ constant distance = constant phase
- ▶ waves interfere constructively, leading to a focus

Requirements:

- ▶ high reflectivity of the surface
- ▶ good surface quality
- ▶ 3D shape or 2 crossed 2D shapes



typical figure errors, 2010: ~ nm over 10 cm



wave-optical simulations of an ideal and real mirror; focal spot size < 100 nm (point-source)

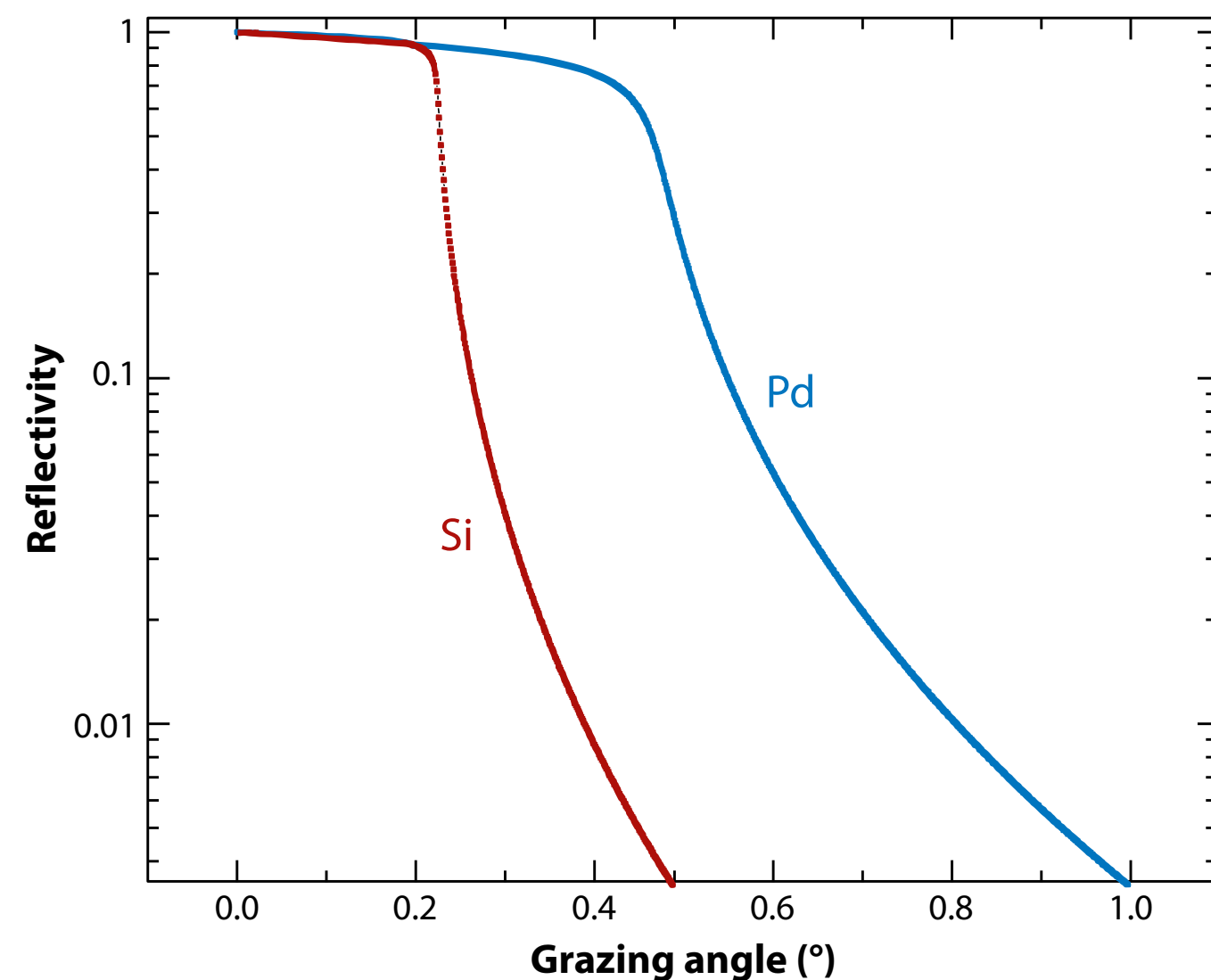
Total Reflection, Coating

3. X-RAY MIRRORS

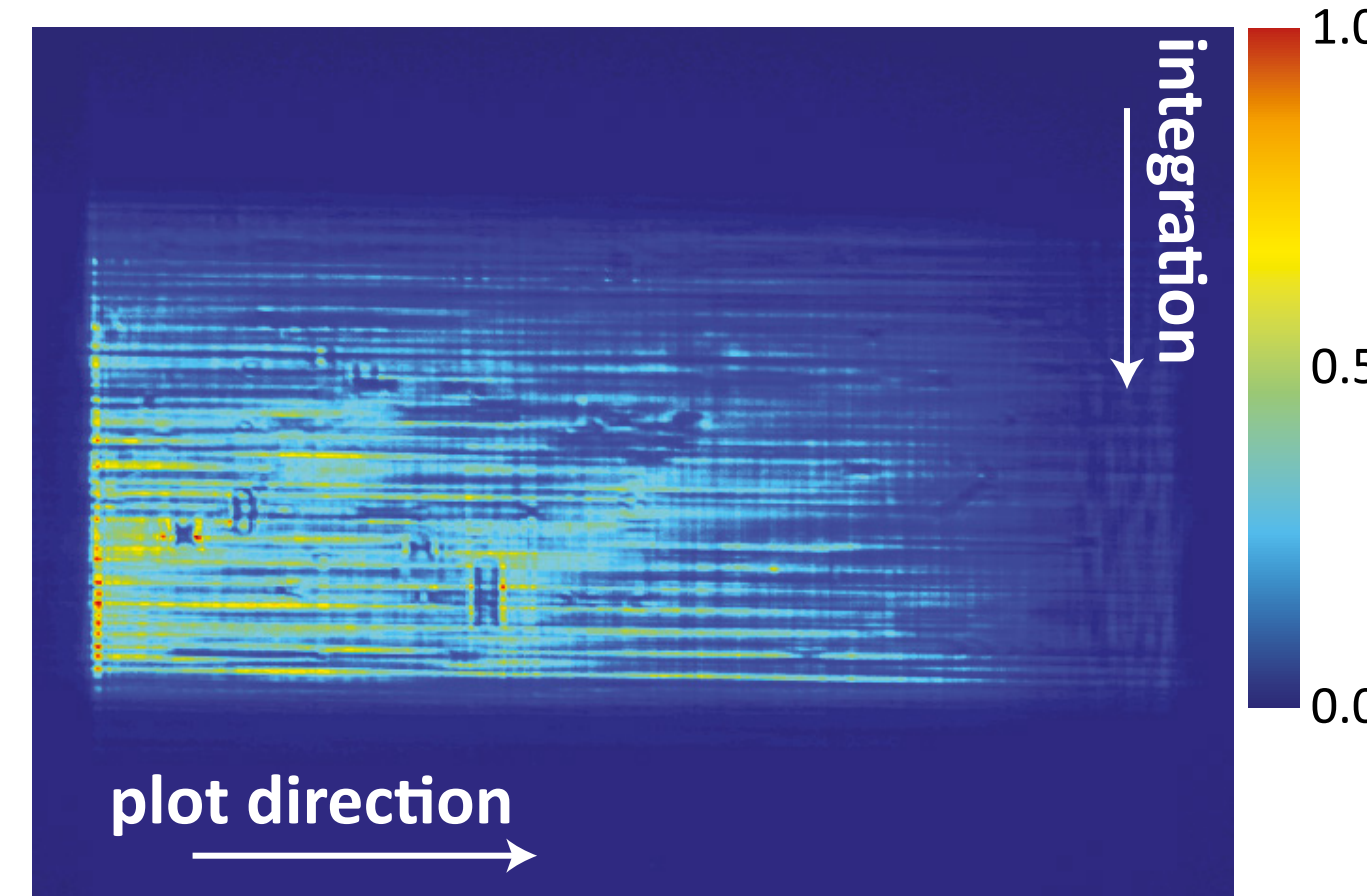
X-ray mirrors rely on total external reflection. The real part of the index of refraction is given by (6, 7)

$$n = 1 - \delta = 1 - \lambda^2 r_e \rho / 2\pi. \quad 2.$$

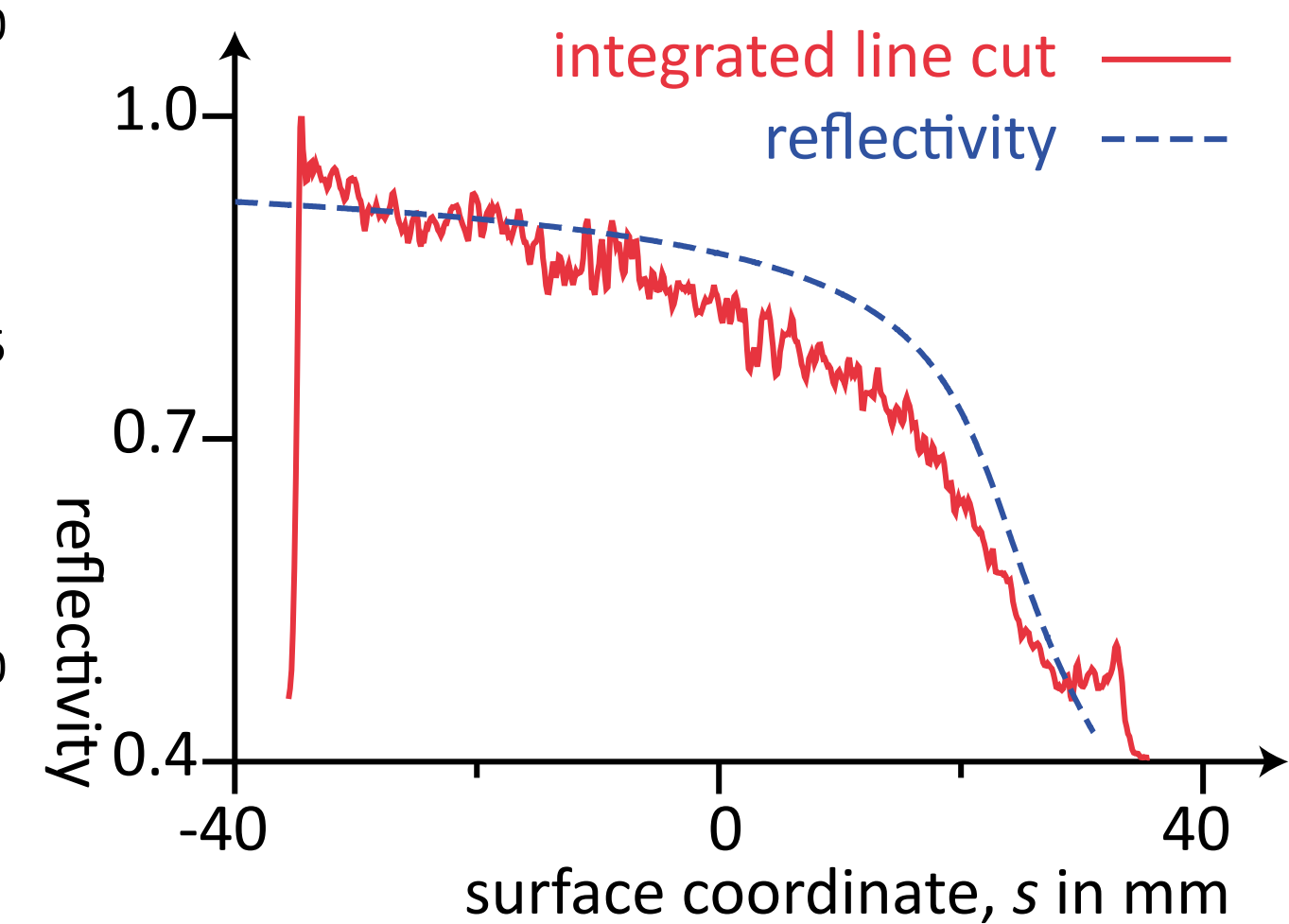
Here λ is the wavelength; r_e is the classical electron radius, which equals 2.814×10^{-5} ; and ρ is the electron density. The result is that n is less than unity so that, according to Snell's law, there is total external reflection, and because δ is very small ($\sim 10^{-5}$), reflection occurs only at low grazing angles. The reflectivity of smooth surfaces can be computed from Fresnel formulas (8). The critical grazing angle above which total external reflection does not occur is given by $\theta_c = \sqrt{2\delta}$. **Figure 5** shows calculated (9) specular reflectivity curves at 8 keV for a Si mirror without any coating as well as for one coated with Pd. At extremely grazing angles, an evanescent wave to a depth of $\lambda/(2\pi\theta_c)$ propagates just below the surface. The thickness of the coating should be chosen to be much larger than the penetration depth of the evanescent wave, which is 3 nm in the case of a Pd mirror.



(a) KB mirror far-field

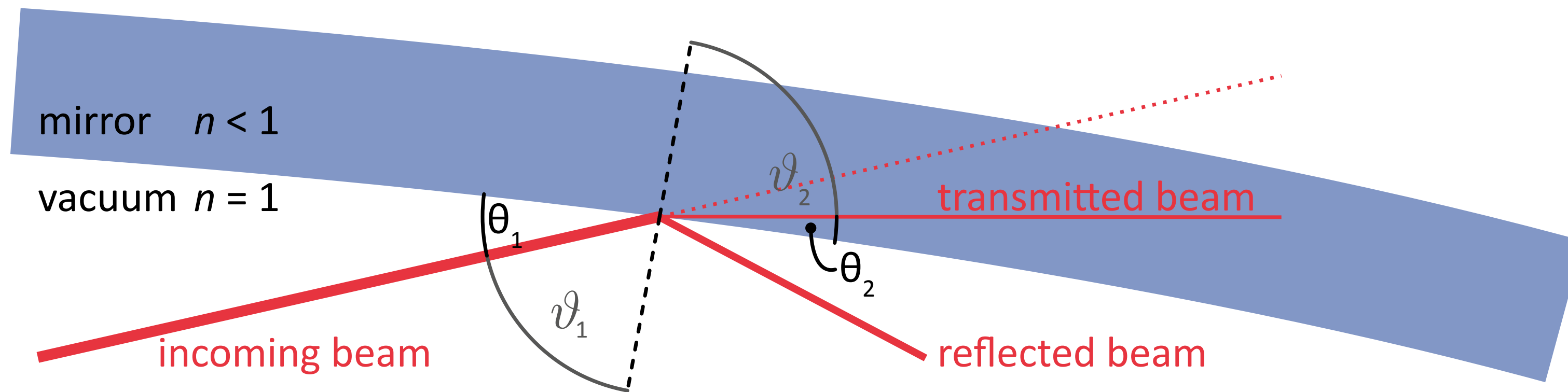


(b) Fresnel reflectivity



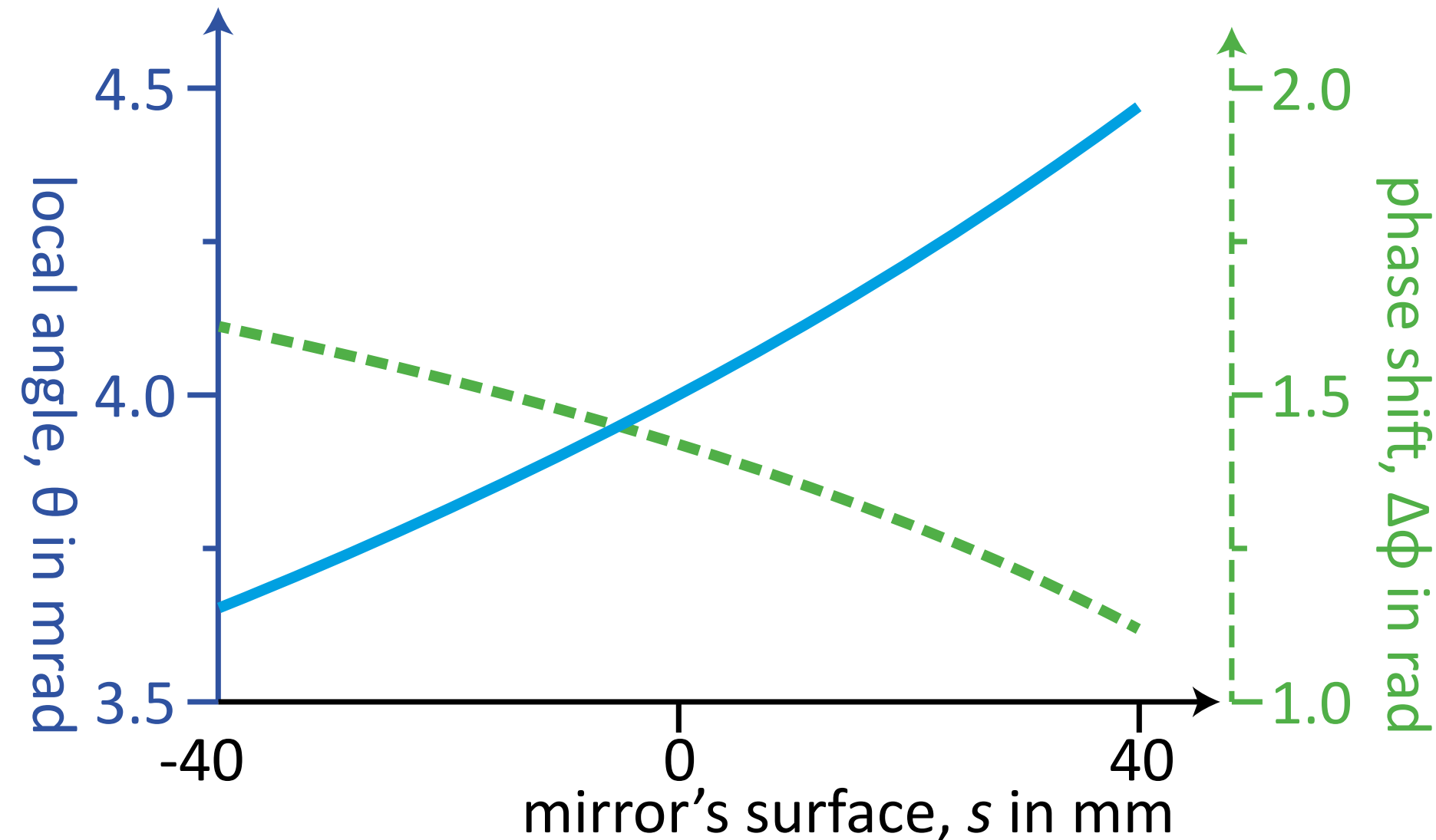
- ▶ total external reflection for grazing incidence
- ▶ typical angles: 0.5° - few milli radian
- ▶ proportional to electron density \times wavelength

Gouy Phase

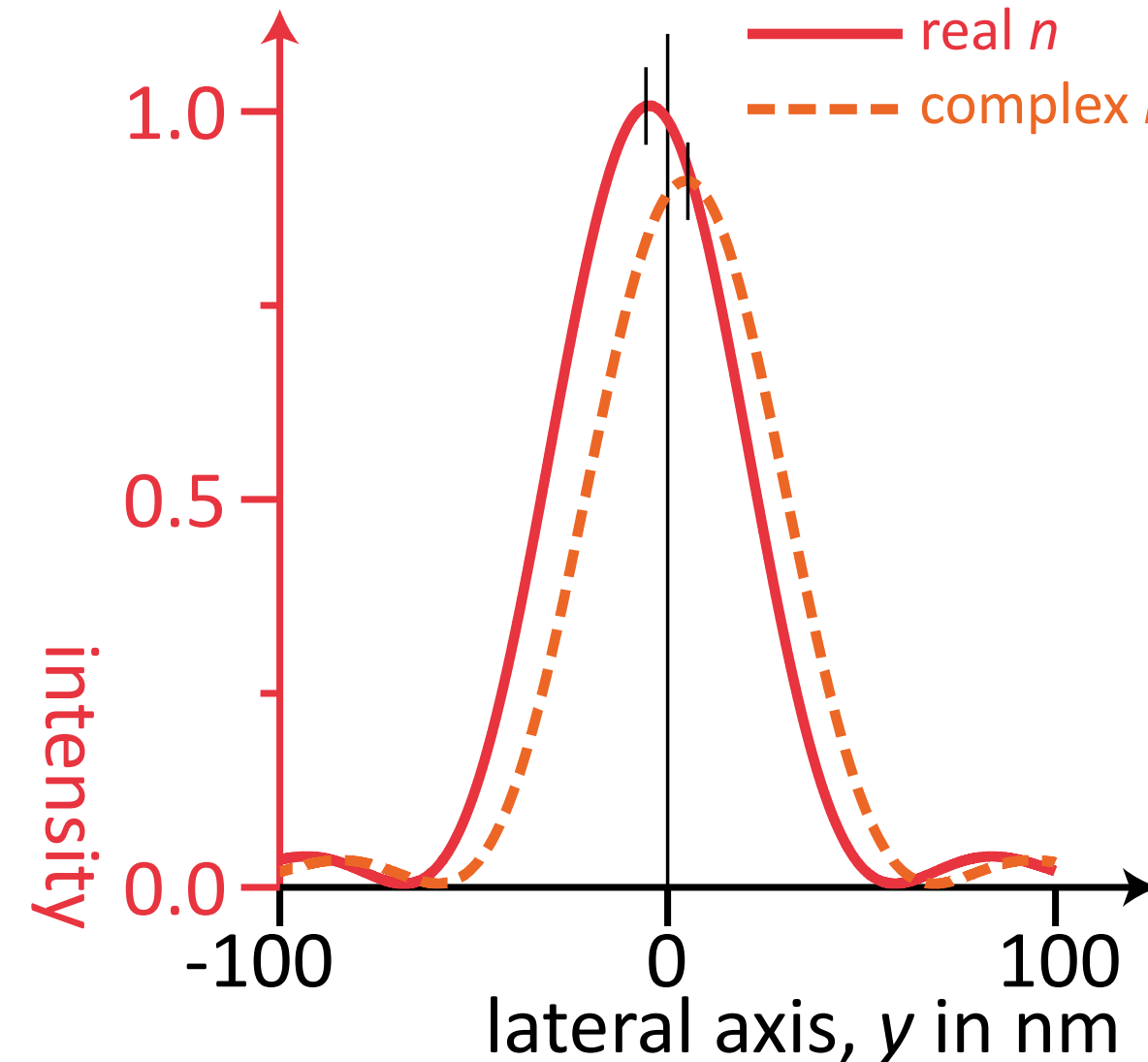


$$\phi(z_m) = 2 \arctan \left(\frac{-\sqrt{2\delta - \sin^2 \theta_z}}{\sin \theta_z} \right)$$

(a) Local angle and phase shift

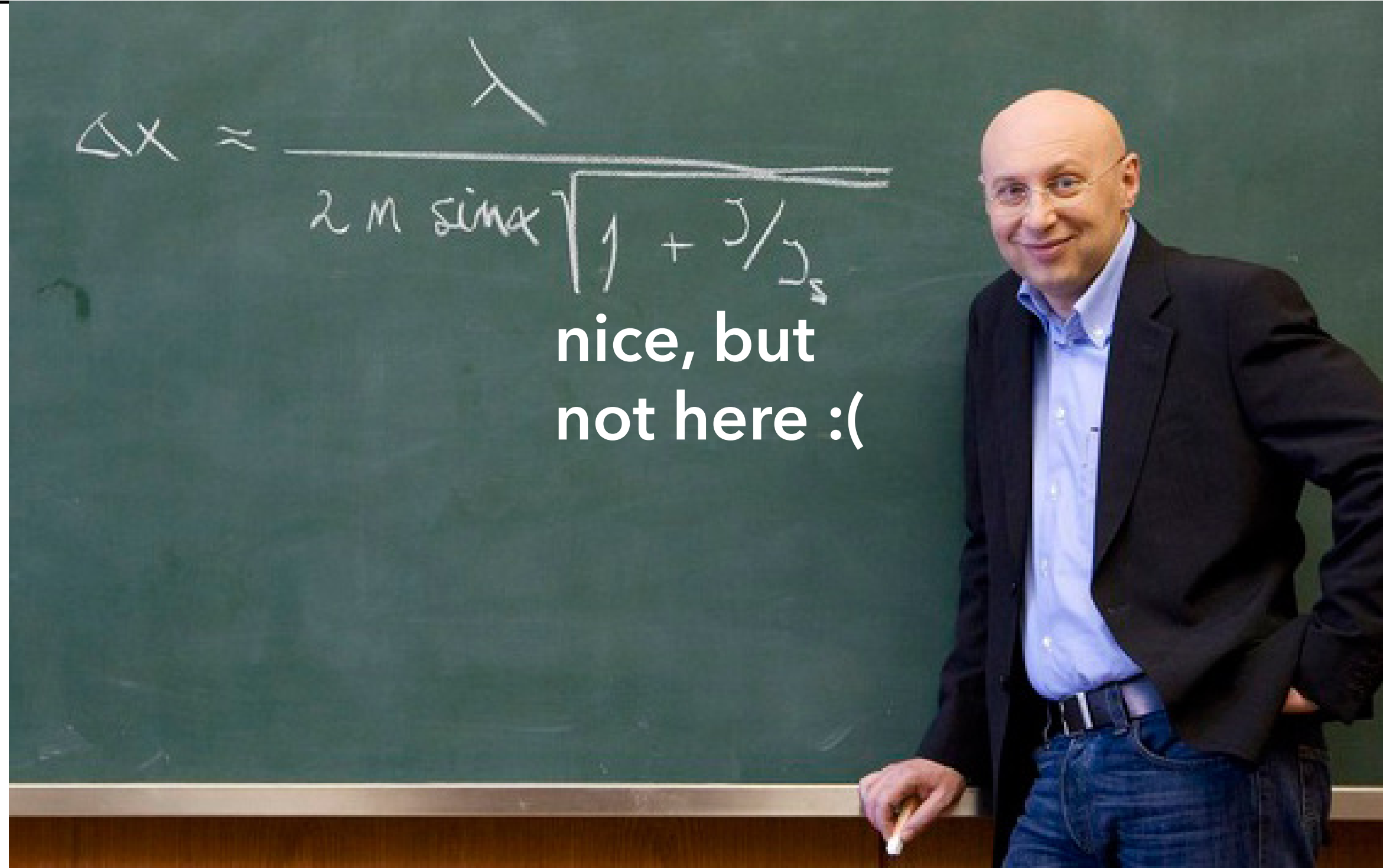


(b) Simulated focus



- ▶ evanescent wave enters even under total reflection
- ▶ surface: phase shift gradient
- ▶ shift of focus position
- ▶ reduced intensity due to absorption
- ▶ but no impact on focus size, no aberrations

Maximum Aperture - Minimum Focus Size



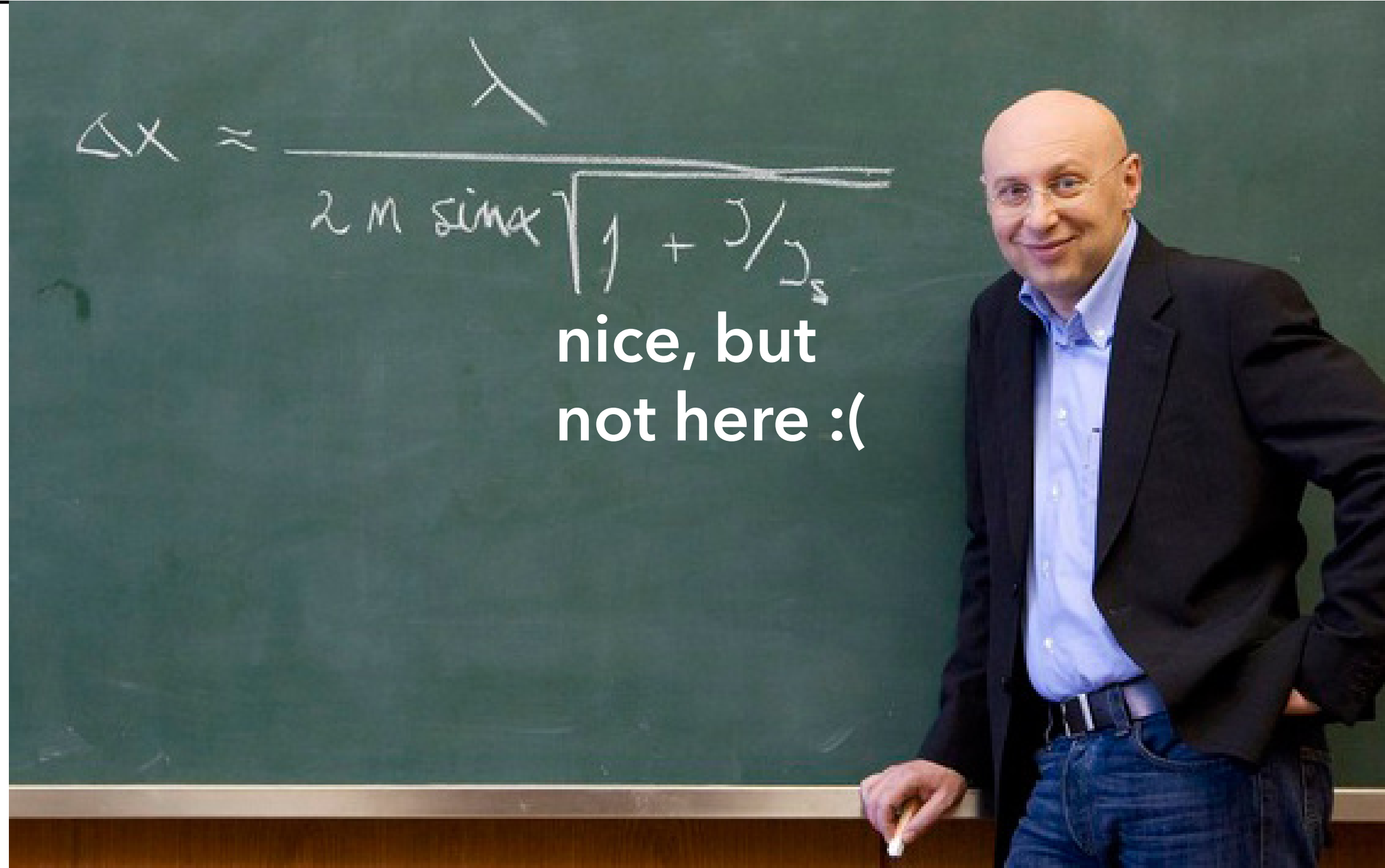
In the TRM case one assumes a full opening of up to half of the critical angle

$$4\varepsilon \leq \theta_c \tag{7}$$

leading to a diffraction limit of

$$D_{\text{diff}}(\text{TRM}) \approx \frac{1.76 \lambda}{\sqrt{2} \delta} = 1.76 \sqrt{\frac{\pi}{r_0 \rho_e}} \tag{8}$$

Maximum Aperture - Minimum Focus Size



In the TRM case one assumes a full opening of up to half of the critical angle

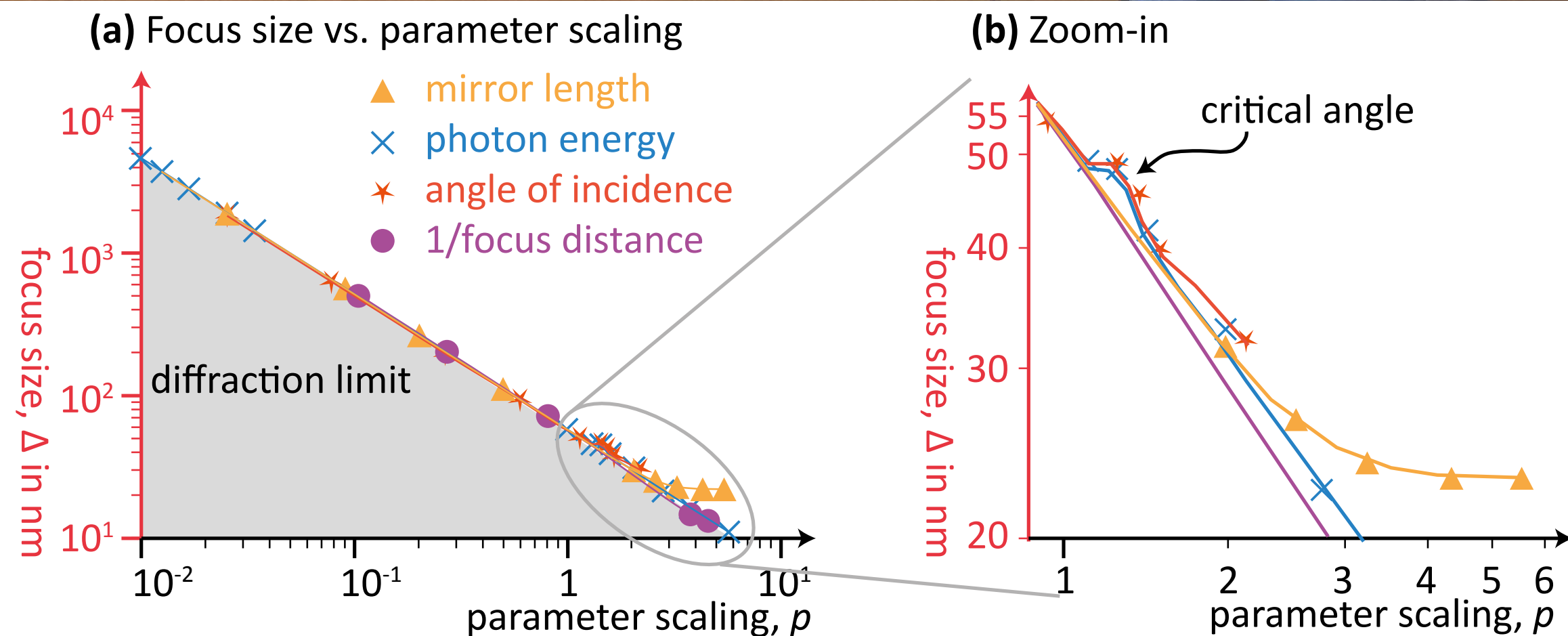
$$4\varepsilon \leq \theta_c \tag{7}$$

leading to a diffraction limit of

$$D_{diff}(TRM) \approx \frac{1.76 \lambda}{\sqrt{2 \delta}} = 1.76 \sqrt{\frac{\pi}{r_0 \rho_e}} \tag{8}$$

The beam size limit $\sim W_c$, derived here for waveguiding geometries, also applies to other x-ray focusing devices. For example, the spot size achievable with a Fresnel

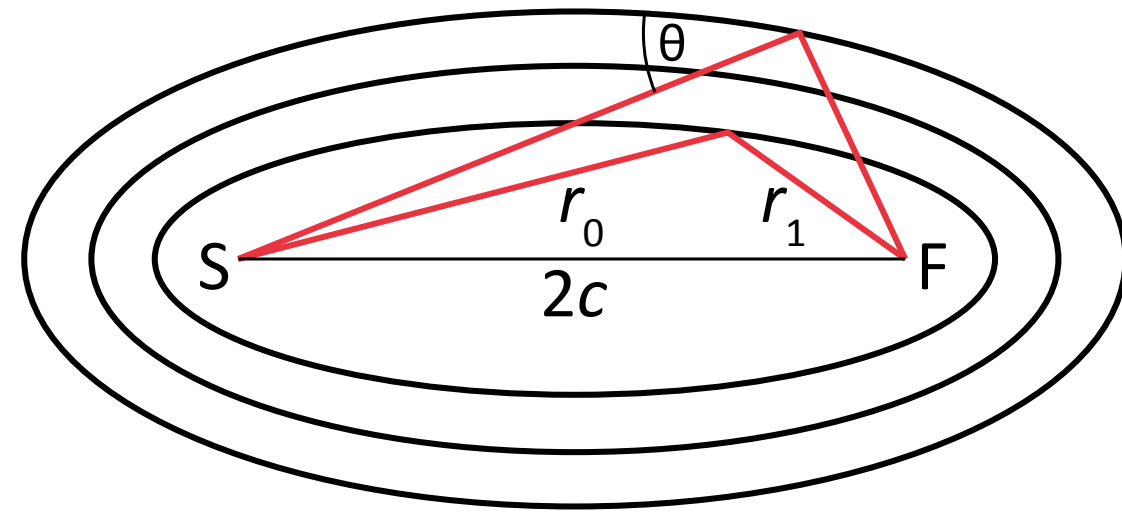
- ▶ index of refraction scales as λ^2
- ▶ numerical aperture vanishes
- ▶ fundamental focus limit (!/?)



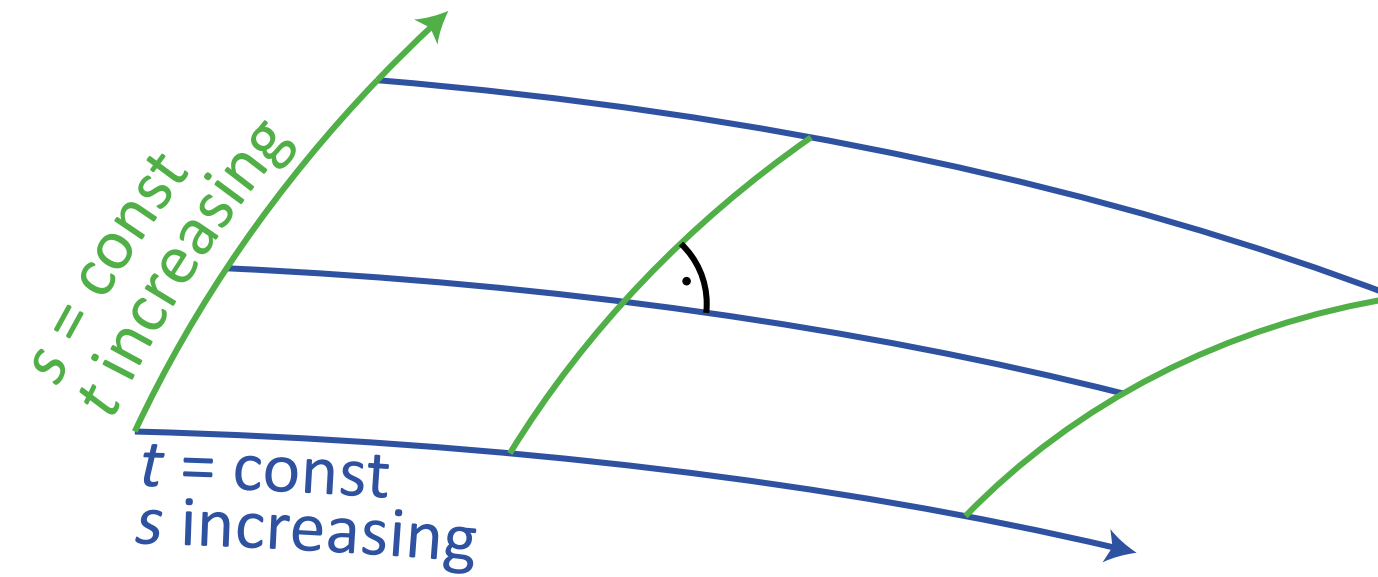
Harke, Hell et al, Optics Express, 2008 Morawe, Osterhoff, NIMA, 2010
 Osterhoff, PhD thesis, 2011 Bergemann et al, PRL, 2003

Multilayer Coatings, Takagi-Taupin

(a) Confocal ellipses

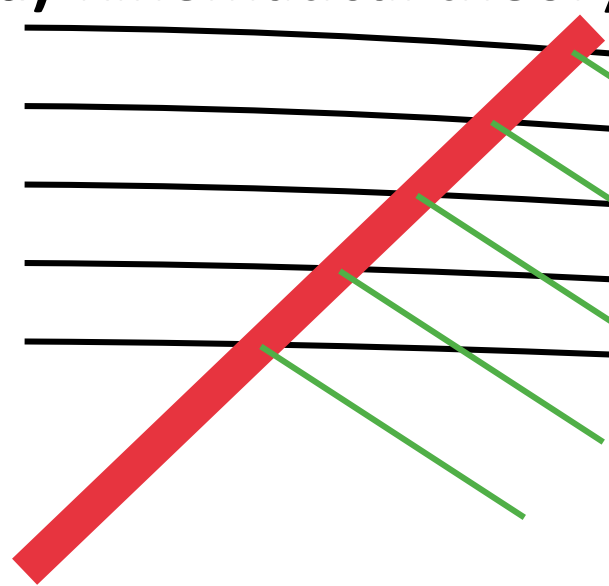


(b) Elliptical coordinates

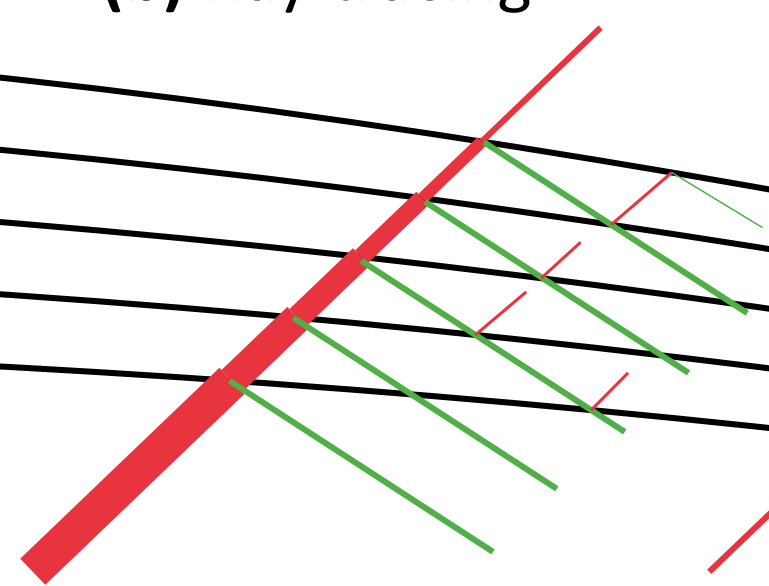


ML mirror as nested confocal ellipses

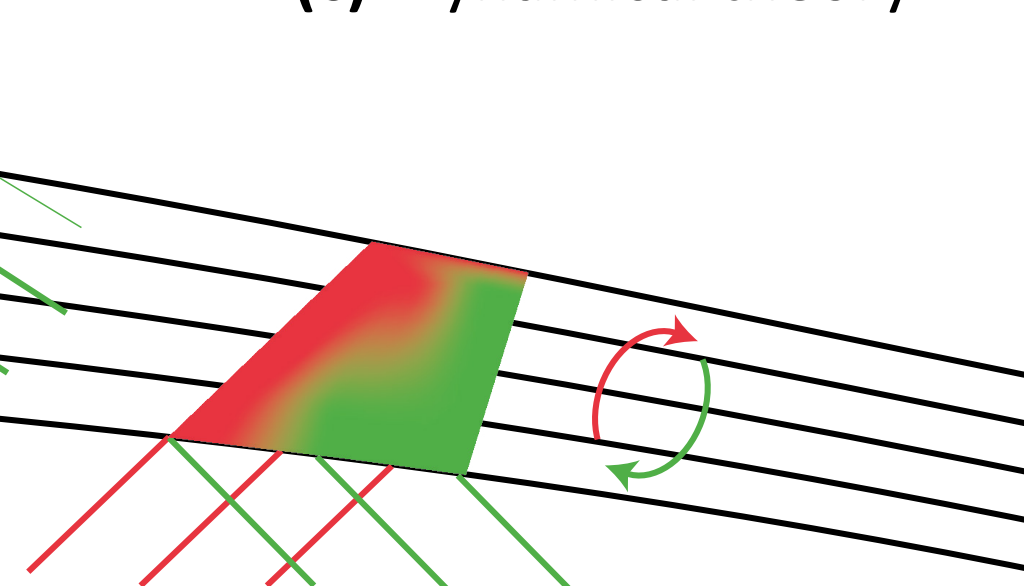
(a) Kinematical theory



(b) Ray-tracing

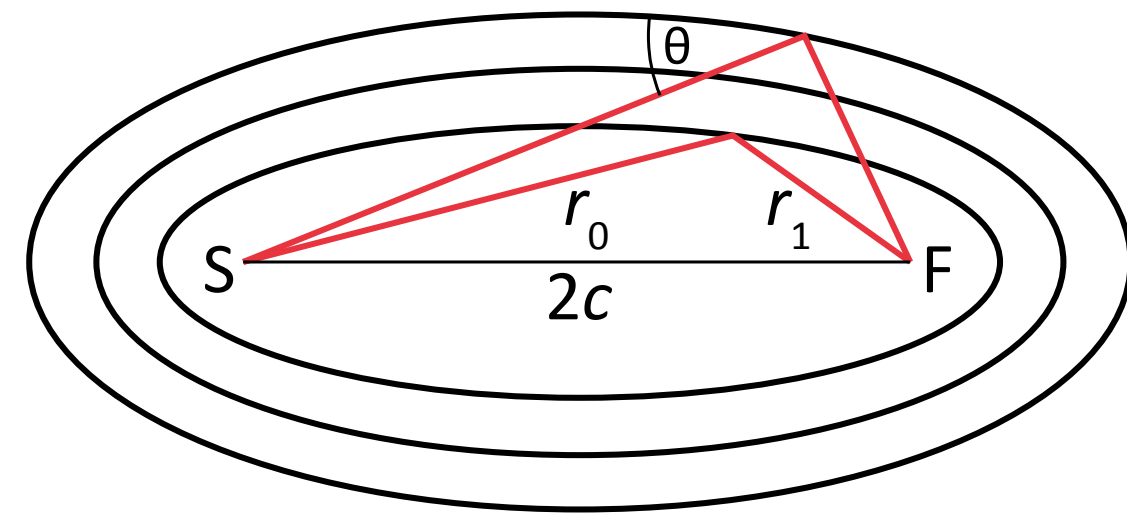


(c) Dynamical theory

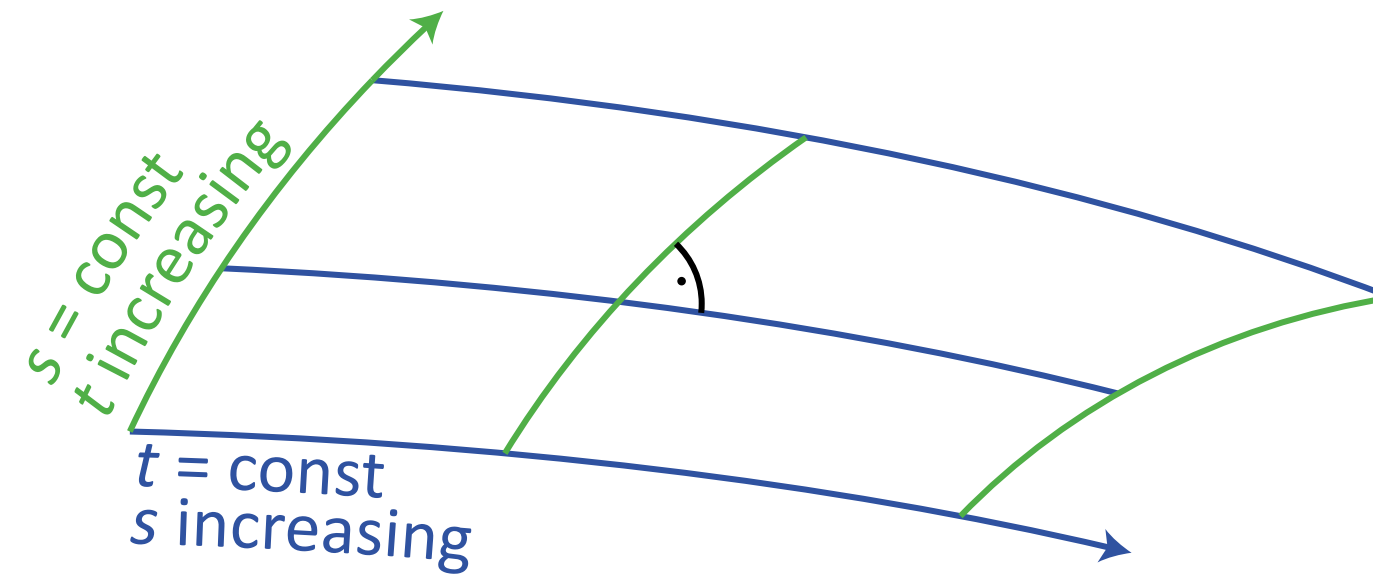


Multilayer Coatings, Takagi-Taupin

(a) Confocal ellipses



(b) Elliptical coordinates

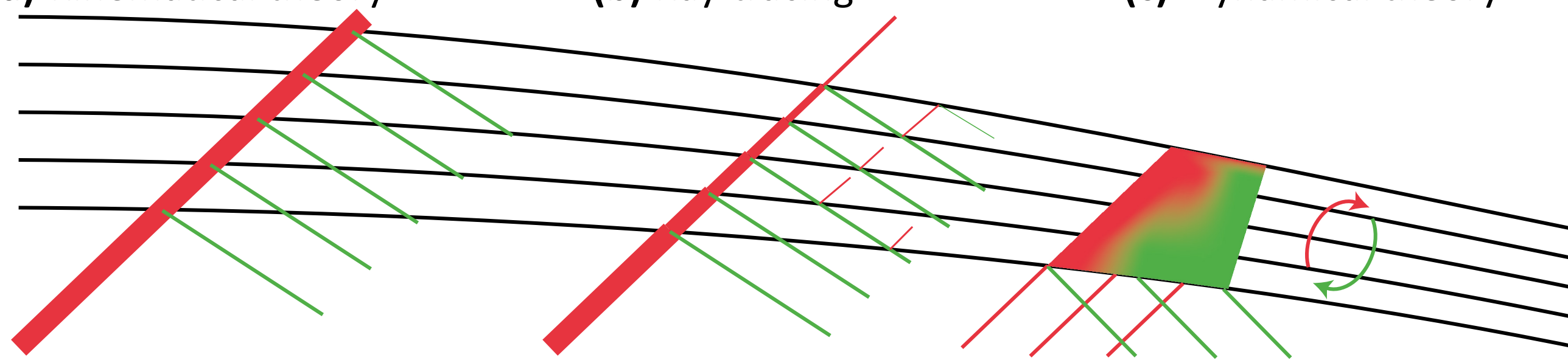


ML mirror as nested confocal ellipses

(a) Kinematical theory

(b) Ray-tracing

(c) Dynamical theory



models of increasing complexity: single reflection;
multiple reflection; coupled wave-theory

$$(\alpha^2 \partial_s + \beta^2 \partial_t) \psi_0 = i(u_0 \psi_0 + u_1 \psi_1) - \gamma^+ \psi_0$$

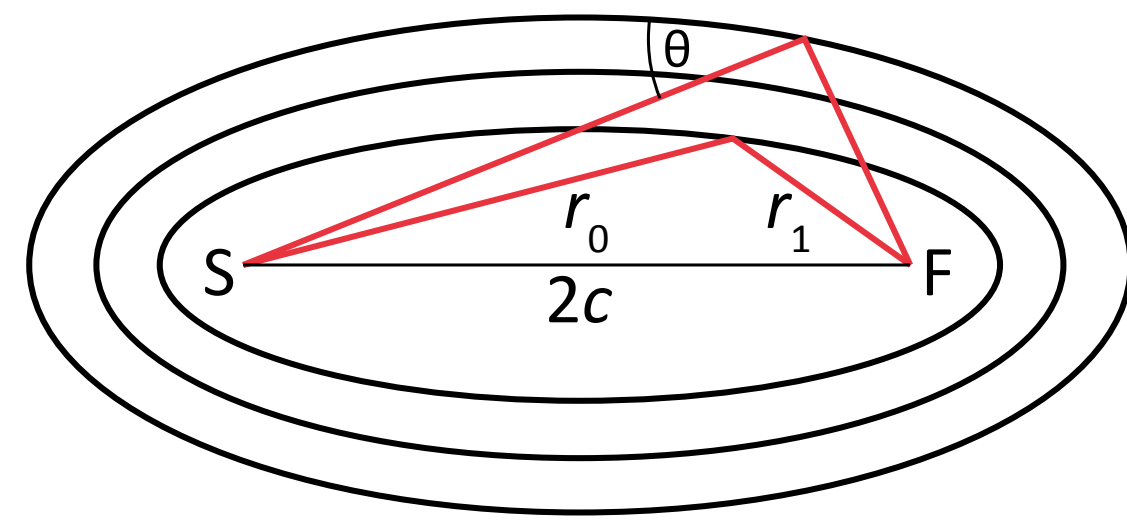
$$(\alpha'^2 \partial_s - \beta'^2 \partial_t) \psi_1 = i \left((u_0 - \varepsilon) \psi_1 + u_{\text{I}} \psi_0 \right) + \gamma'^- \psi_1$$

Takagi-Taupin description in elliptical geometry:
incoming wave and reflected wave
are coupled by quasi-periodic susceptibility

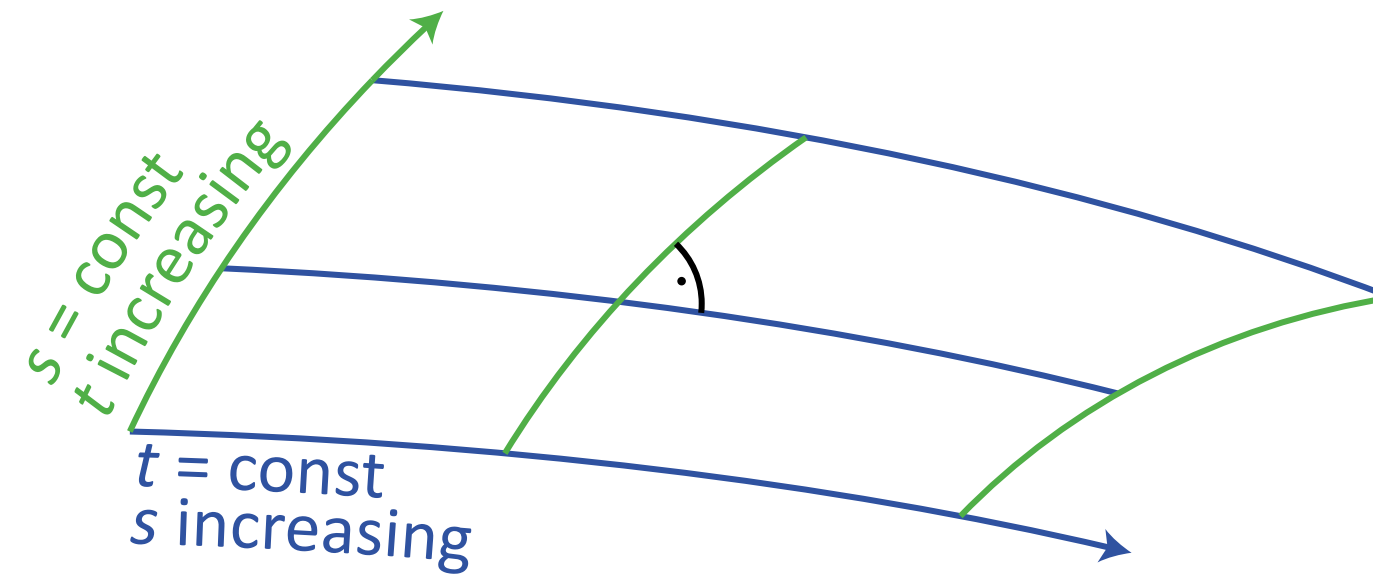
Multilayer Coatings, Takagi-Taupin



(a) Confocal ellipses



(b) Elliptical coordinates

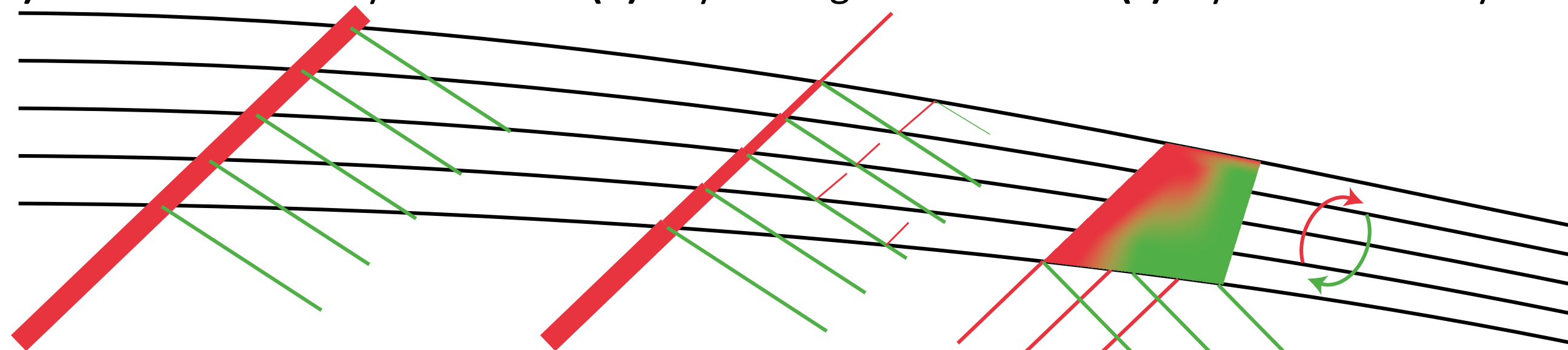


ML mirror as nested confocal ellipses

(a) Kinematical theory

(b) Ray-tracing

(c) Dynamical theory

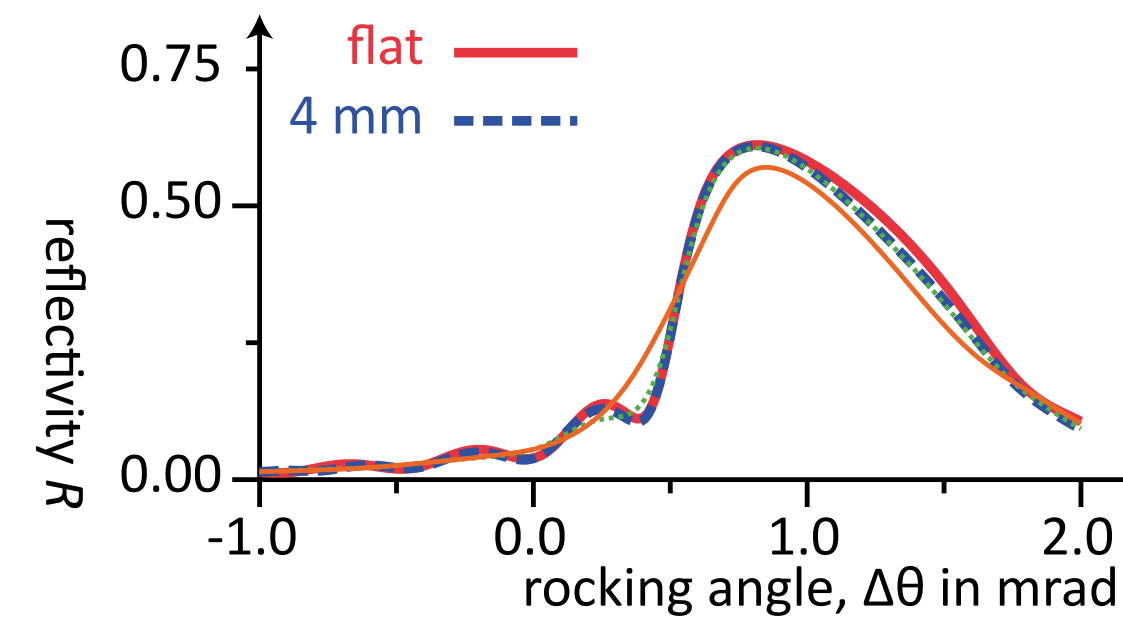


models of increasing complexity: single reflection; multiple reflection; coupled wave-theory

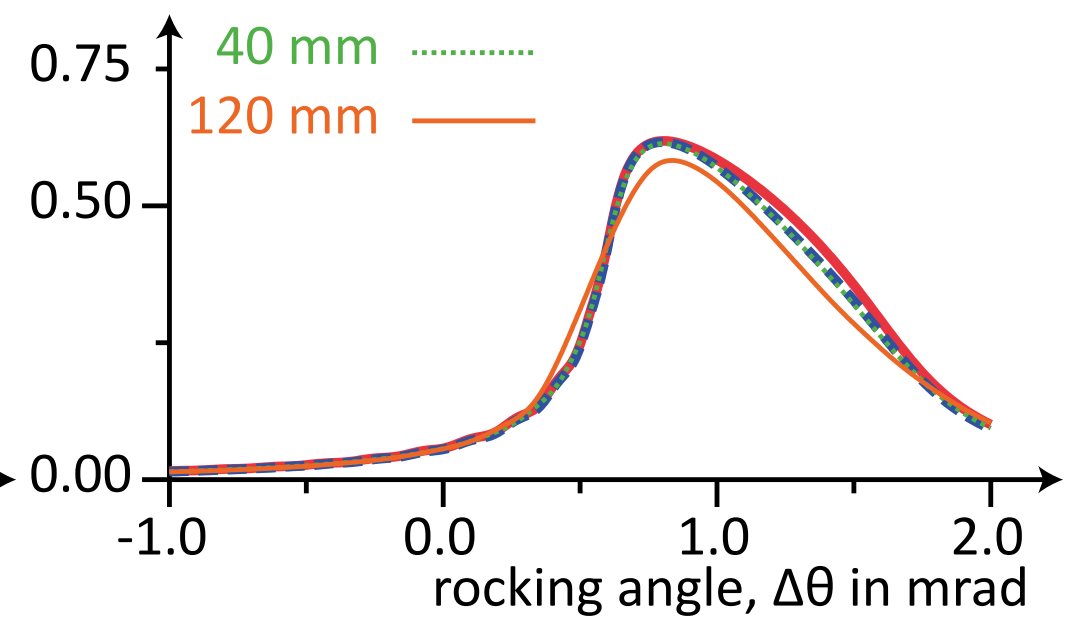
$$(\alpha^2 \partial_s + \beta^2 \partial_t) \psi_0 = i(u_0 \psi_0 + u_1 \psi_1) - \gamma^+ \psi_0$$

$$(\alpha'^2 \partial_s - \beta'^2 \partial_t) \psi_1 = i((u_0 - \varepsilon) \psi_1 + u_{\text{I}} \psi_0) + \gamma'^- \psi_1$$

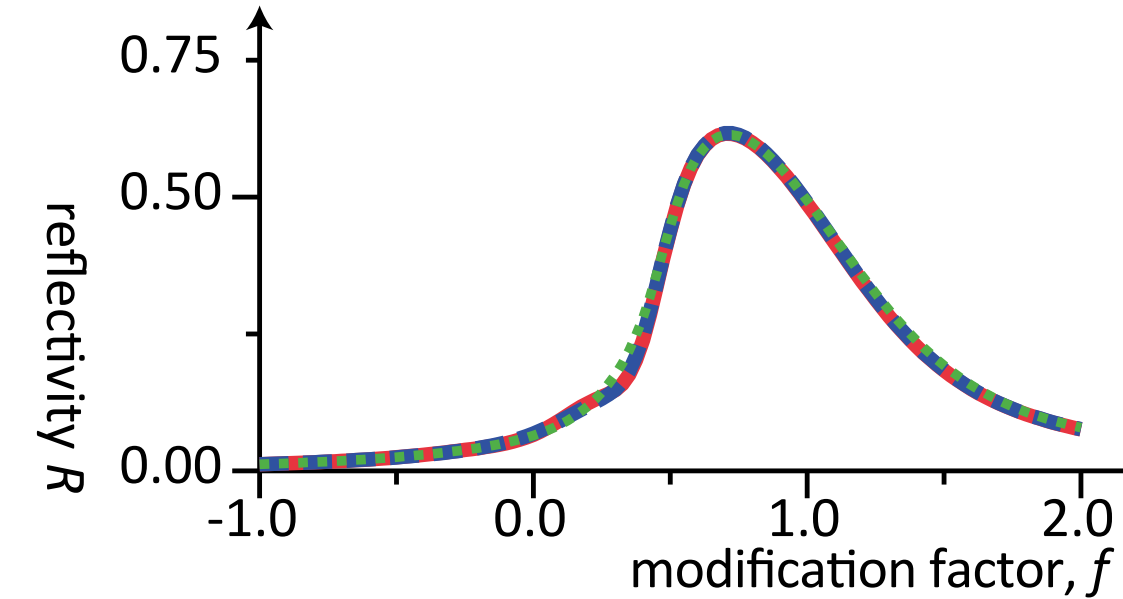
(a) 12.4 keV, 20 layers



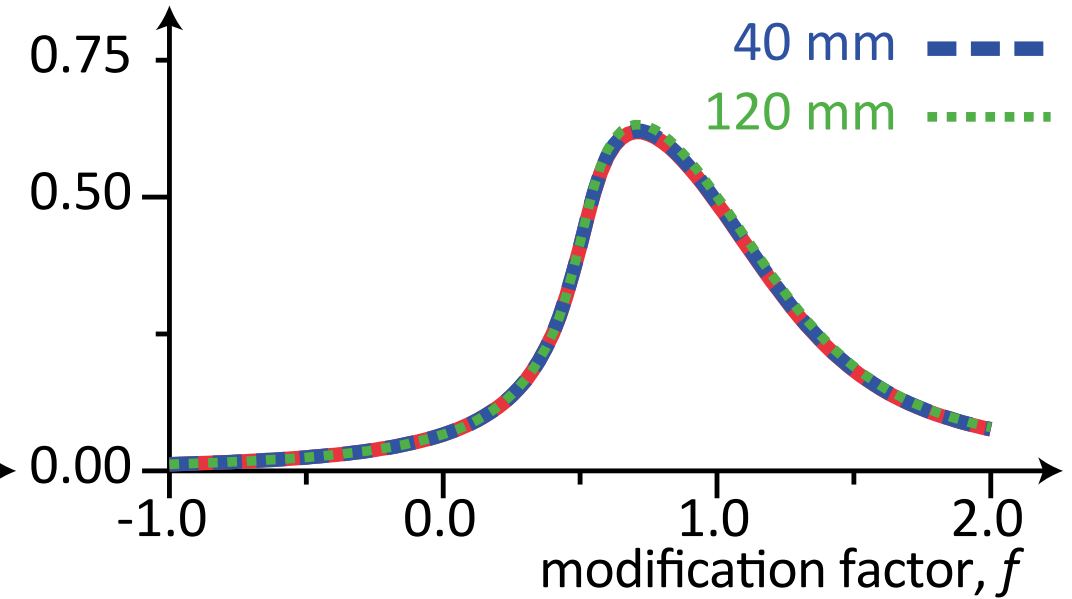
(b) 12.4 keV, 50 layers



(a) 12.4 keV, 20 layers



(b) 12.4 keV, 50 layers



simulated reflectivity of curved ML mirror; top: without, bottom: with correction for refraction inside ML

Takagi-Taupin description in elliptical geometry: incoming wave and reflected wave are coupled by quasi-periodic susceptibility

Recent Progress

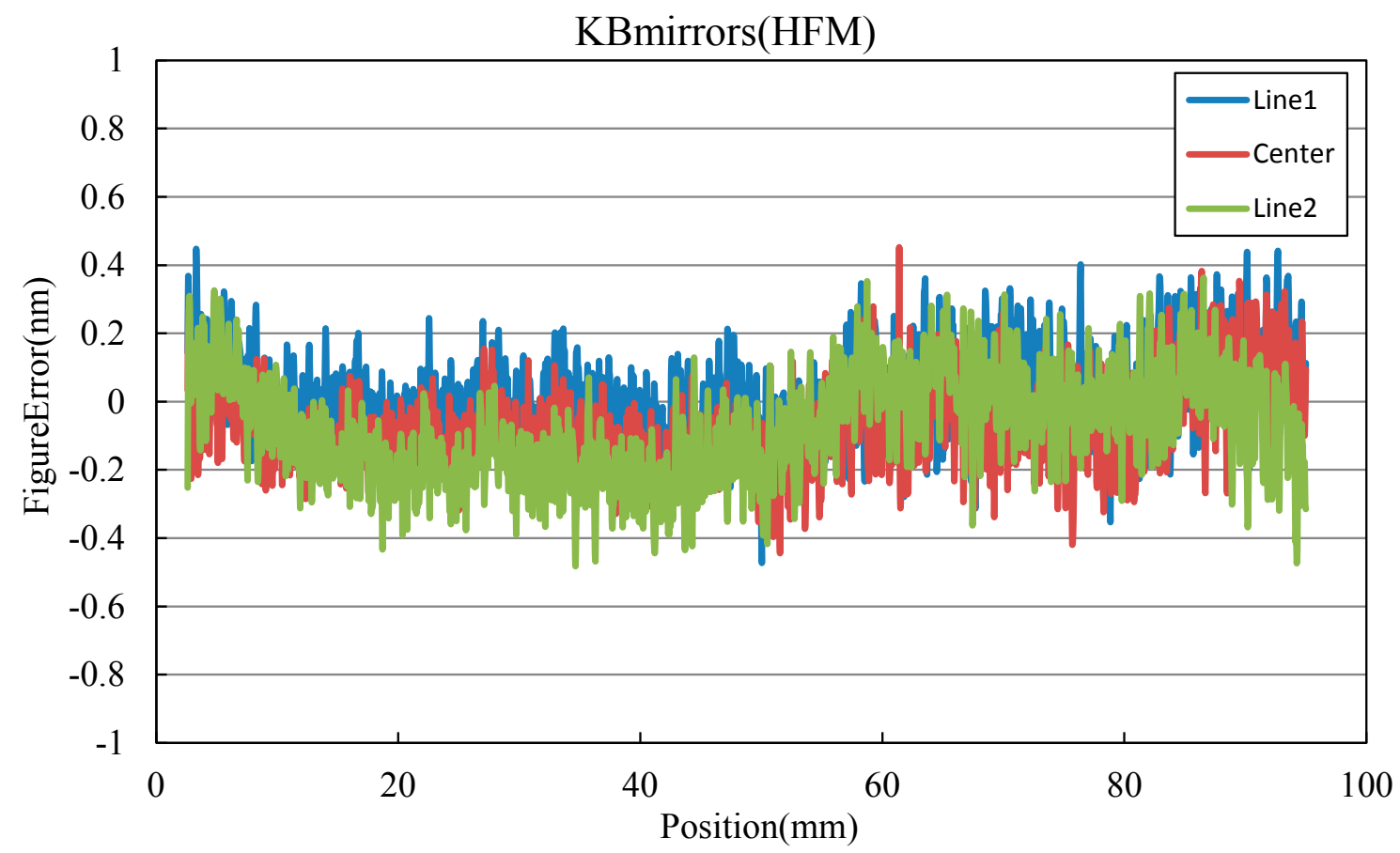
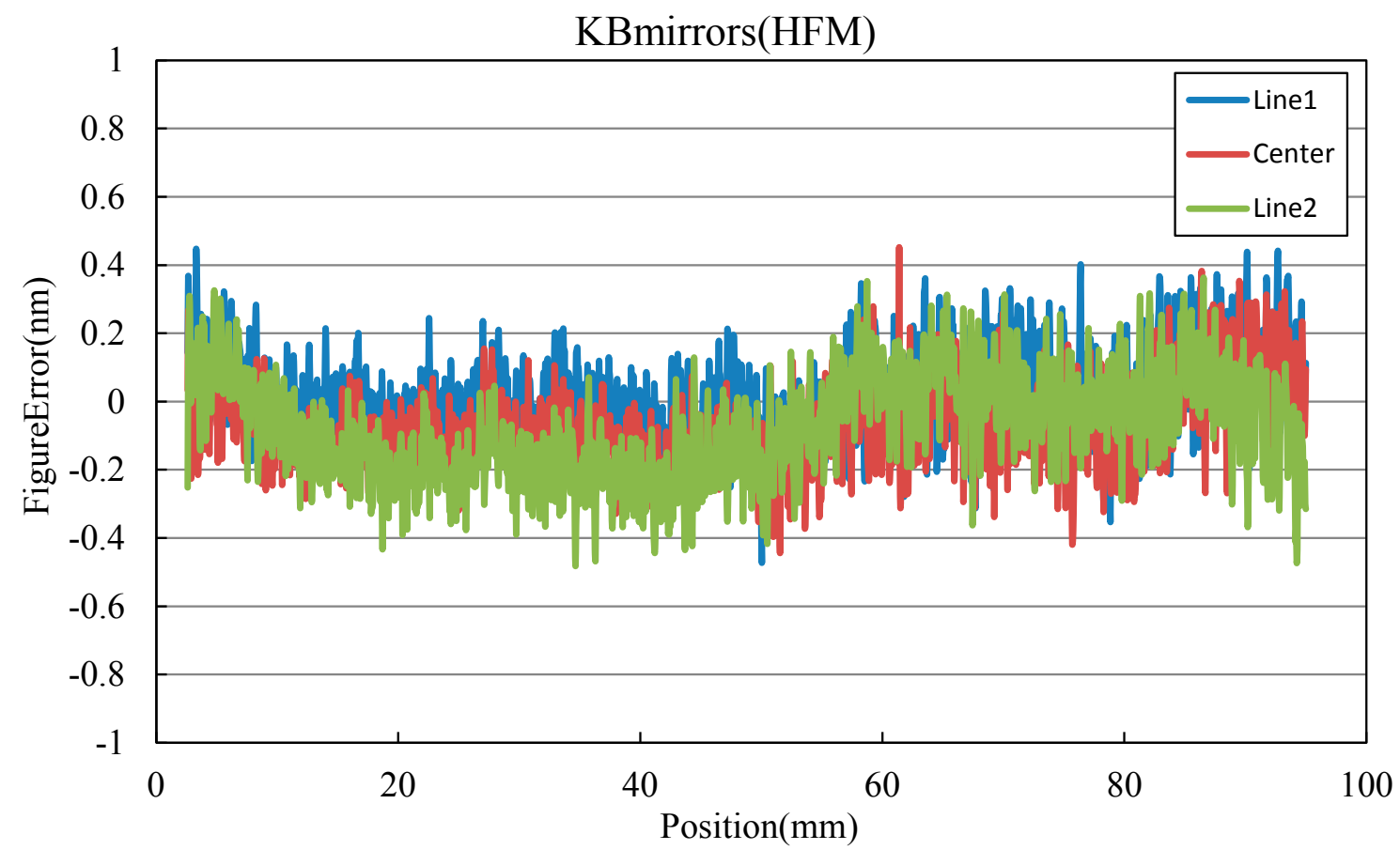


Figure 2-3: Tangential Figure error profiles of HFM

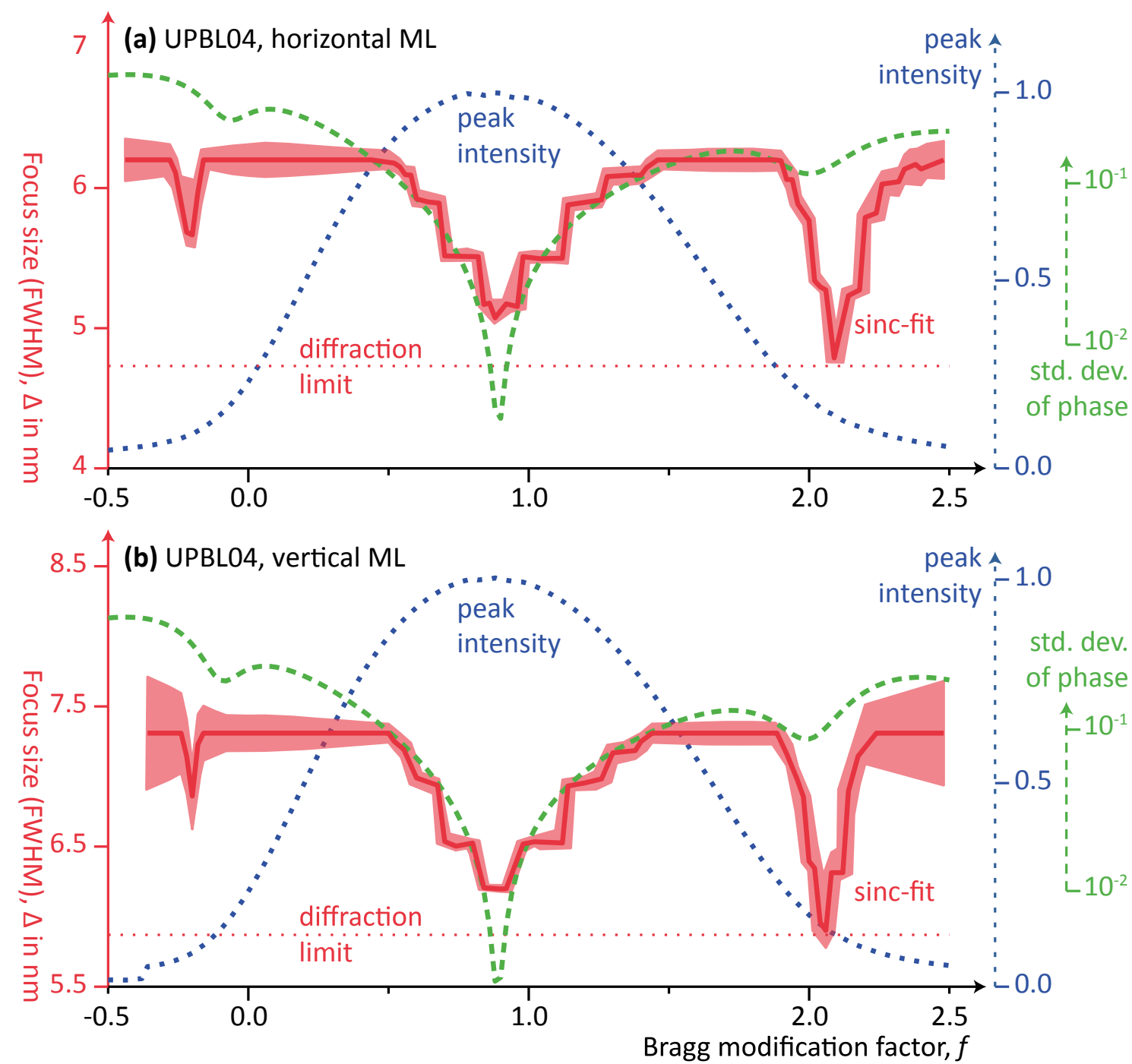
► smooth surfaces
sub-nm figure error

Recent Progress



- ▶ smooth surfaces
sub-nm figure error
- ▶ simulations to
single nano metre

Figure 2-3: Tangential Figure error profiles of HFM



Recent Progress

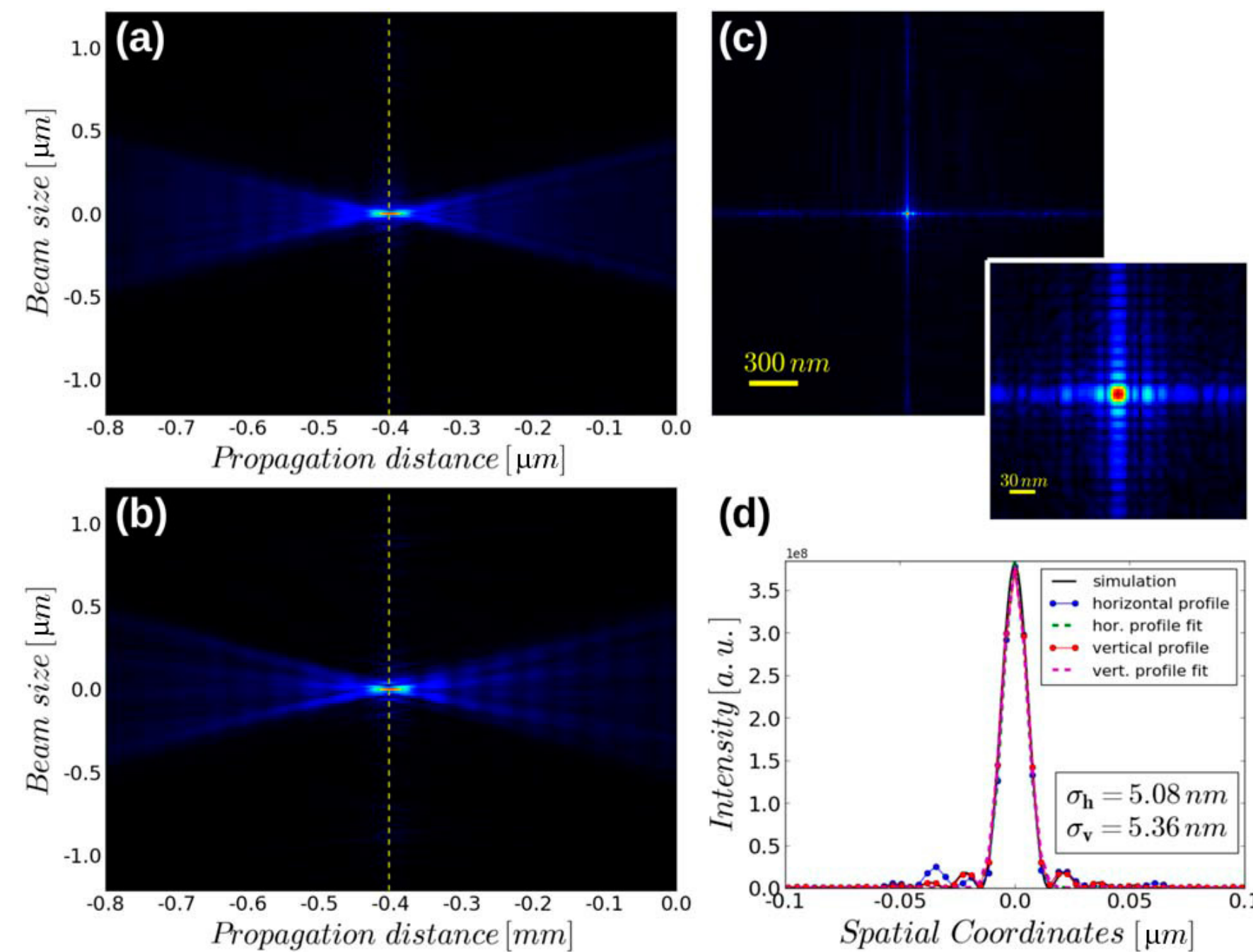
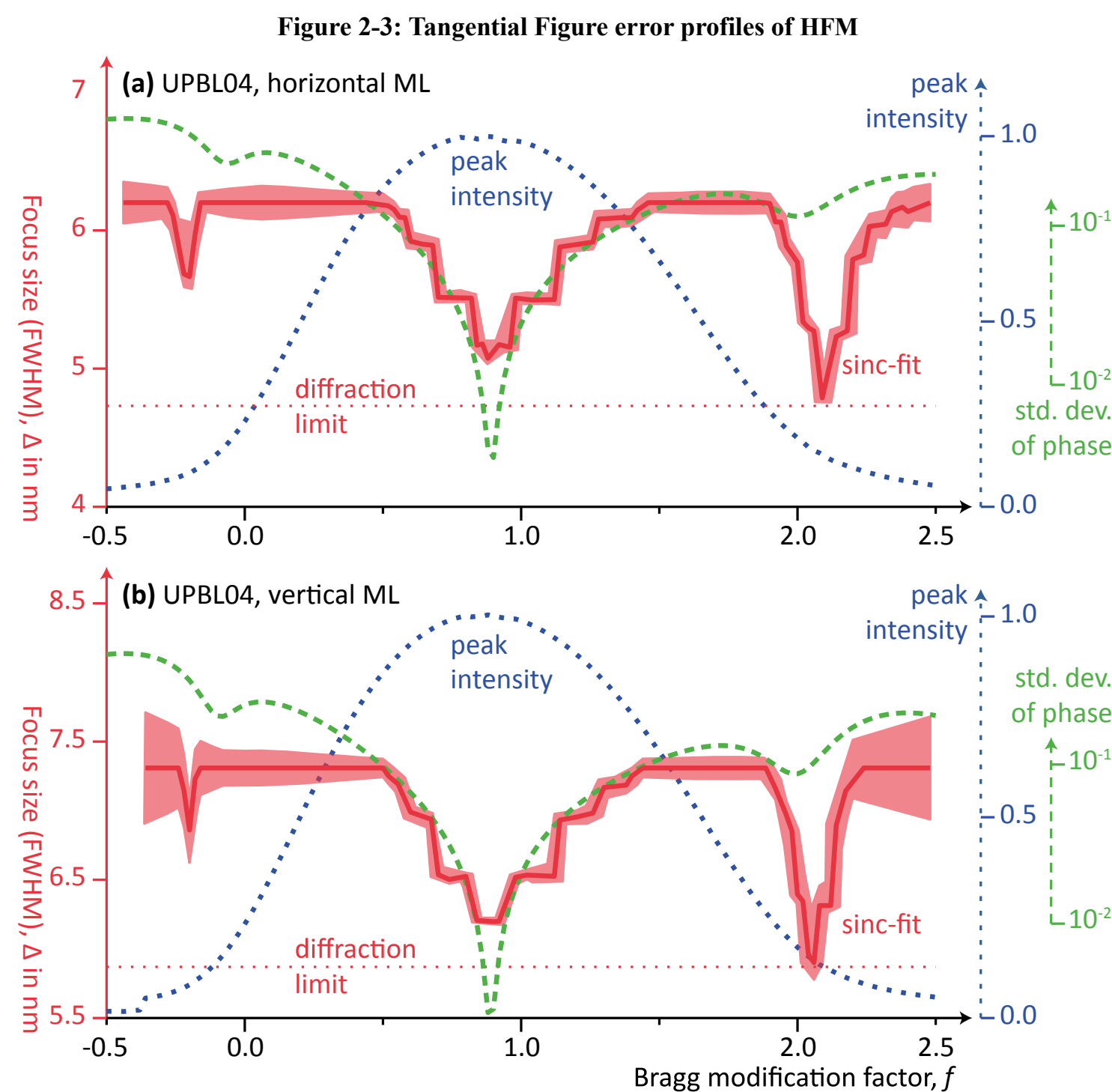
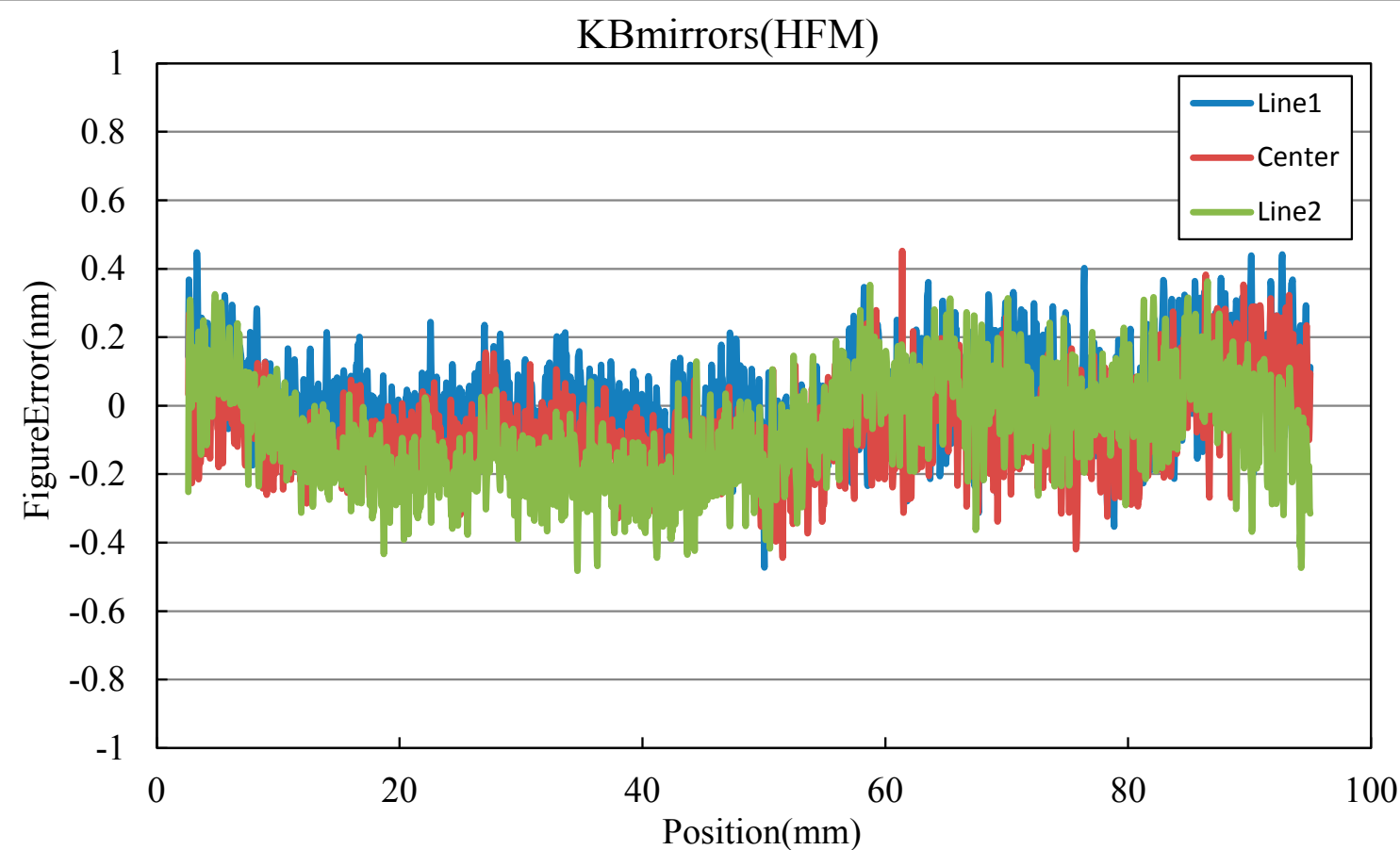


Fig. 3. X-ray wavefront characterization and focus size. (a) Vertical cross-section of the propagation of the wavefront. (b) Horizontal cross-section of the propagation of the wavefront. In (a) and (b), the sample is at position 0 and the focus is indicated by the dashed yellow line. (c) Beam at the focus position. The inset displays a zoomed-in view of the central part. (d) Horizontal and vertical profiles of the intensity of the beam at the focus position plotted together with a simulated profile of an ideal optical system. The FWHM values calculated by $2\sqrt{2 \log(2)\sigma}$ were 12.0 nm for the horizontal focus and 12.6 nm for the vertical focus.

- ▶ smooth surfaces
sub-nm figure error
- ▶ simulations to
single nano metre
- ▶ ML mirrors down to
12 nm, above 20 keV

12.0 nm ×
12.6 nm
(FWHM),
≥ 20 keV

Fresnel Zone Plates, ML Laue Lenses, ML Zone Plates



Outline

- ▶ Introduction + History
- ▶ Reflective Optics
- ▶ *Diffractive Optics*
- ▶ Refractive Optics
- ▶ Waveguides
- ▶ Discussion

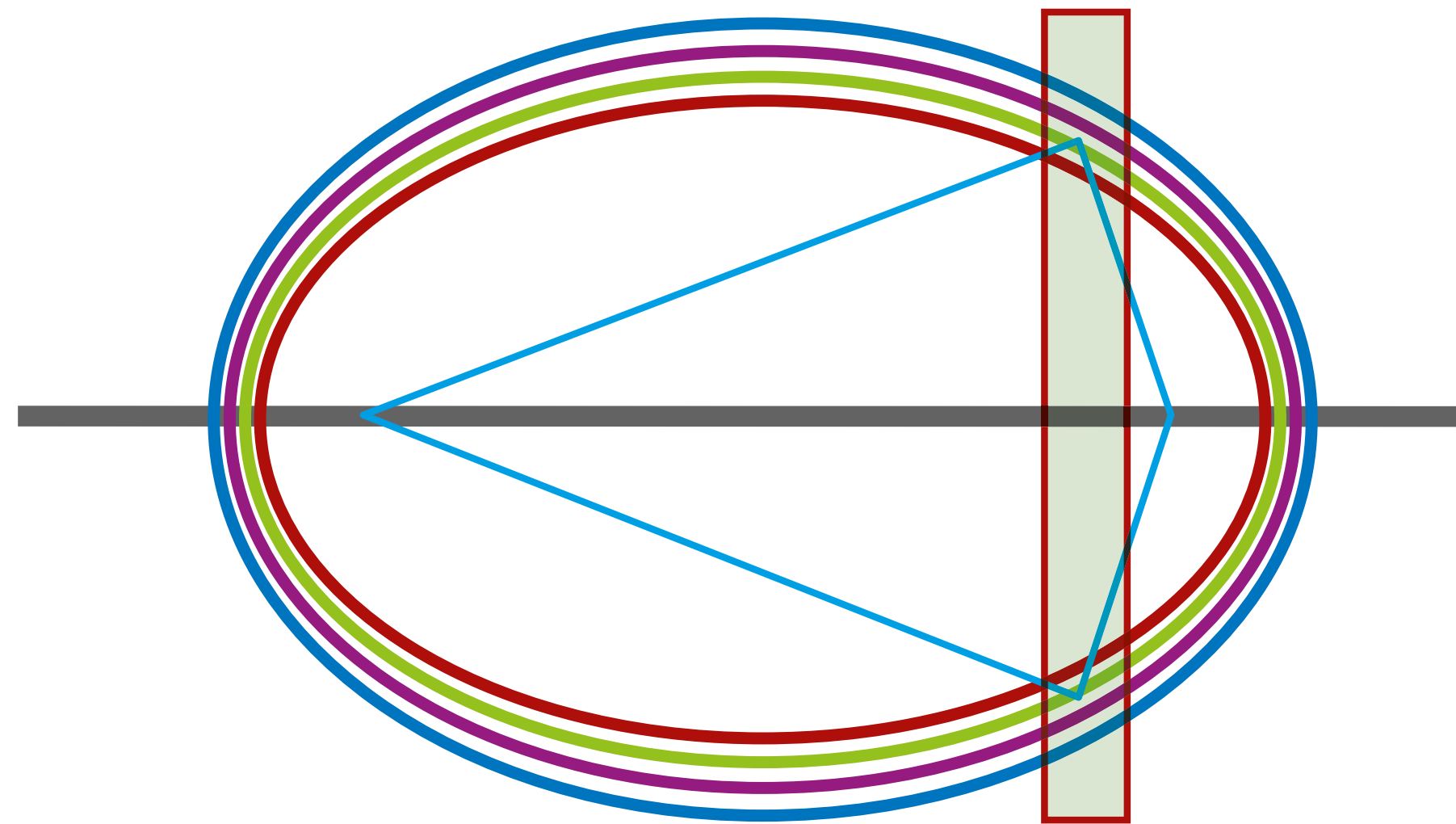


Figure 2

A set of concentric ellipses along with a depiction of a multilayer Laue lens.

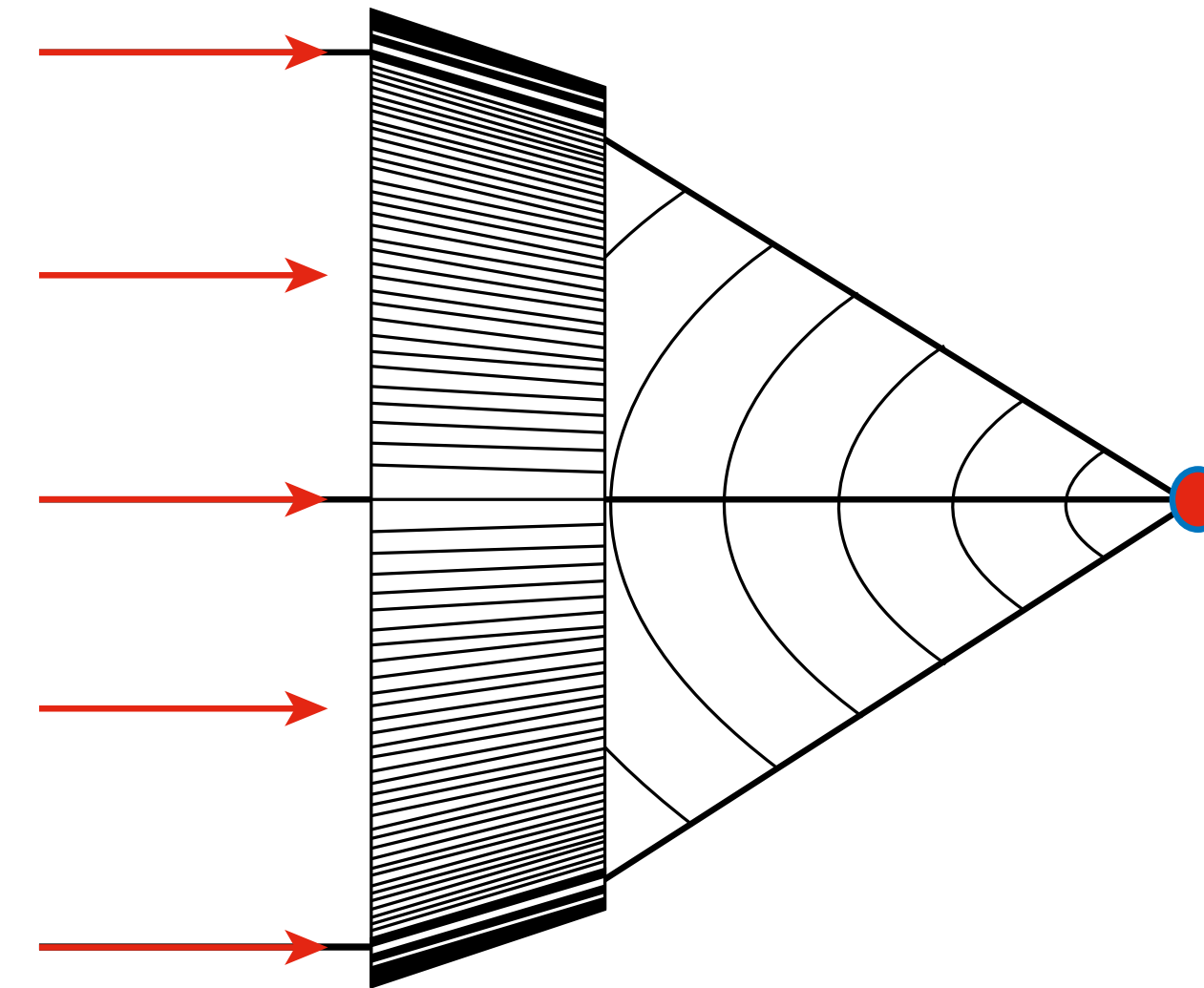


Figure 10

A schematic wedged multilayer Laue lens in which each interface is slanted to achieve a Bragg condition.

$$r_n = \sqrt{(n\lambda/2)^2 + n\lambda f}$$

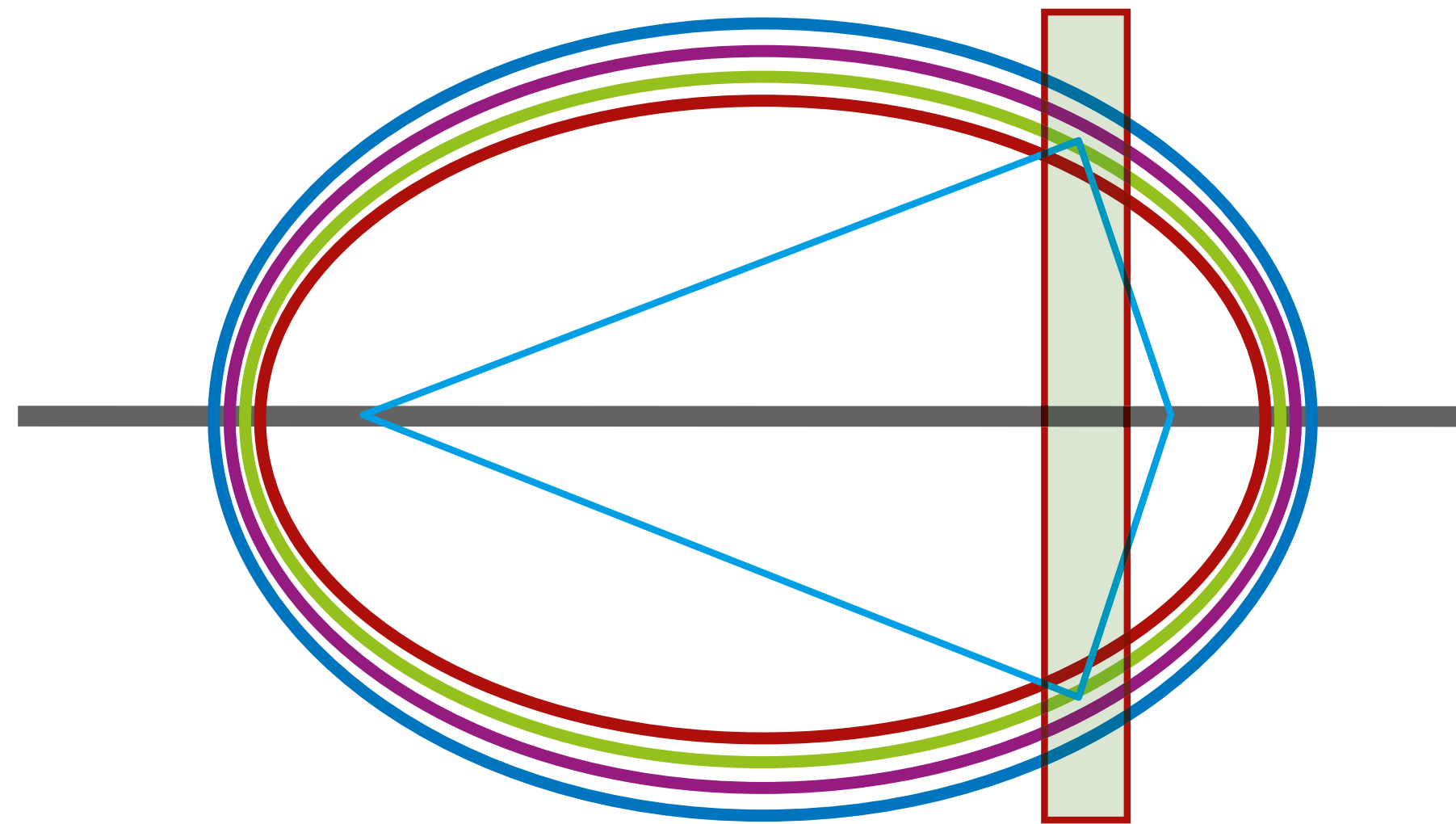


Figure 2

A set of concentric ellipses along with a depiction of a multilayer Laue lens.

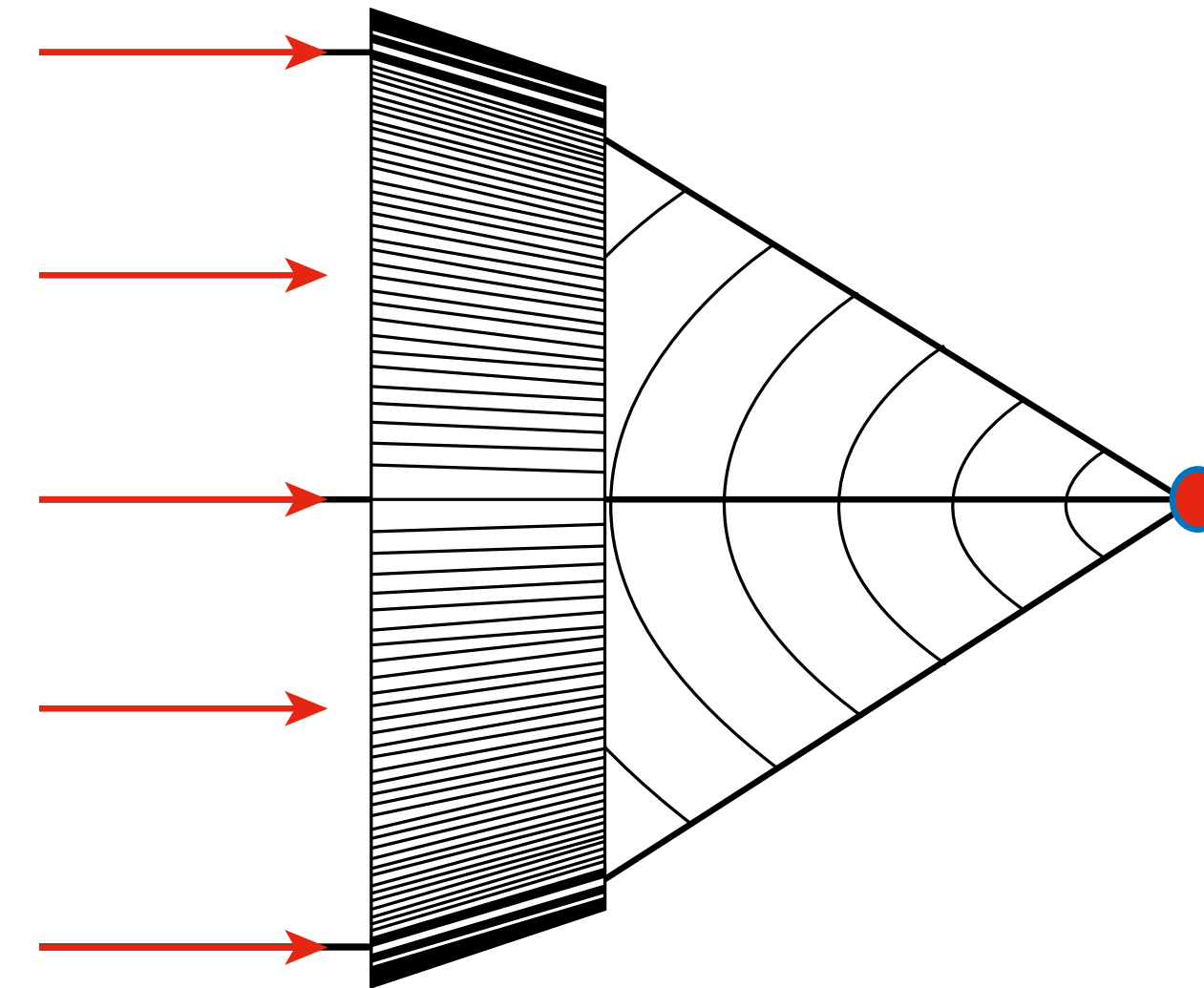


Figure 10

A schematic wedged multilayer Laue lens in which each interface is slanted to achieve a Bragg condition.

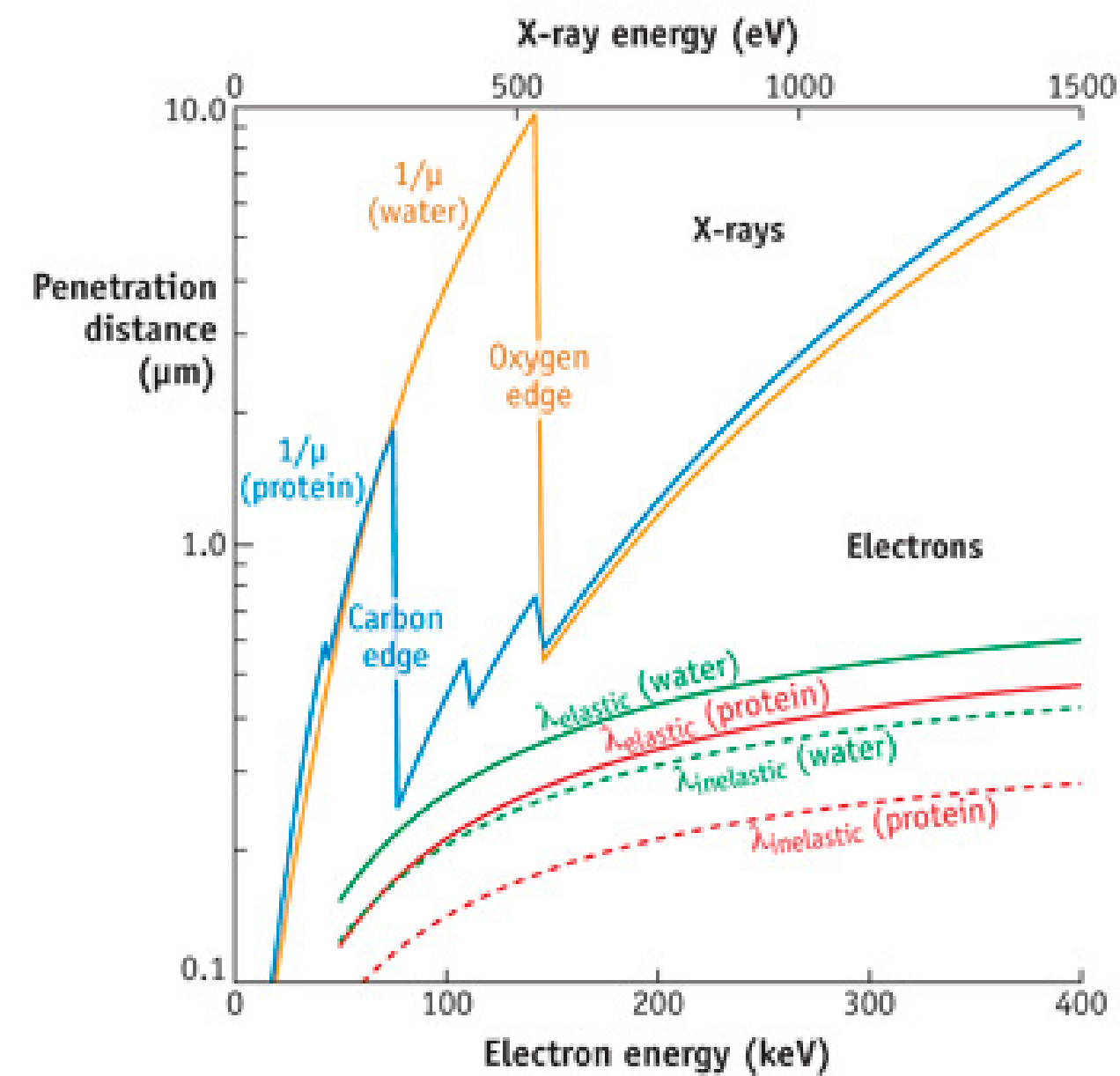
$$r_n = \sqrt{(n\lambda/2)^2 + n\lambda f}$$

Zone Plate Laws

- ▶ resolution given by outermost zone width
- ▶ zone width limited by fabrication
- ▶ efficiency limited by optical thickness
- ▶ thin and long zones: volume diffraction; "Bergemann-Limit"

Water Window

- ▶ high contrast between C (cell) and O (water)
- ▶ soft x-rays, good optics



1980ies: Soft X-Ray Microscopy

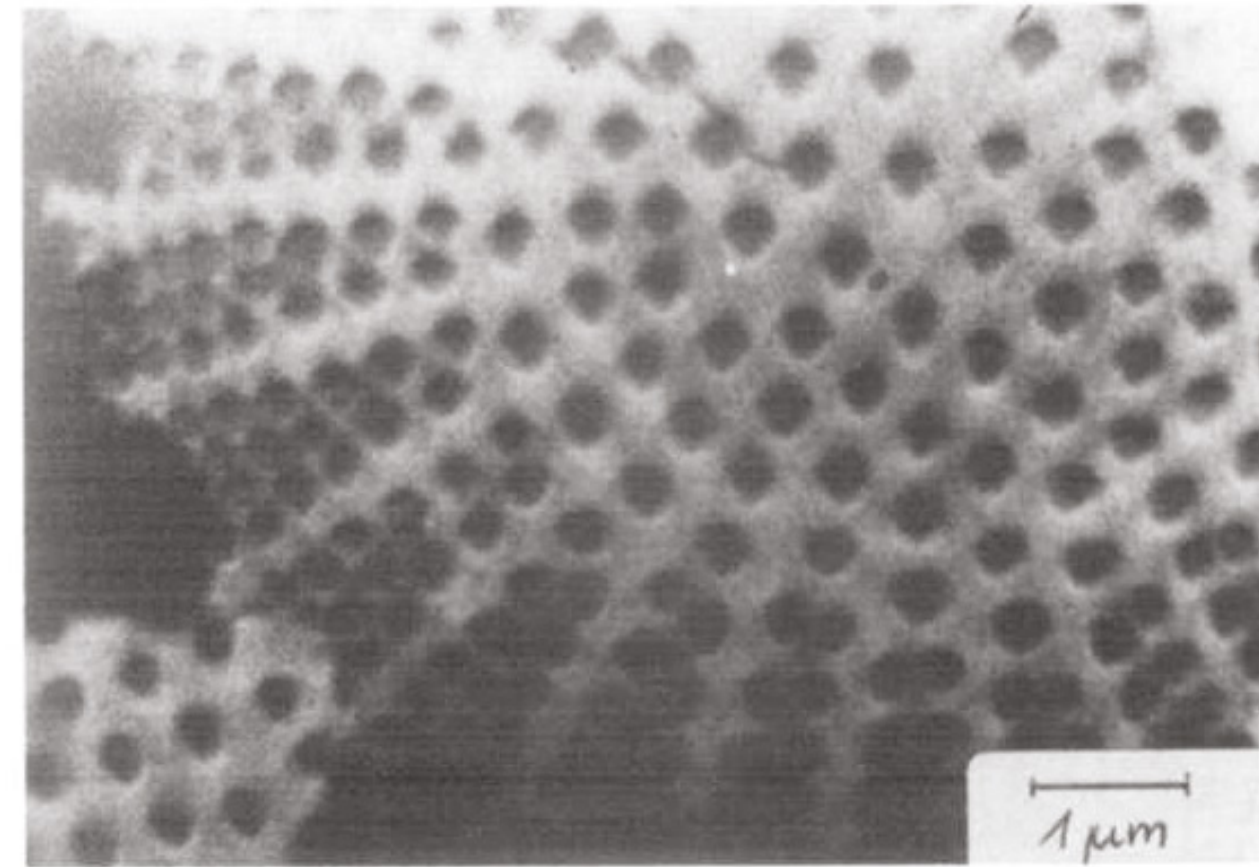
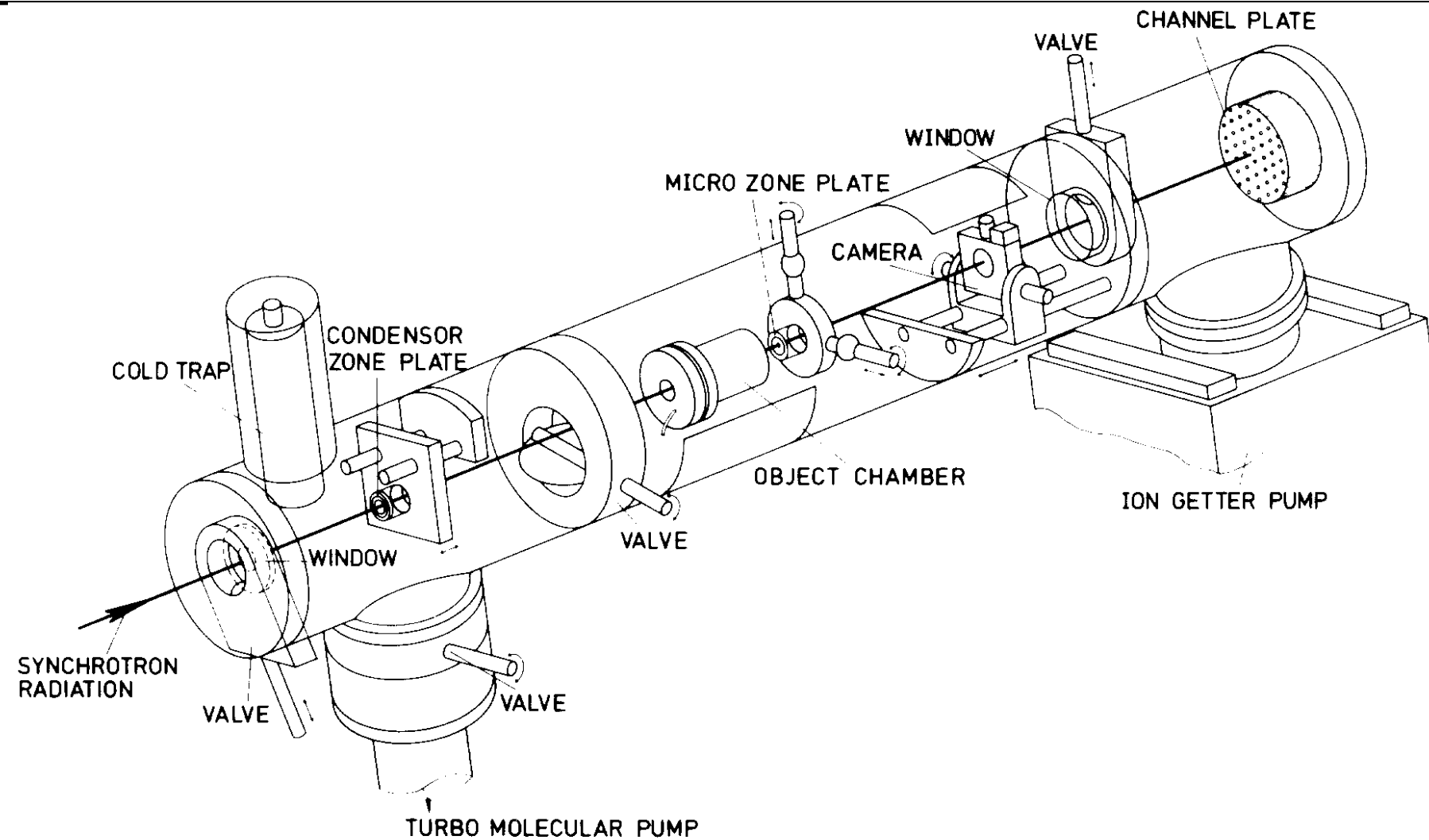


Fig. 4. Diatom, imaged with 4.5 nm X-rays, X-ray magnification 250×, exposure time 20 s, storage ring current 100 mA.

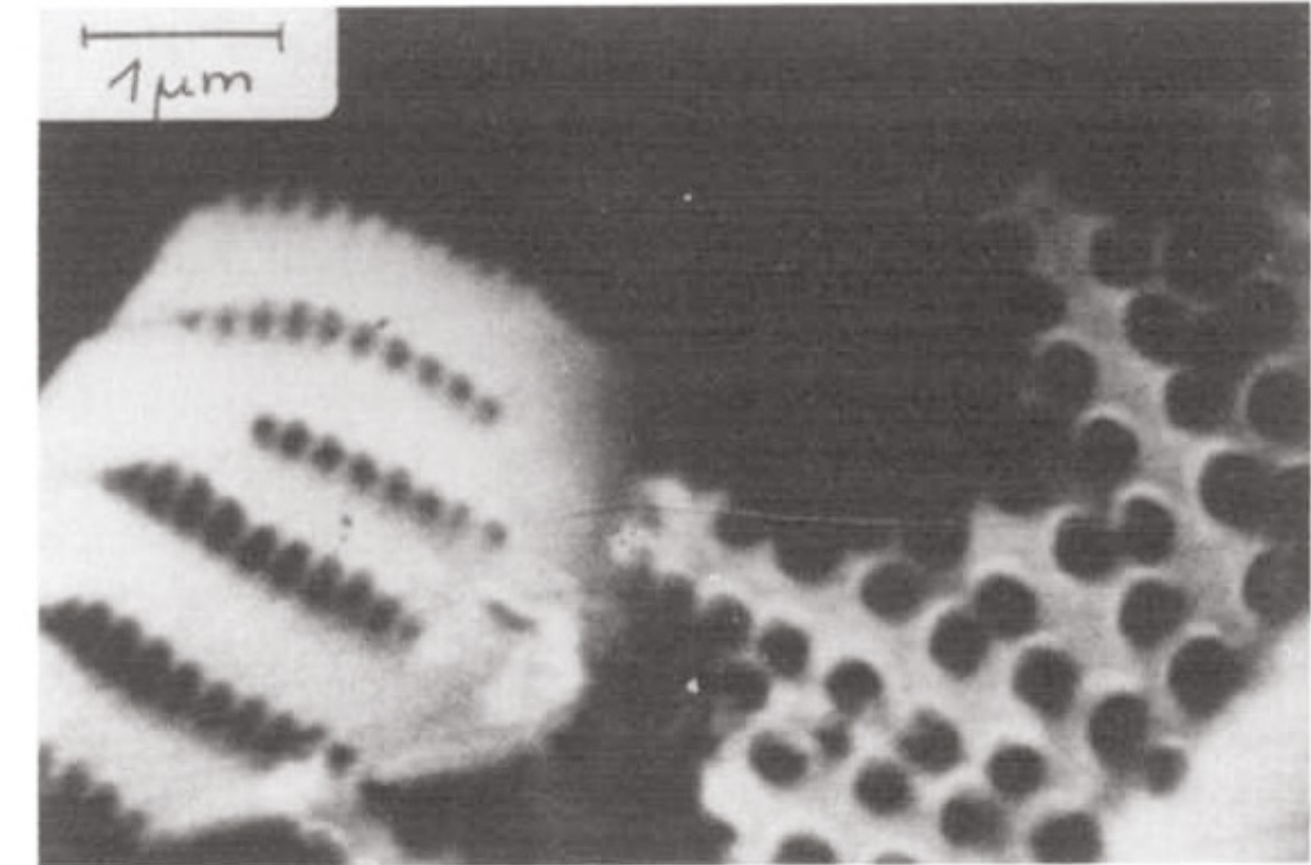
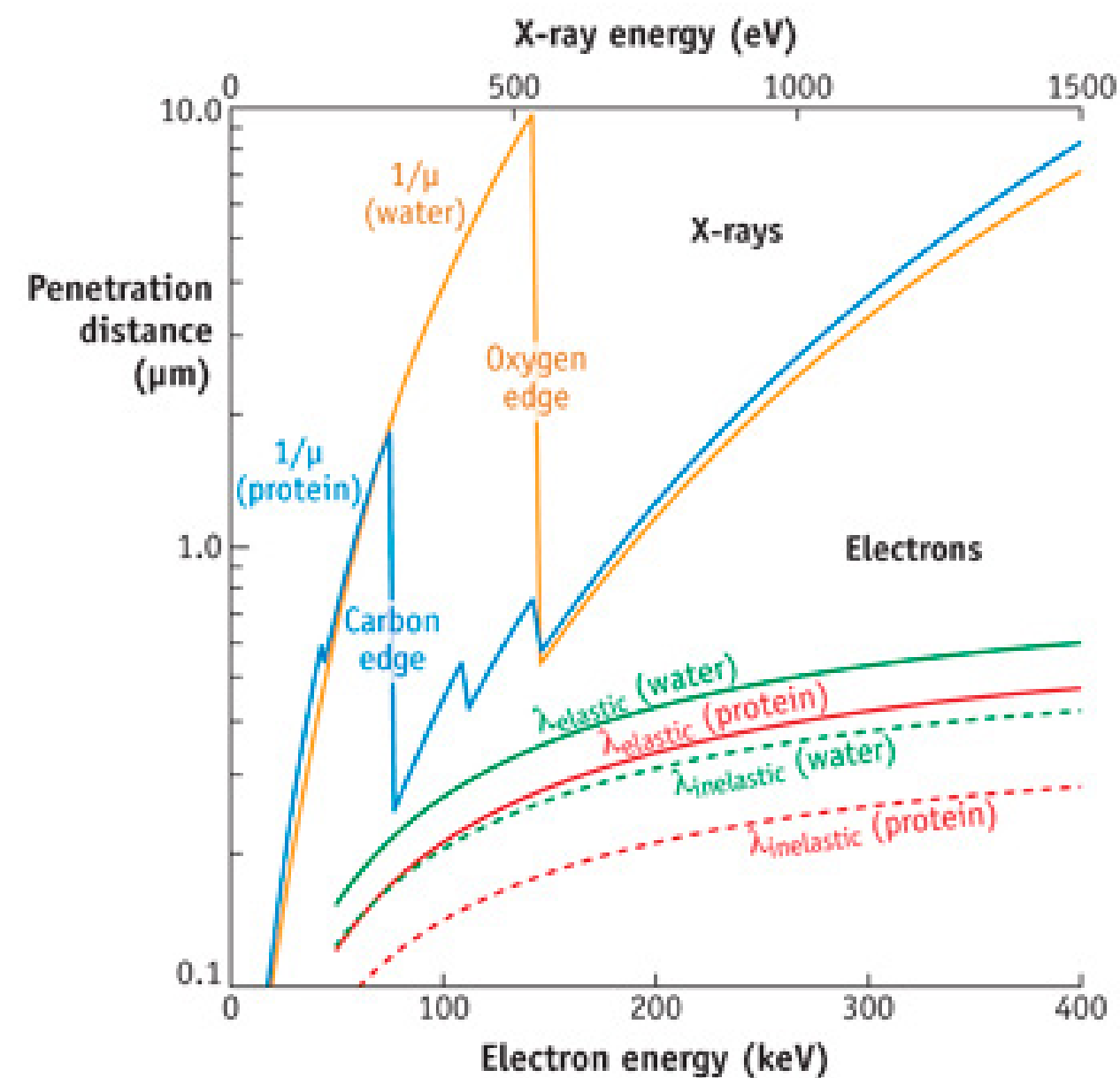


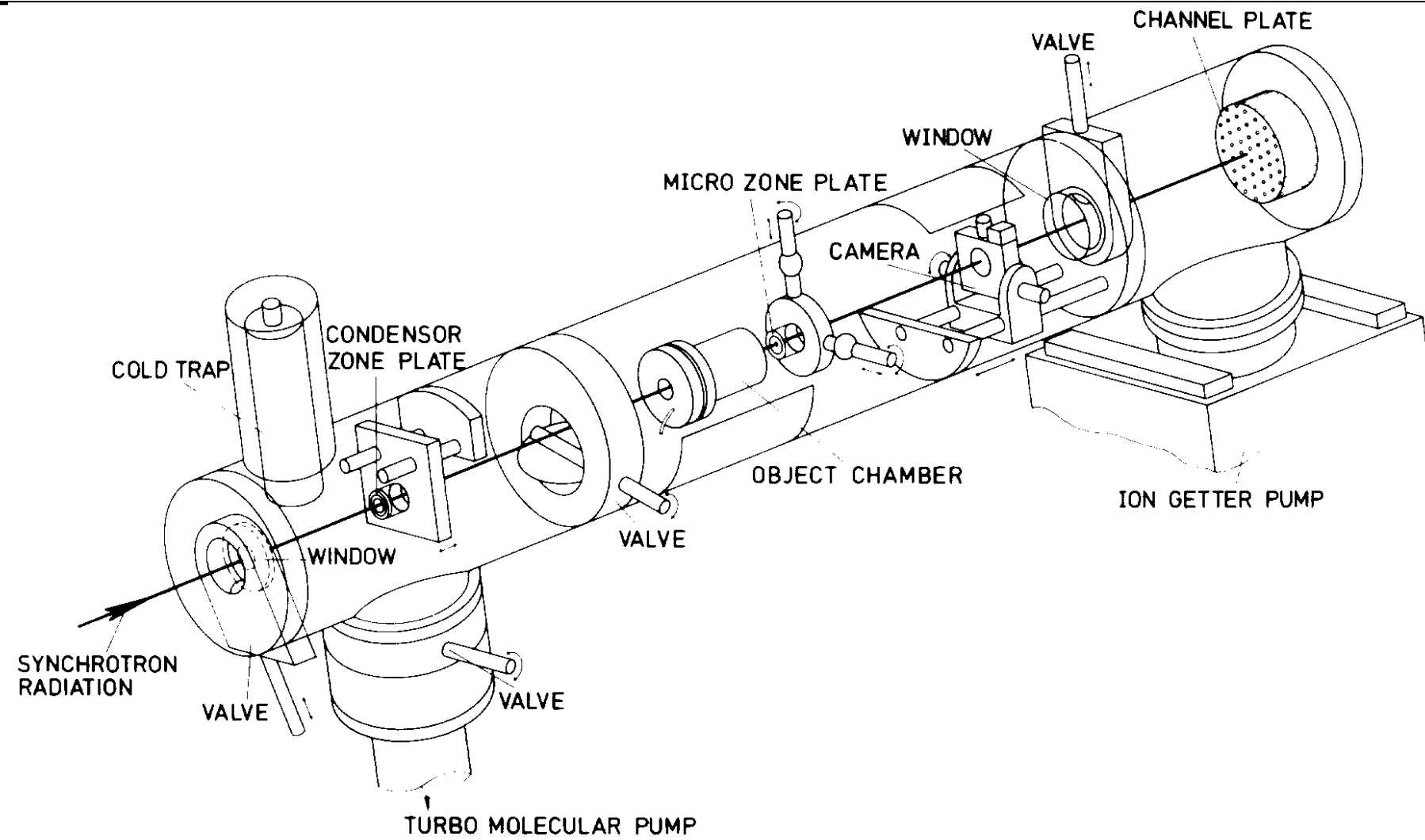
Fig. 6. Diatoms, imaged with 4.5 nm X-rays, X-ray magnification 500×, exposure time 60 s, storage ring current 150 mA.

Water Window

- ▶ high contrast between C (cell) and O (water)
- ▶ soft x-rays, good optics

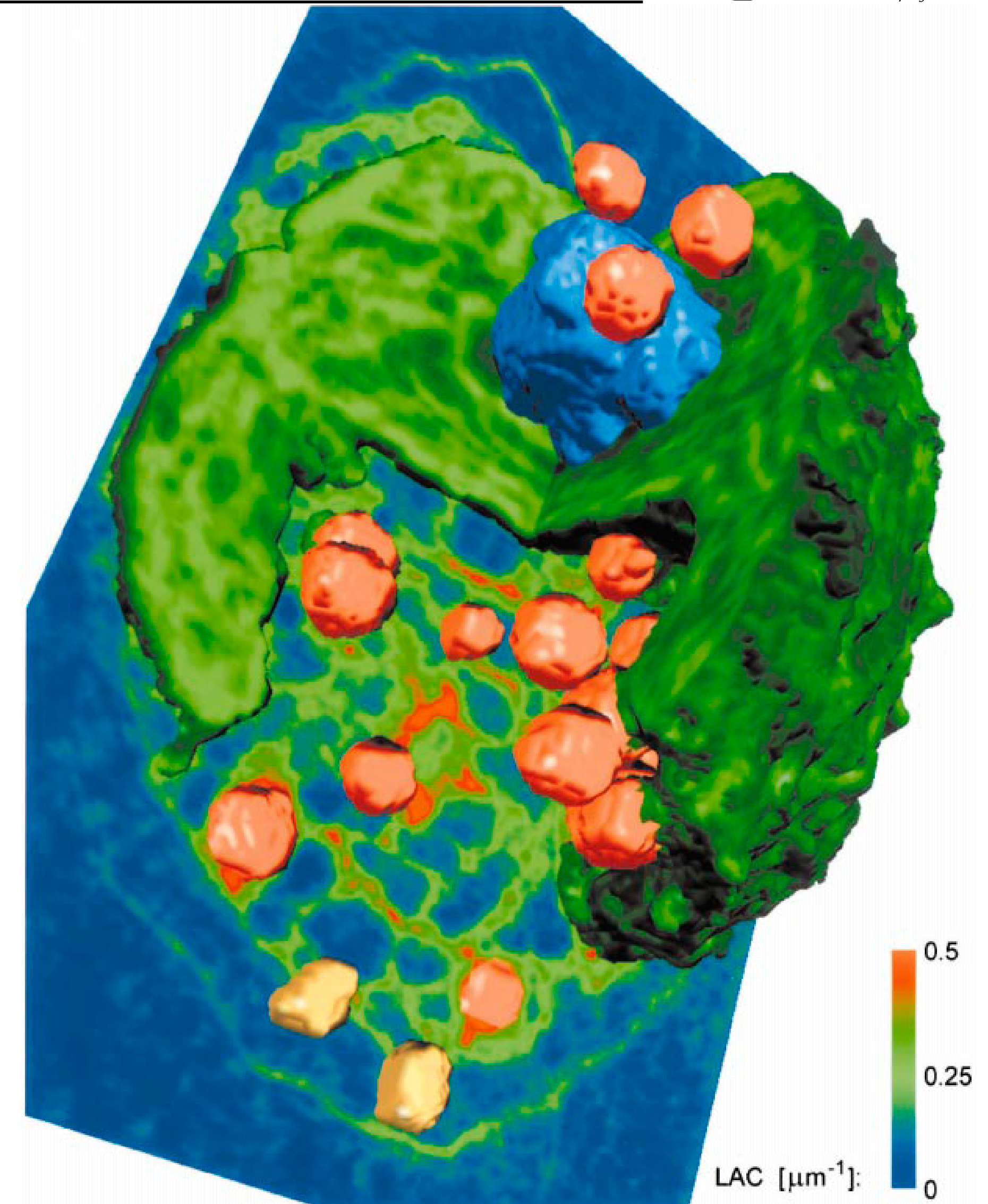
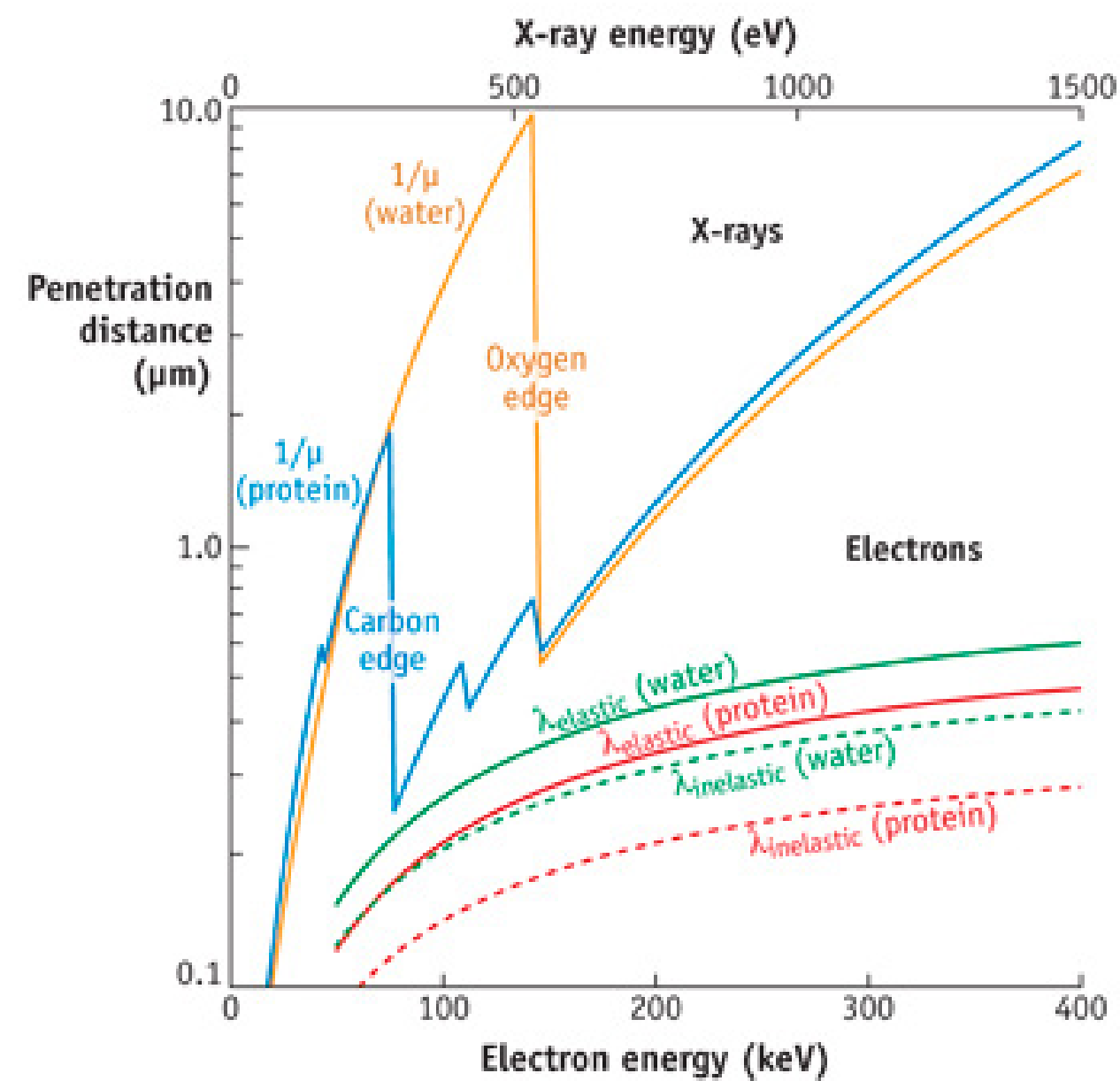


1980ies: Soft X-Ray Microscopy



Water Window

- ▶ high contrast between C (cell) and O (water)
- ▶ soft x-rays, good optics



Volume Diffraction - Multilayer Zone Plates

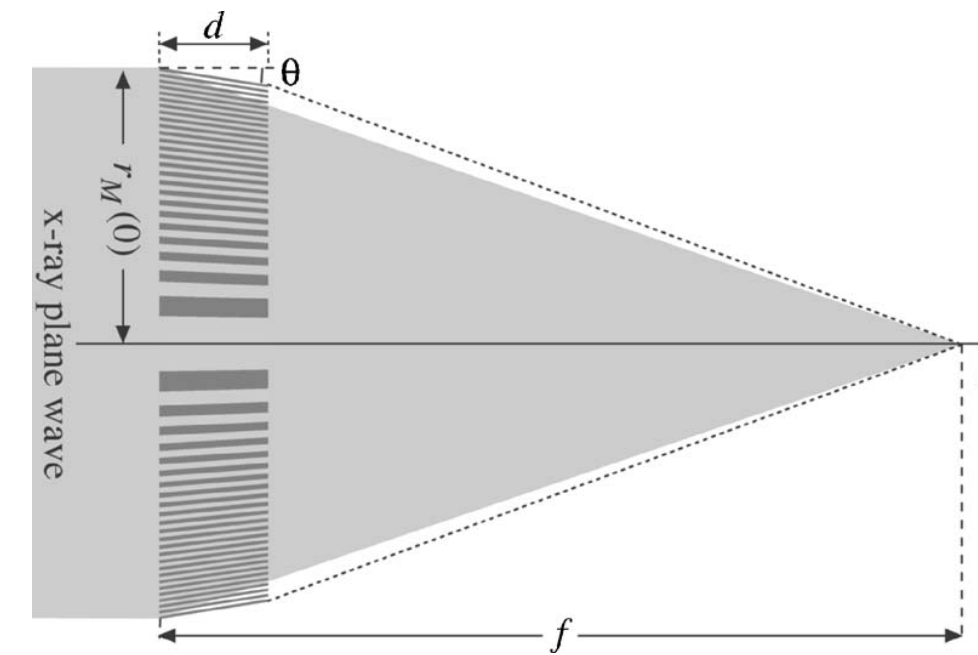


FIG. 1. Focusing geometry for a thick Fresnel zone plate with tilted zones.

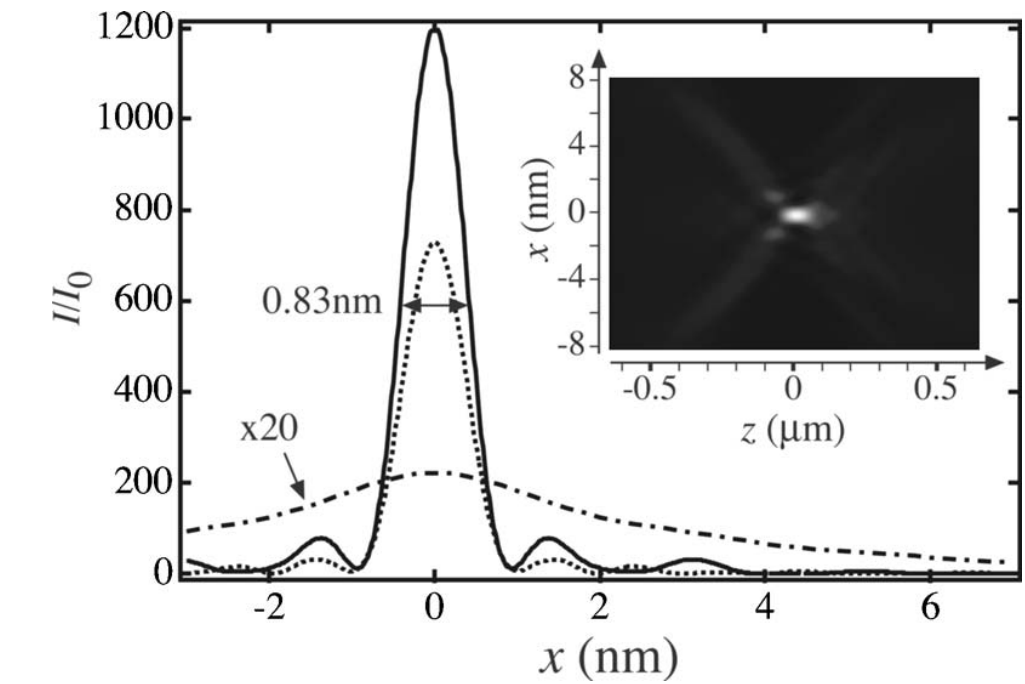


FIG. 2. First-order focus of a parabolically tilted zone plate (solid line), an equivalent ideal thin zone plate (dotted line), and a straight (not tilted) zone plate (dash-dotted line). The inset shows the beam intensity distribution around the focus along the optical axis for the parabolically tilted zone plate.

Efficiency for hard x-rays?

- ▶ vanishing absorption
no absorption-based zone plate
- ▶ small phase shift per μm
optically thick, "long" zone plates needed
- ▶ aspect ratio $\sim 1:1000$ and more
outermost zone width vs. optical thickness

Volume Diffraction - Multilayer Zone Plates

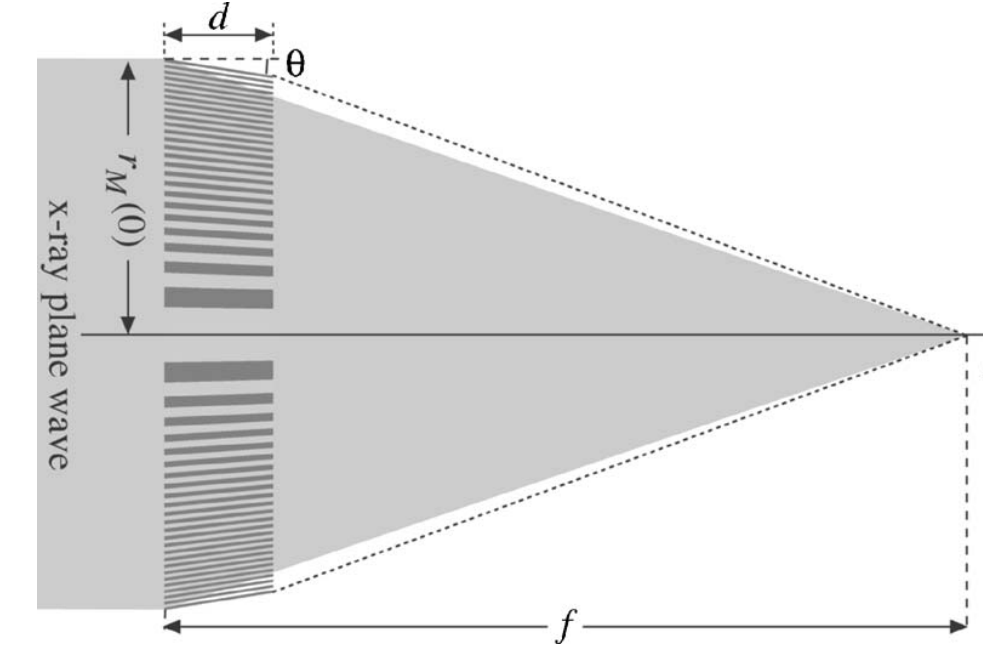
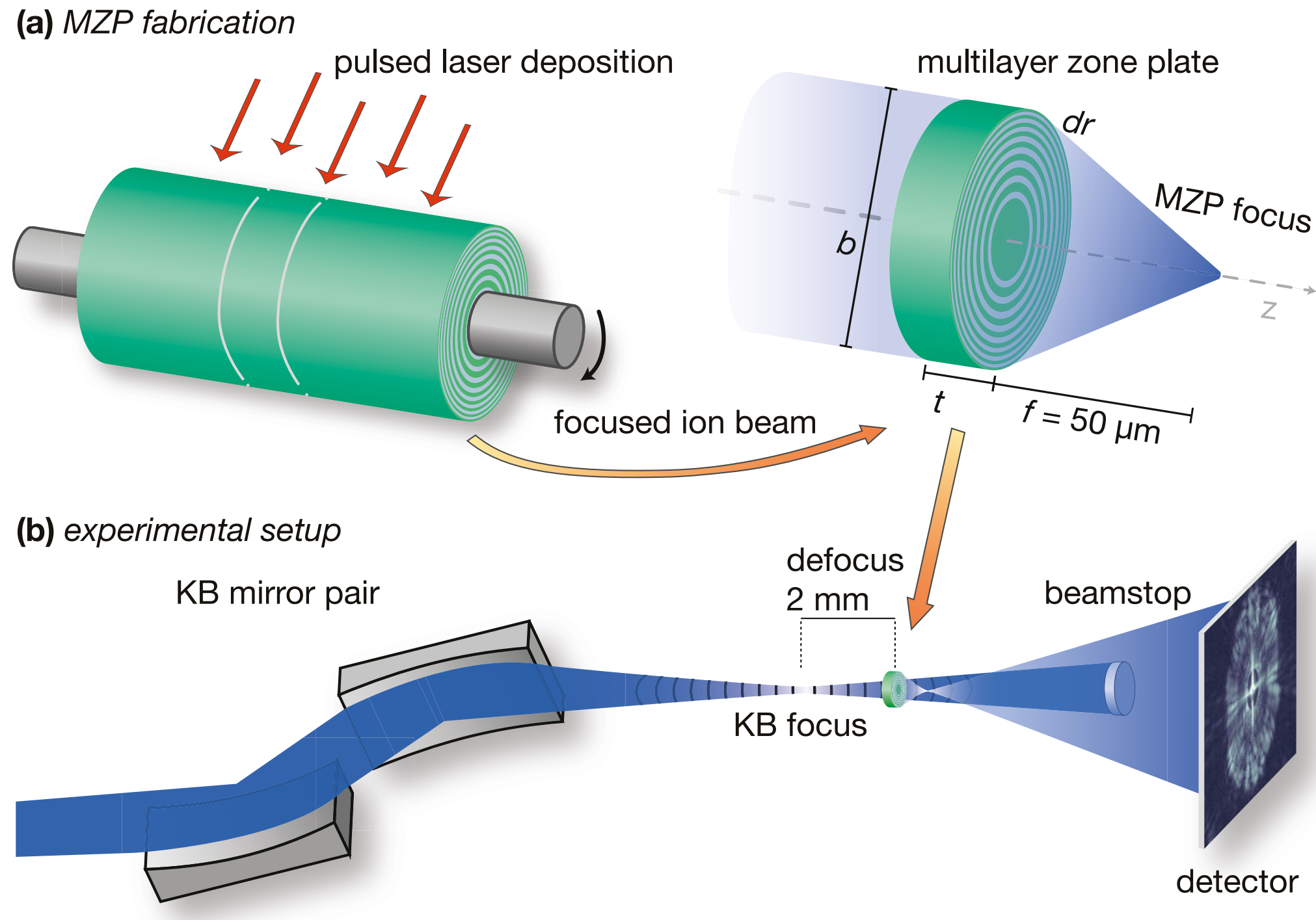


FIG. 1. Focusing geometry for a thick Fresnel zone plate with tilted zones.

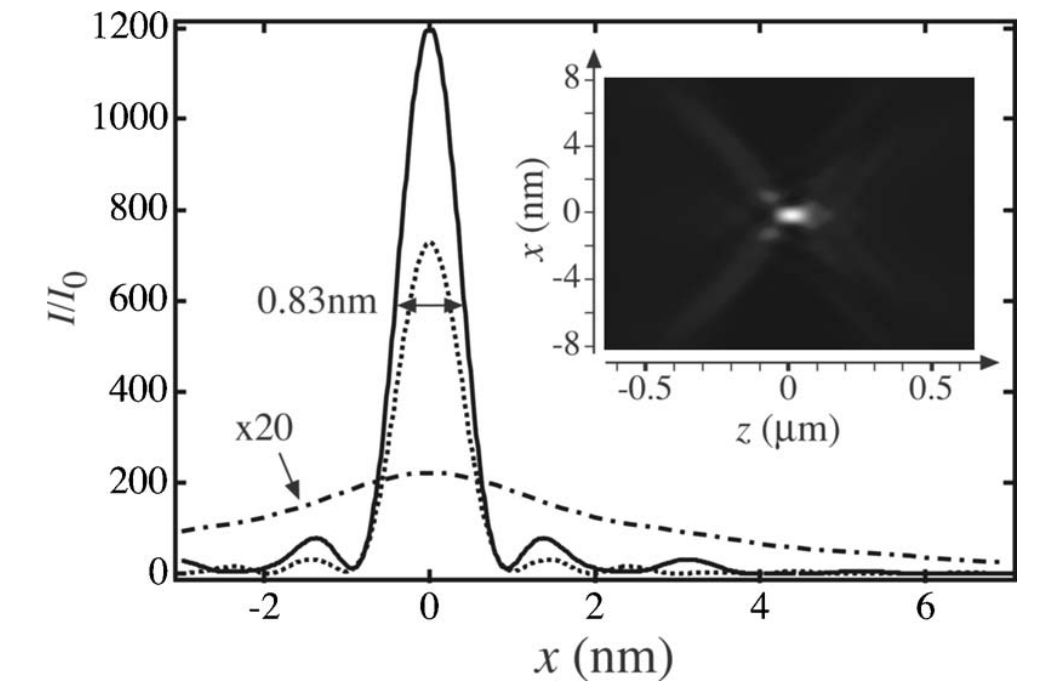
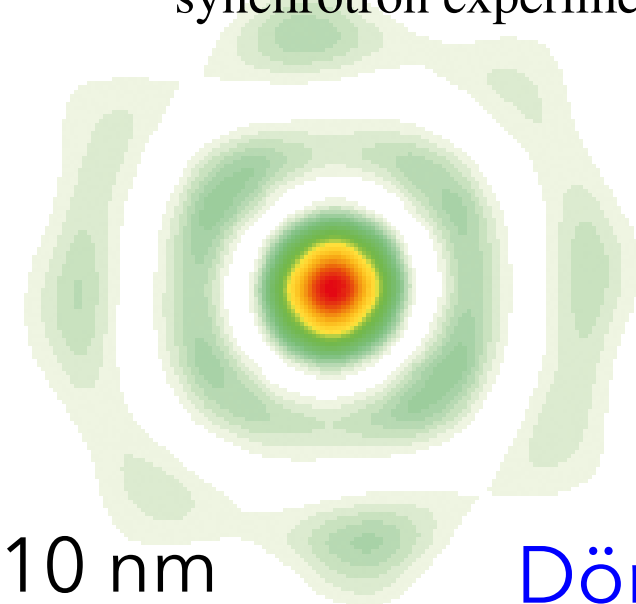


FIG. 2. First-order focus of a parabolically tilted zone plate (solid line), an equivalent ideal thin zone plate (dotted line), and a straight (not tilted) zone plate (dash-dotted line). The inset shows the beam intensity distribution around the focus along the optical axis for the parabolically tilted zone plate.

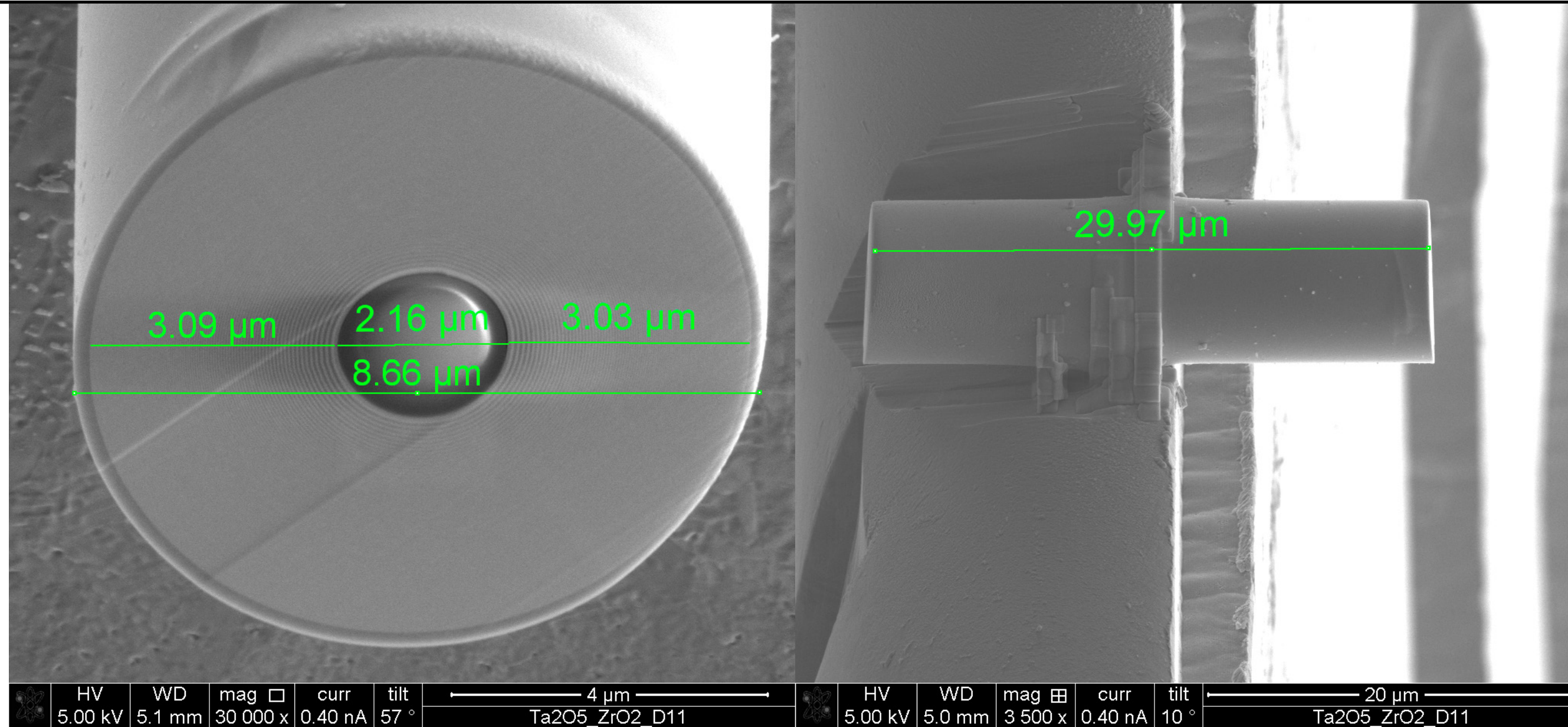
Efficiency for hard x-rays?

- ▶ vanishing absorption
no absorption-based zone plate
- ▶ small phase shift per μm
optically thick, "long" zone plates needed
- ▶ aspect ratio $\sim 1:1000$ and more
outermost zone width vs. optical thickness

Fig. 1. (a) Schematic fabrication process: Pulsed laser deposition of W and Si multilayer onto a rotating wire according to the Fresnel zone plate law. Focused ion beam fabrication of the MZP by cutting a slice out of the coated wire, placing it onto a sample holder and polishing it down to the optimal optical thickness of $0.7 \mu\text{m}$. (b) Experimental setup of the synchrotron experiment: The MZP is positioned 2 mm downstream of the KB focus.



Recent Progress



- ▶ Multilayer Zone Plate for high x-ray energies designed for 60 keV, tested also at 100 keV
 - ▶ outermost zones: 10 nm
 - ▶ optical thickness: 30 μm
- Eberl, Soltau, Osterhoff et al (work in progress)

Recent Progress

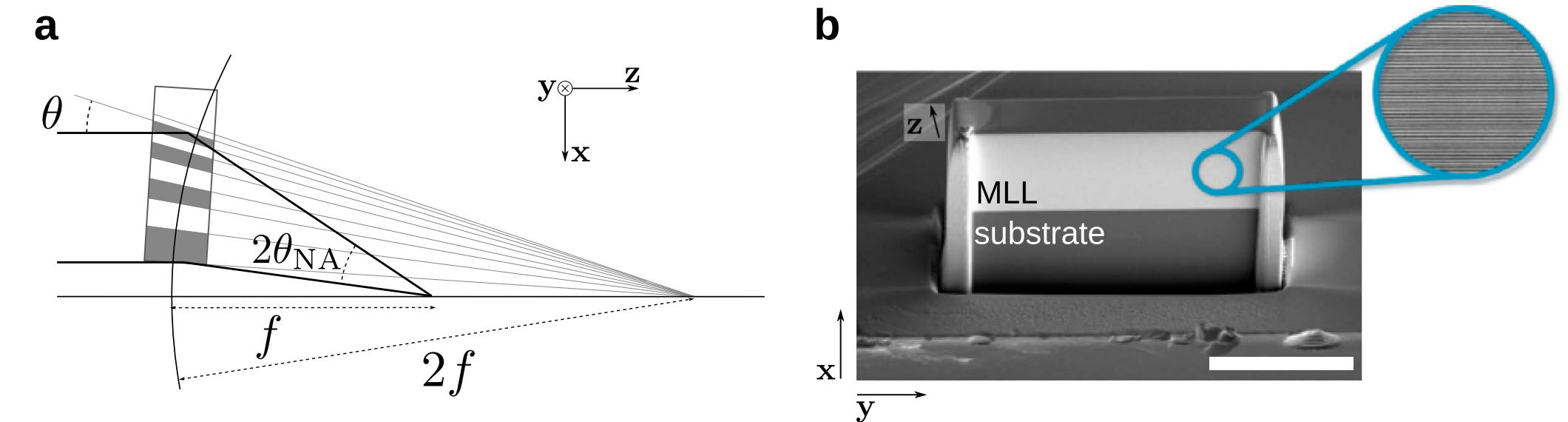
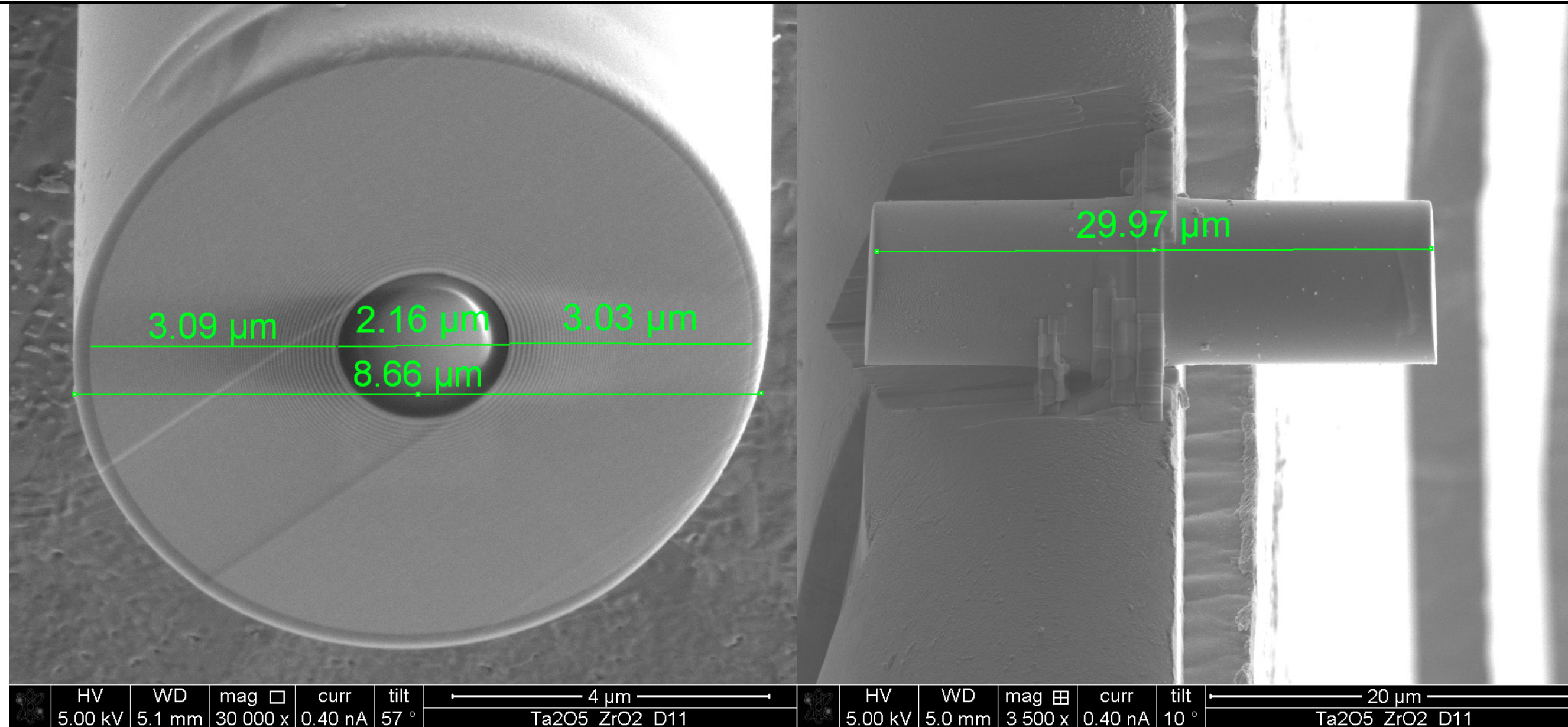
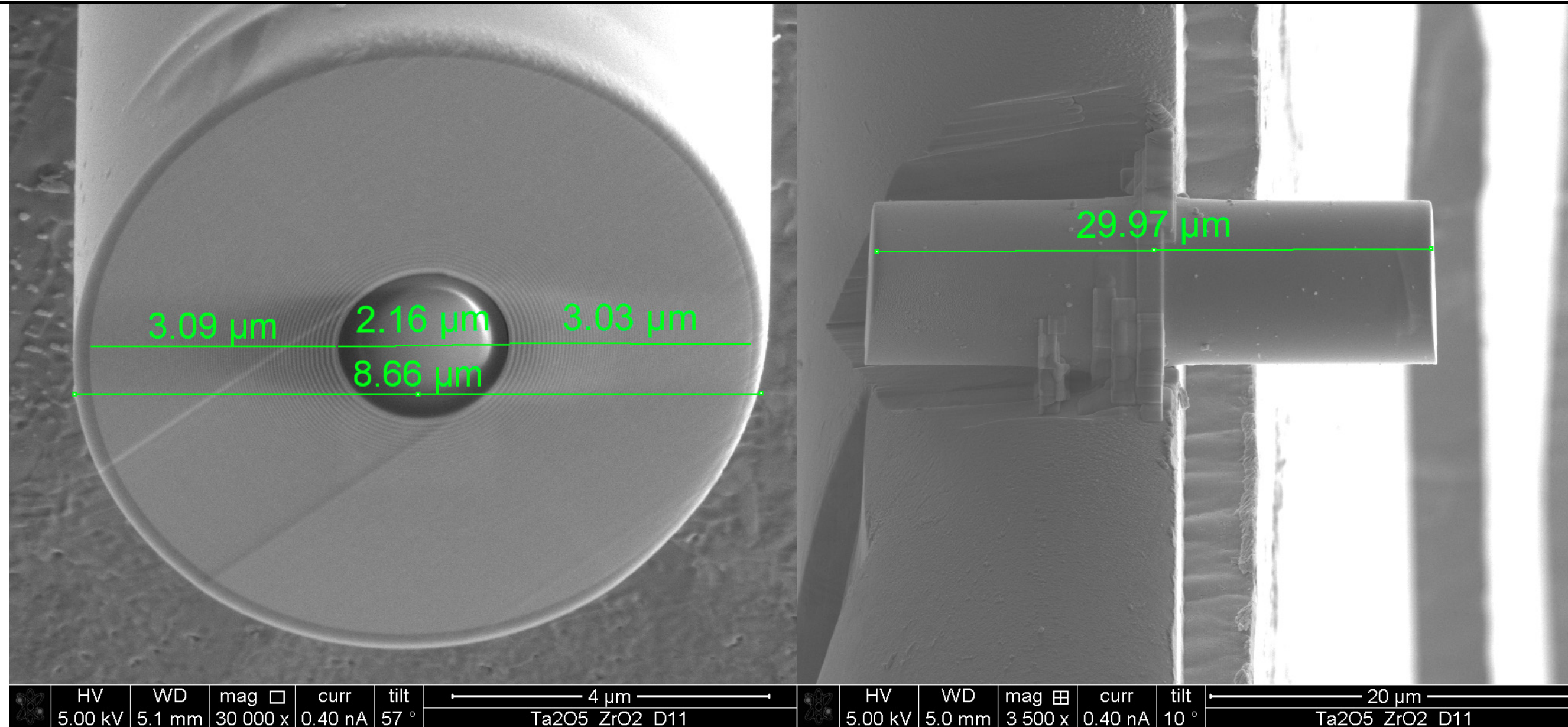


Figure 1. (a) A wedged multilayer Laue lens of focal length f is constructed from layers whose spacing follows the zone-plate condition. To achieve high efficiency the lens must be thick, in which case diffraction is a volume effect described by dynamical diffraction. In this case the layers should be tilted to locally obey Bragg's law, which places them normal to a circle of radius $2f$. (b) SEM image of the 2750-bilayer wedged MLL used in this study. The regions corresponding to the multilayered materials and the Si substrate are indicated. The white scale bar is $20\ \mu\text{m}$ and the inset shows a magnified TEM image of the layered materials.

- ▶ Multilayer Zone Plate for high x-ray energies designed for 60 keV, tested also at 100 keV
 - ▶ outermost zones: 10 nm
 - ▶ optical thickness: $30\ \mu\text{m}$
- Eberl, Soltau, Osterhoff et al (work in progress)

Recent Progress



- ▶ Multilayer Zone Plate for high x-ray energies designed for 60 keV, tested also at 100 keV
 - ▶ outermost zones: 10 nm
 - ▶ optical thickness: 30 μm
- Eberl, Soltau, Osterhoff et al (work in progress)

Bajt et al, Scientific Reports, 2015
 Gleber et al, Optics Express, 2014

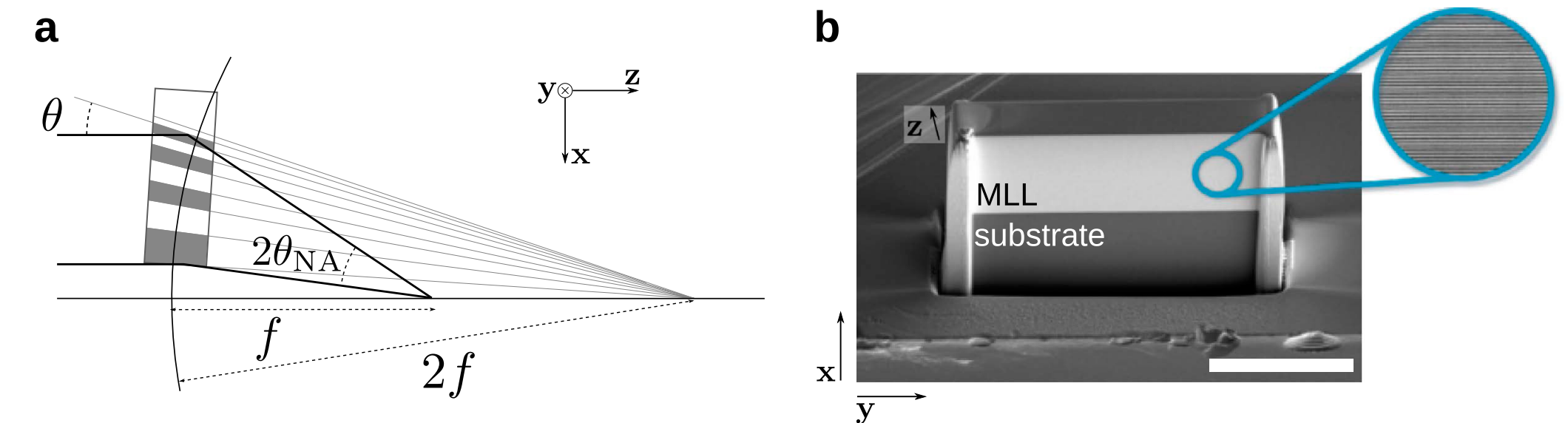


Figure 1. (a) A wedged multilayer Laue lens of focal length f is constructed from layers whose spacing follows the zone-plate condition. To achieve high efficiency the lens must be thick, in which case diffraction is a volume effect described by dynamical diffraction. In this case the layers should be tilted to locally obey Bragg's law, which places them normal to a circle of radius $2f$. (b) SEM image of the 2750-bilayer wedged MLL used in this study. The regions corresponding to the multilayered materials and the Si substrate are indicated. The white scale bar is 20 μm and the inset shows a magnified TEM image of the layered materials.

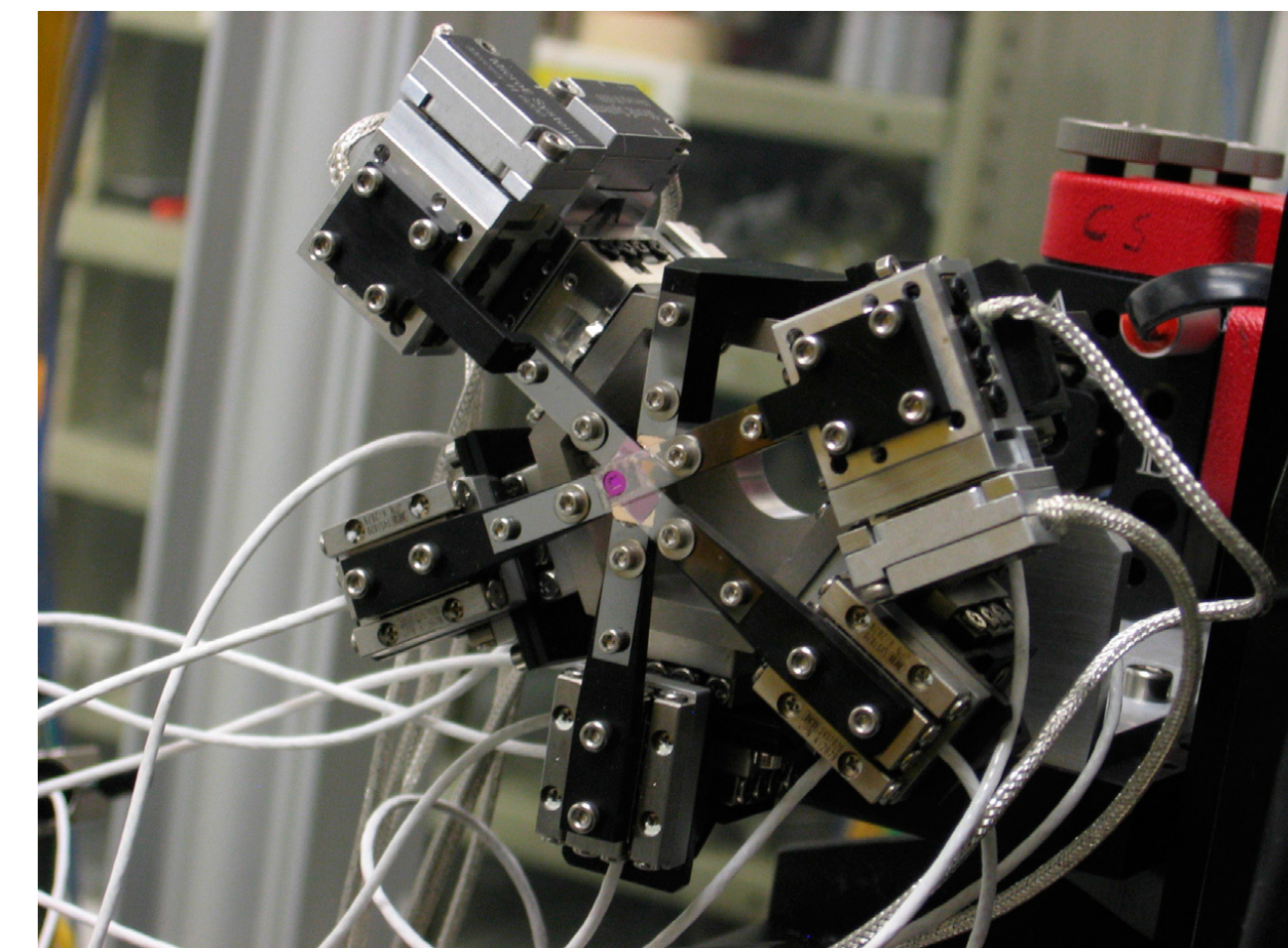


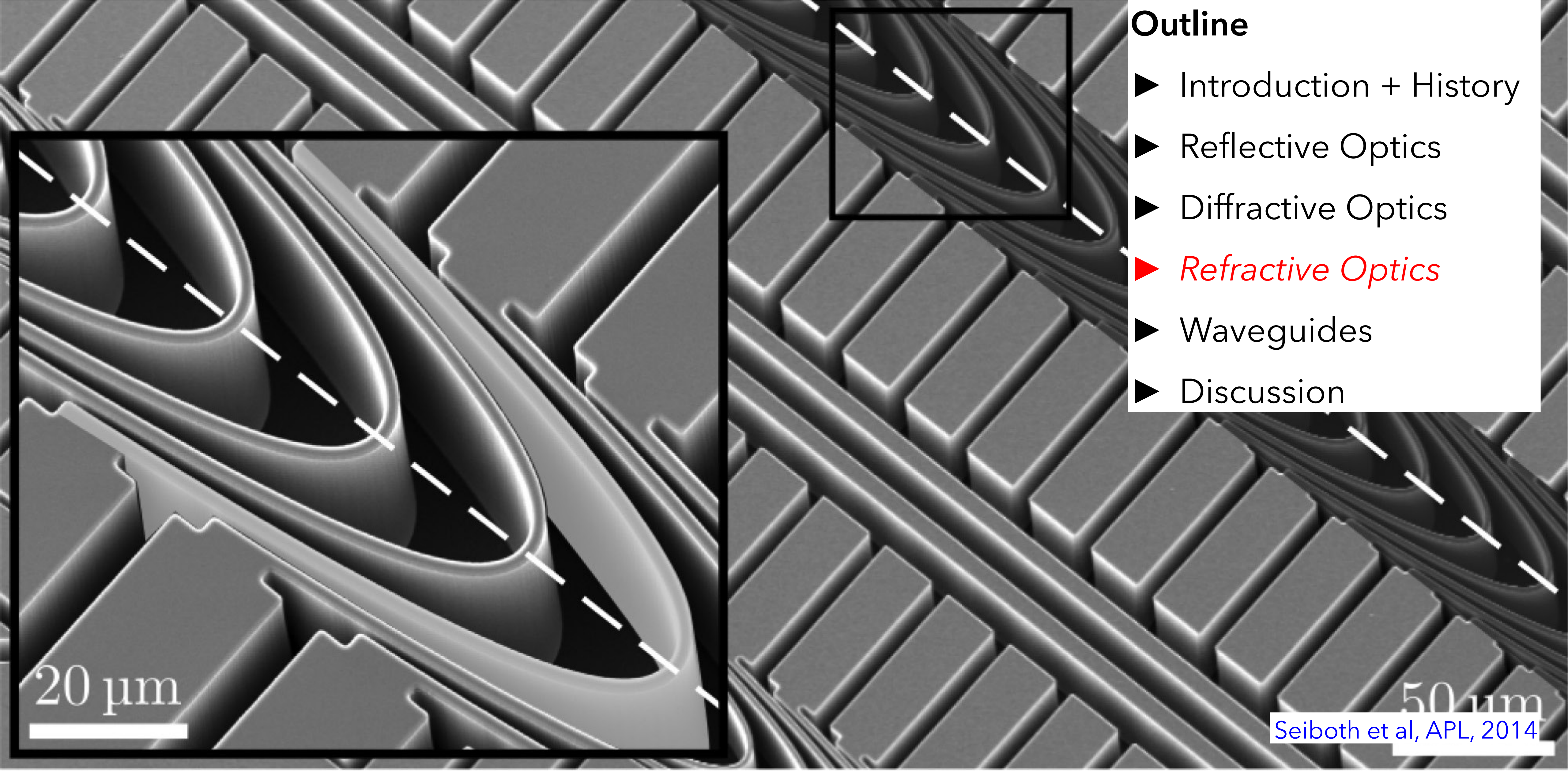
Fig. 4. Picture of the ANL Z2-37 precision alignment apparatus for intermediate-field stacking of up to six zone plates. In-house fabricated arrays of Fresnel zone plates are mounted on diamond holders. The apparatus is shown as integrated to the microprobe setup. [D. Shu, J. Liu, S. C. Gleber, J. Vila-Comamala, B. Lai, J. Maser, C. Roehrig, M. J. Wojcik, and S. Vogt, U. S. Patent application in progress for ANL-IN-13-092]

Compound Refractive Lenses



Outline

- ▶ Introduction + History
- ▶ Reflective Optics
- ▶ Diffractive Optics
- ▶ *Refractive Optics*
- ▶ Waveguides
- ▶ Discussion



20 μm

50 μm

Seiboth et al, APL, 2014

Principle and Geometry

“Let’s drill holes into Aluminium,
and use that as a lens” ...

really? yes!

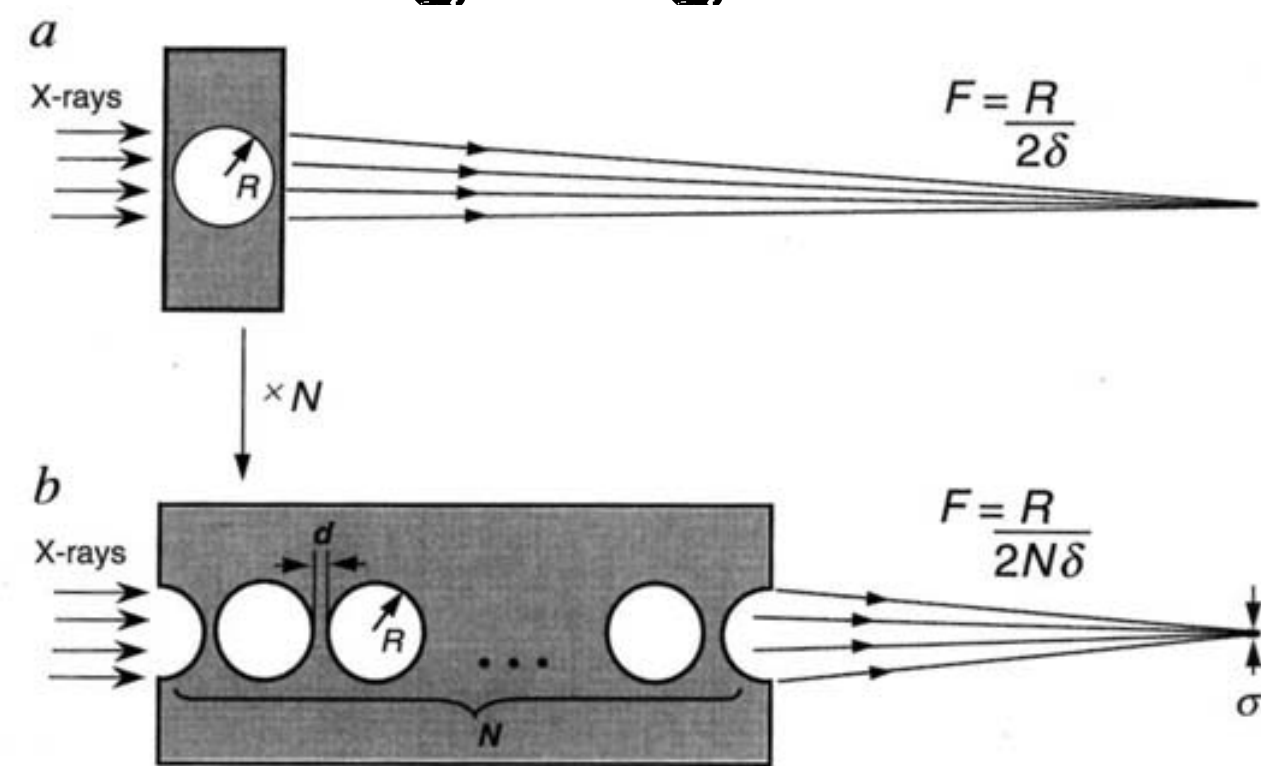
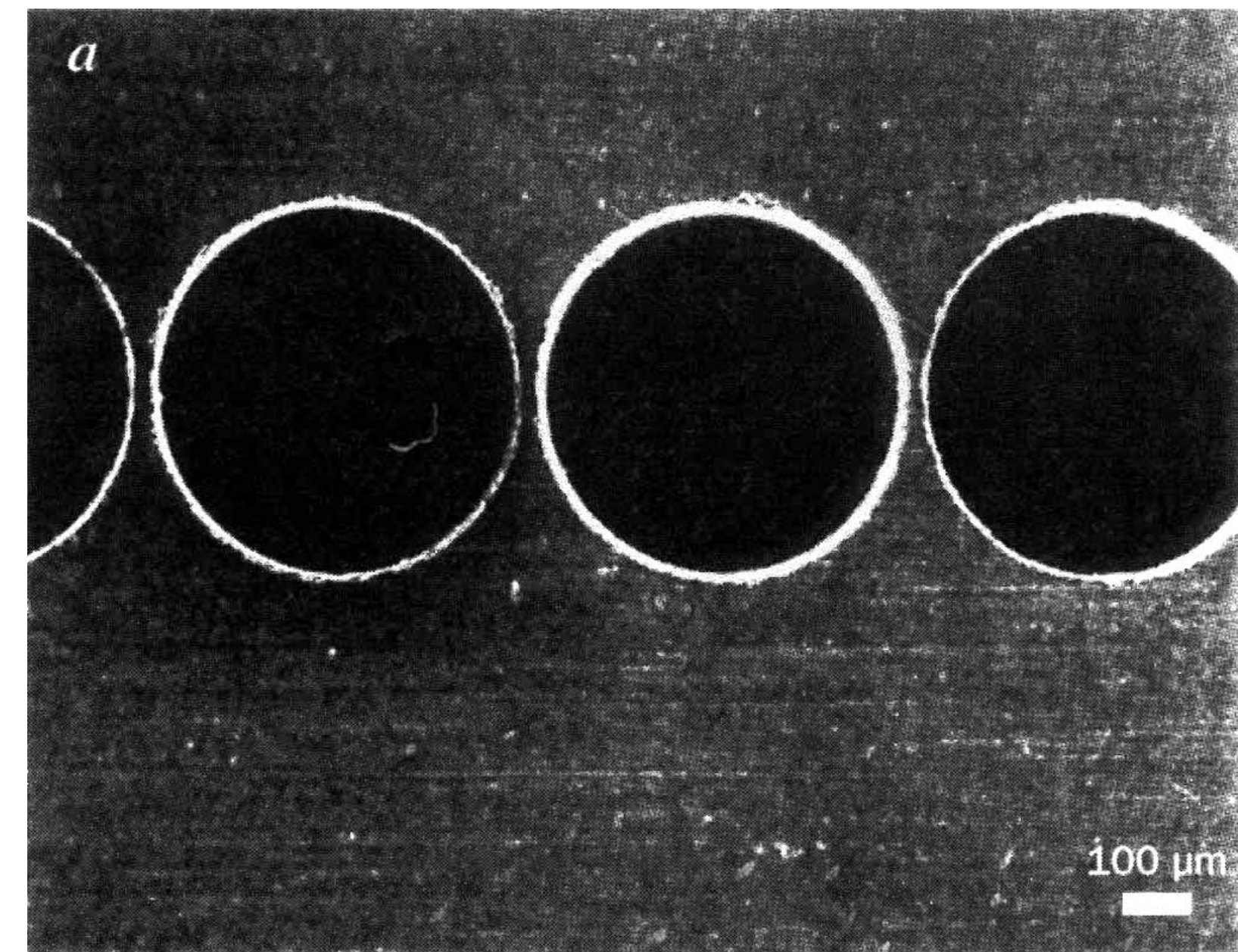


FIG. 1 Schematic diagram showing the principles of X-ray focusing by a compound refractive lens (CRL). As $(1 - \delta)$ is smaller than 1 (where δ is the decrement of the refractive index), a collecting lens for X-rays must have a concave shape. *a*, A simple concave lens fabricated as a cylindrical hole in the material. *b*, A CRL consisting of a number (N) of cylindrical holes placed close together in a row along the optical axis, focuses the X-rays at a distance that is N times shorter compared to a single lens. R is the radius of the holes, d is the spacing between the holes, λ is the X-ray wavelength, and F is the focal distance for a parallel input beam.

- ▶ focal length:
radius / $2 N \delta$
- ▶ with radius $\sim 200 \mu\text{m}$,
 $\delta \sim 10^{-5}$:
 $f \sim 10 \text{ m} / N$
- ▶ with ≥ 50 lenses,
 $f \leq 0.2 \text{ m}$ possible



First Results

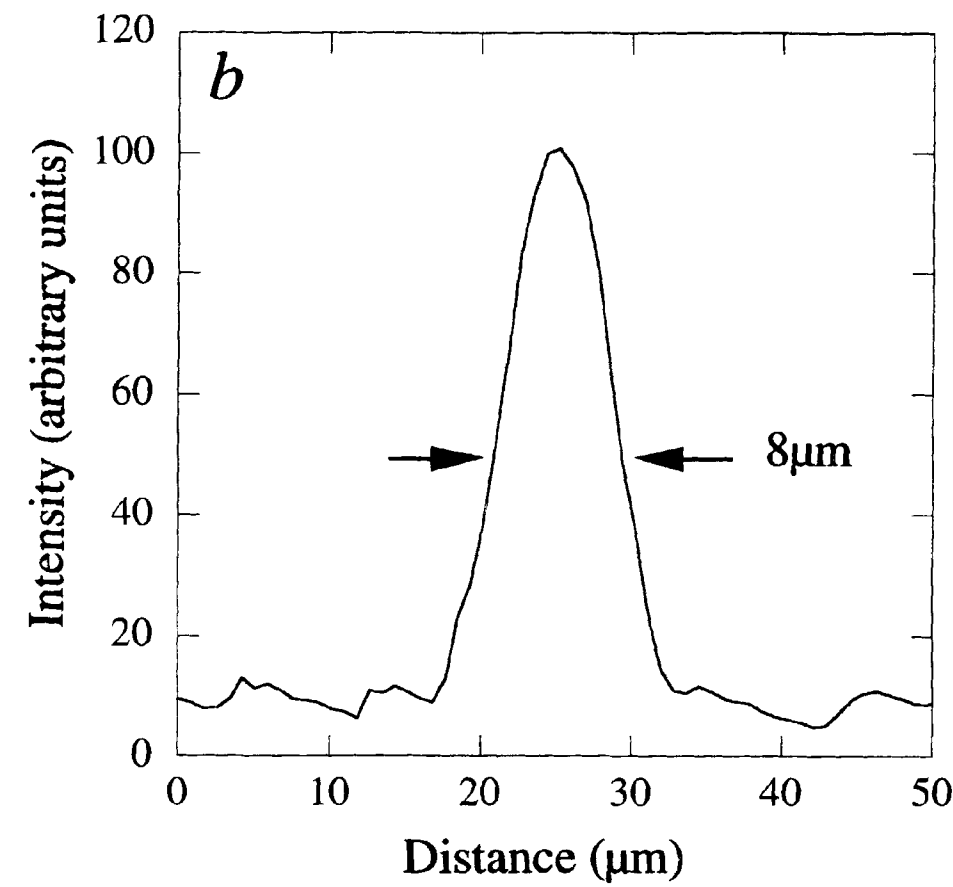


FIG. 3 a, Scanning electron microscope image of the tested compound refractive lens (CRL). 30 cylindrical holes of 300- μm radius were produced in an Al-Cu alloy (with 4 wt% Cu) plate using a computer-controlled drilling machine. Spacing d , the minimum alloy thickness between the holes, was $\sim 25 \mu\text{m}$. The length of the CRL was 19 mm. *b*, Measured profile of the focused X-ray beam taken at 1.8 m from the CRL. The width of the focal line is $\sim 8 \mu\text{m}$, which almost corresponds to the source size of 150 μm reduced by a demagnification factor $r_o/r_f = 20$.

- ▶ 30 holes
- ▶ 300 μm radius each
- ▶ X-ray energy: 14 keV
- ▶ focal length: 1.8 m
- ▶ line focus: 8 μm

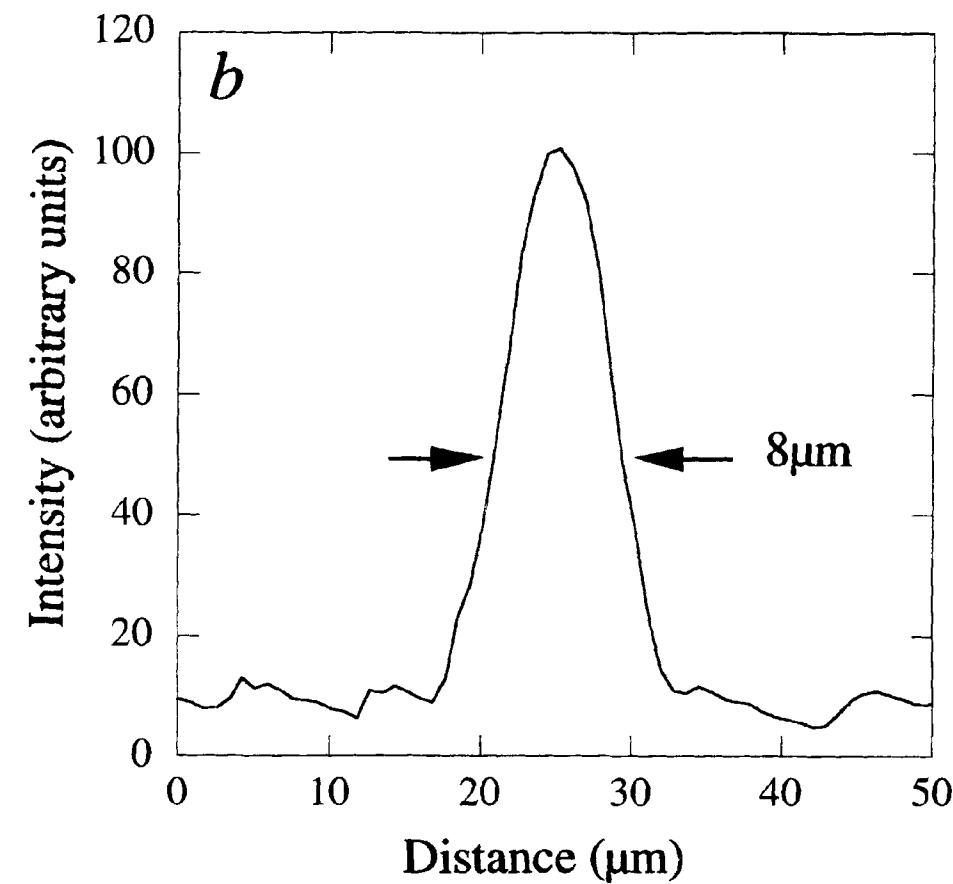


FIG. 3 a, Scanning electron microscope image of the tested compound refractive lens (CRL). 30 cylindrical holes of 300- μm radius were produced in an Al-Cu alloy (with 4 wt% Cu) plate using a computer-controlled drilling machine. Spacing d , the minimum alloy thickness between the holes, was $\sim 25 \mu\text{m}$. The length of the CRL was 19 mm. b, Measured profile of the focused X-ray beam taken at 1.8 m from the CRL. The width of the focal line is $\sim 8 \mu\text{m}$, which almost corresponds to the source size of 150 μm reduced by a demagnification factor $r_o/r_f = 20$.

- ▶ 30 holes
- ▶ 300 μm radius each
- ▶ X-ray energy: 14 keV
- ▶ focal length: 1.8 m
- ▶ line focus: 8 μm

questions for following decades:

- ▶ better fabrication?
- ▶ best material?
- ▶ nanometre possible?
- ▶ flexibility?

If no-one has done it, maybe it's not possible.
If no-one has tried yet, maybe it is possible.

Adiabatic Lenses

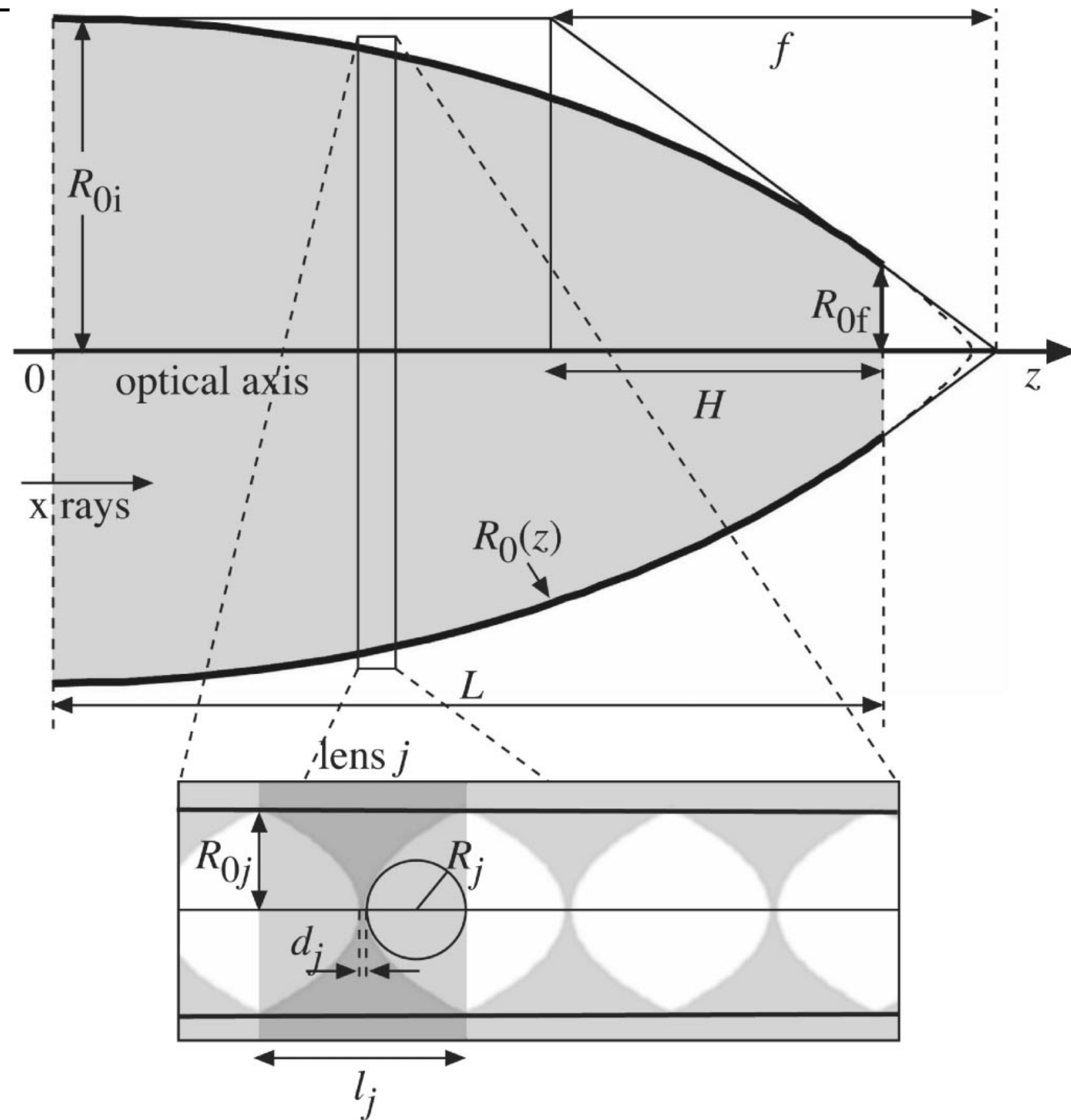


FIG. 1. Adiabatically focusing x-ray lens. The lens is composed of a large number of individual (aspherical) refractive lenses, whose aperture is matched to the converging beam size, increasing the refractive power per unit length along the lens.

Adiabatic Lenses

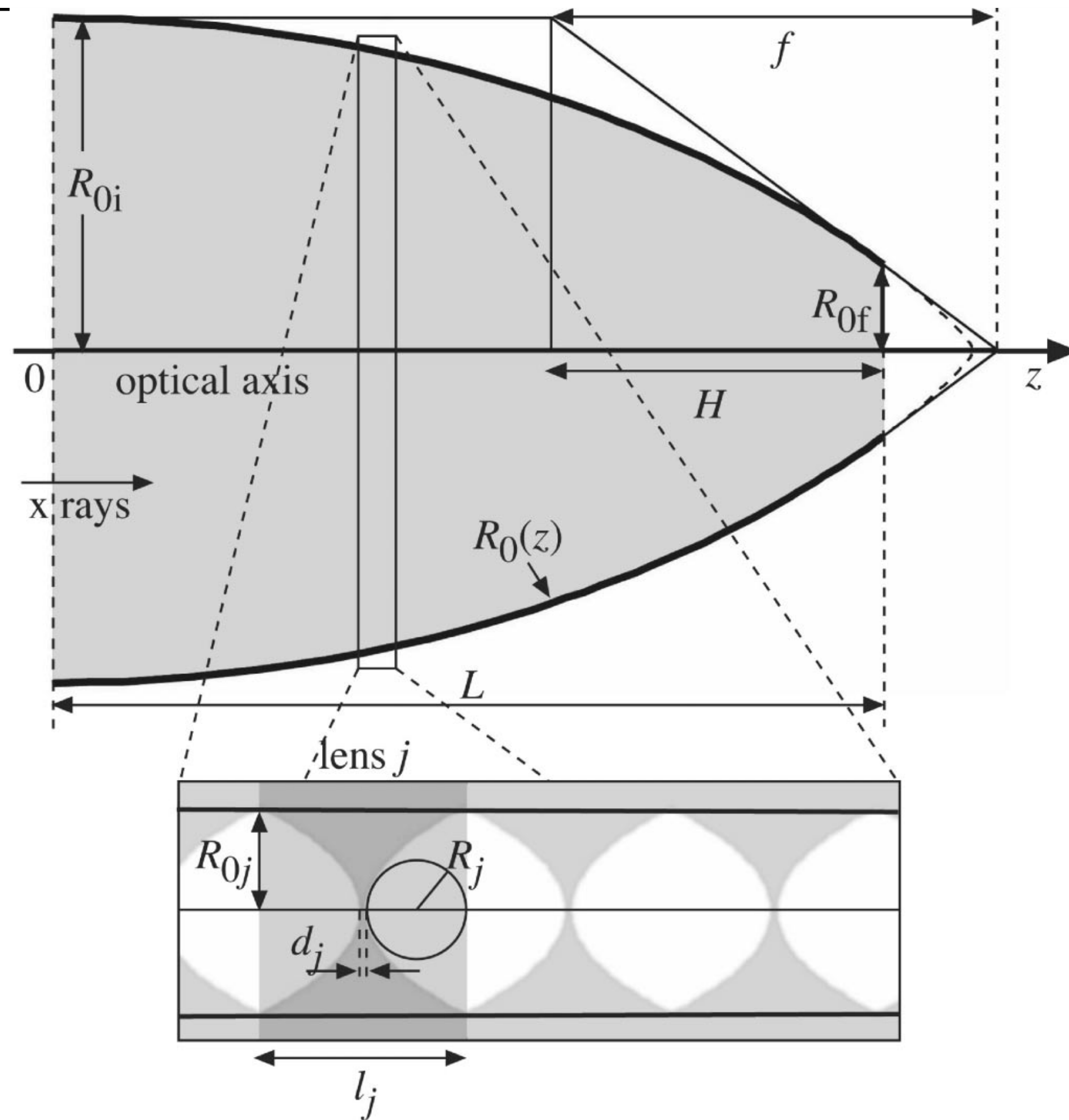


FIG. 1. Adiabatically focusing x-ray lens. The lens is composed of a large number of individual (aspherical) refractive lenses, whose aperture is matched to the converging beam size, increasing the refractive power per unit length along the lens.

where $\mu' = (1 - d_j/l_j)\mu$ and μ is the linear attenuation coefficient. Using Eqs. (4) and (5), the numerical aperture $NA = D_{\text{eff}}/(2f)$ for a distant source is

$$NA = \sqrt{\delta'} \sqrt{4 \frac{a}{R_{0i}} \left[1 - \exp\left(-\frac{R_{0i}}{a}\right) \right] \log \frac{R_{0i}}{R_{0f}}}, \quad (6)$$

where $a = \frac{4\sqrt{\delta'}}{\sqrt{\pi\mu}}$ is a material specific characteristic aperture shown in Fig. 2 for different materials. A larger a yields a larger numerical aperture, favoring materials with low atomic number Z . In addition, the numerical aperture is proportional to $\sqrt{\delta'}$, favoring lens materials with large mass density ρ . The largest numerical apertures are therefore expected for high density low Z materials, such as diamond.

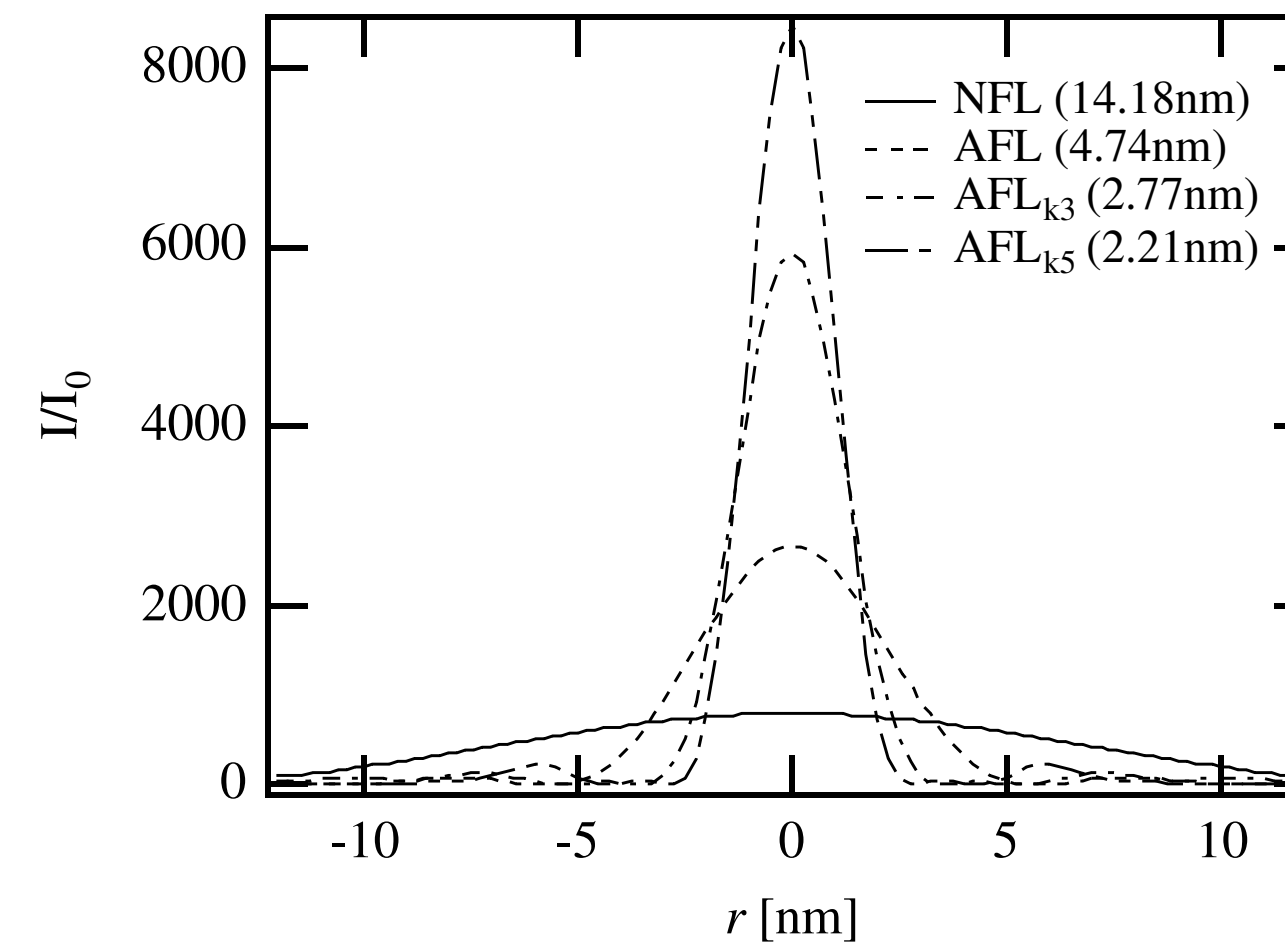


FIG. 5. Lateral beam profiles for a nanofocusing lens, an adiabatically focusing lens, and two kinoform AFLs with three and five segments, respectively.

Adiabatic Lenses

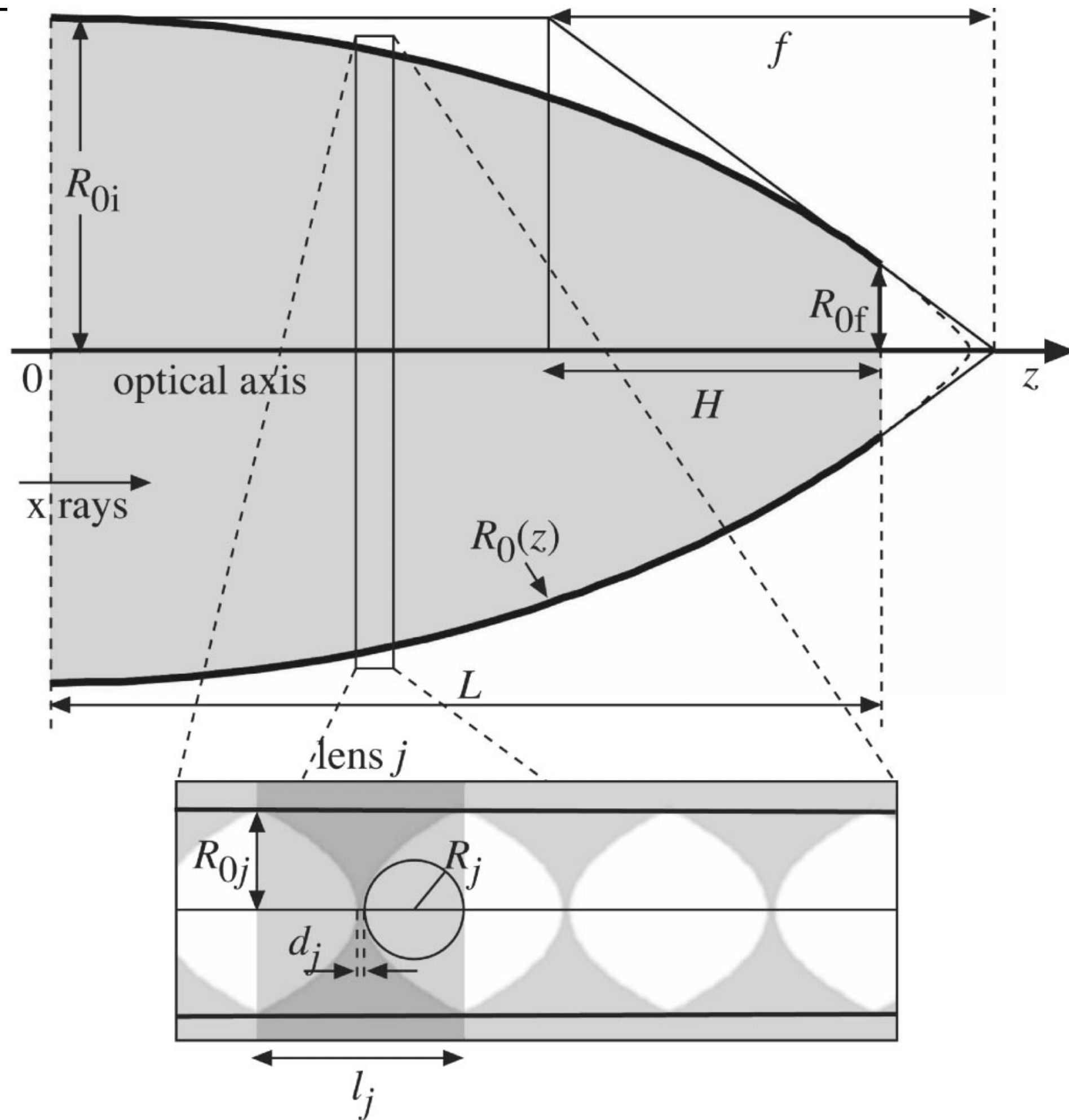


FIG. 1. Adiabatically focusing x-ray lens. The lens is composed of a large number of individual (aspherical) refractive lenses, whose aperture is matched to the converging beam size, increasing the refractive power per unit length along the lens.

where $\mu' = (1 - d_j/l_j)\mu$ and μ is the linear attenuation coefficient. Using Eqs. (4) and (5), the numerical aperture $NA = D_{\text{eff}}/(2f)$ for a distant source is

$$NA = \sqrt{\delta'} \sqrt{4 \frac{a}{R_{0i}} \left[1 - \exp\left(-\frac{R_{0i}}{a}\right) \right] \log \frac{R_{0i}}{R_{0f}}}, \quad (6)$$

where $a = \frac{4\sqrt{\delta'}}{\sqrt{\pi\mu}}$ is a material specific characteristic aperture shown in Fig. 2 for different materials. A larger a yields a larger numerical aperture, favoring materials with low atomic number Z . In addition, the numerical aperture is proportional to $\sqrt{\delta'}$, favoring lens materials with large mass density ρ . The largest numerical apertures are therefore expected for high density low Z materials, such as diamond.

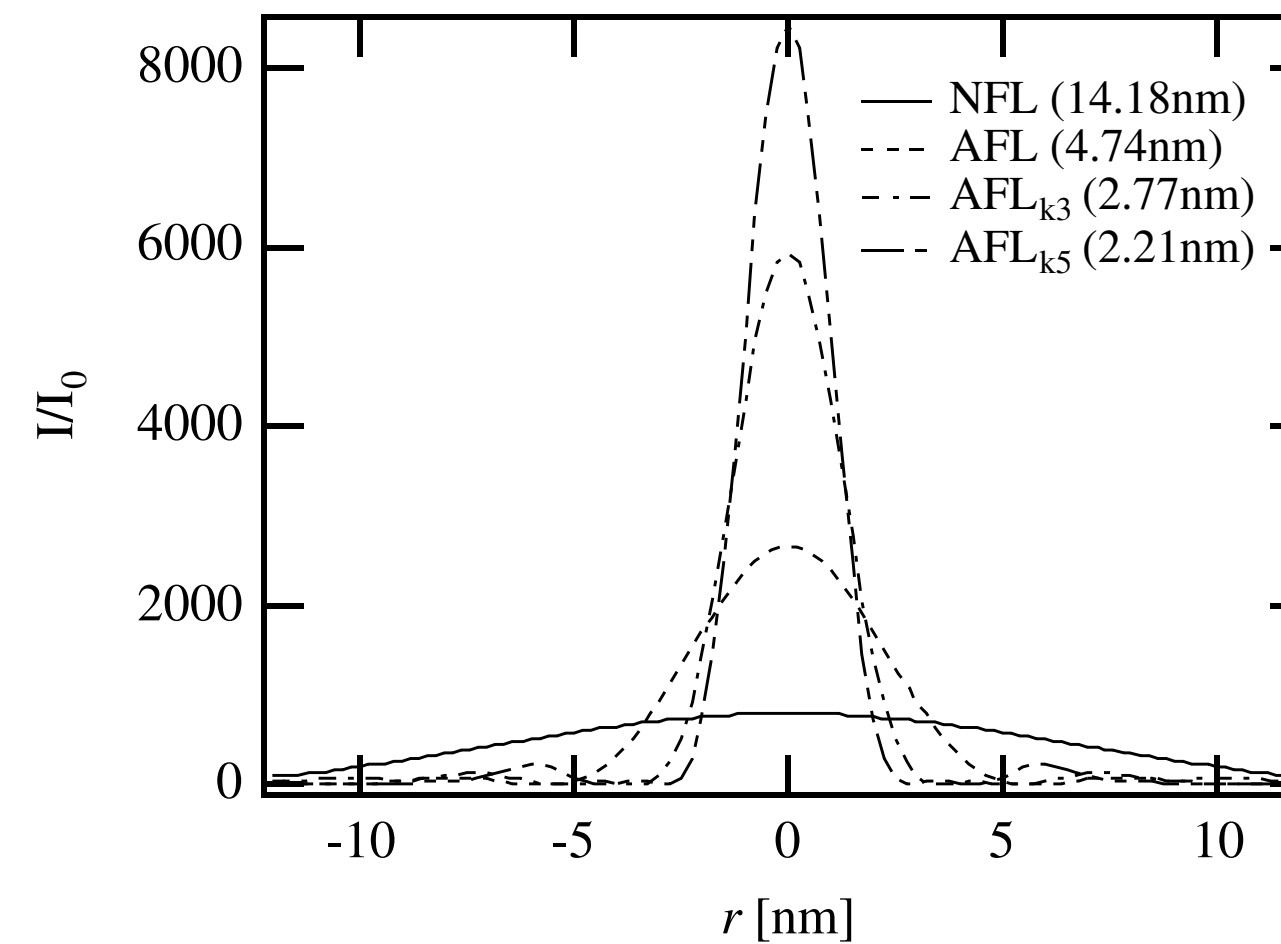
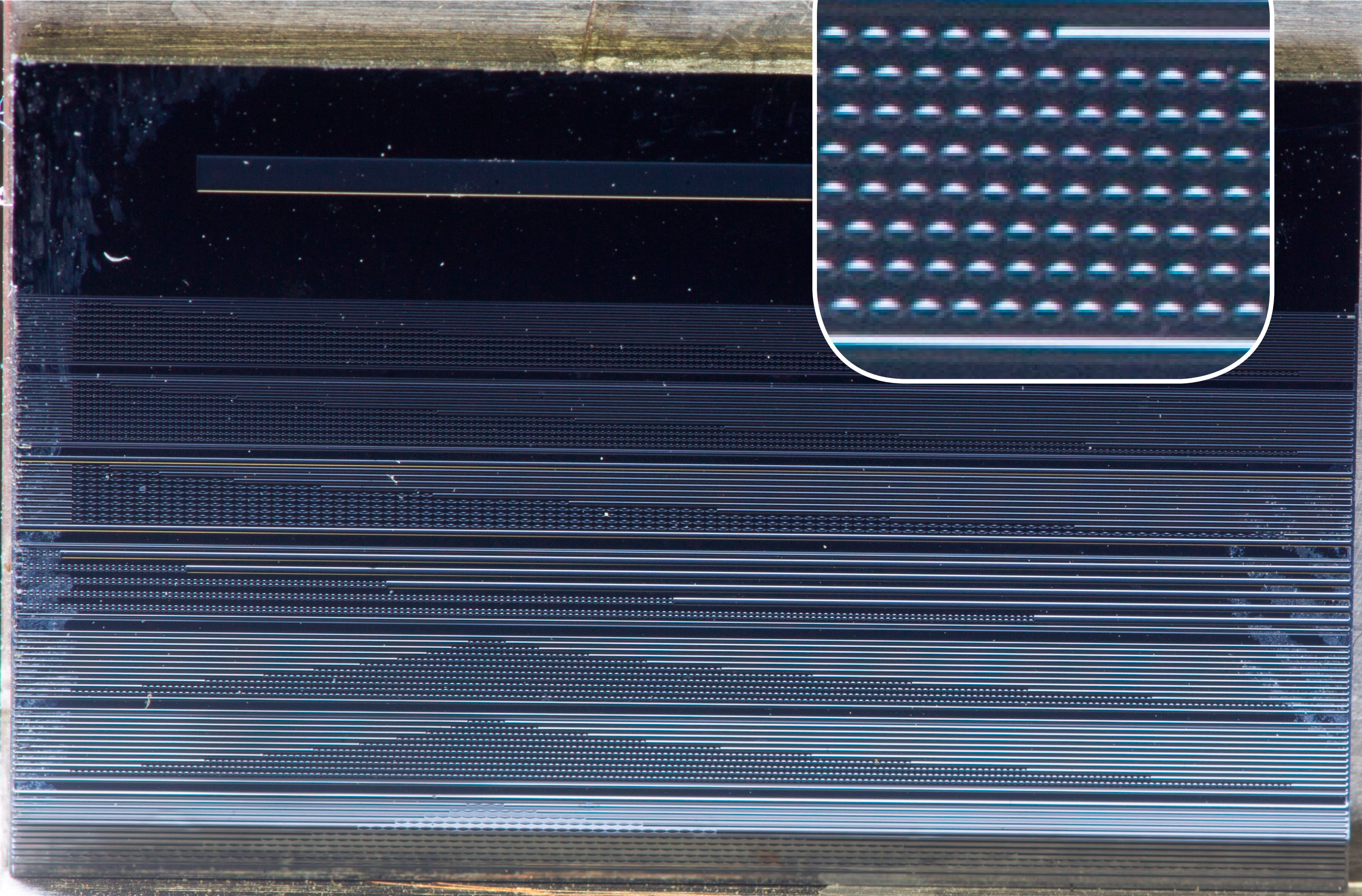
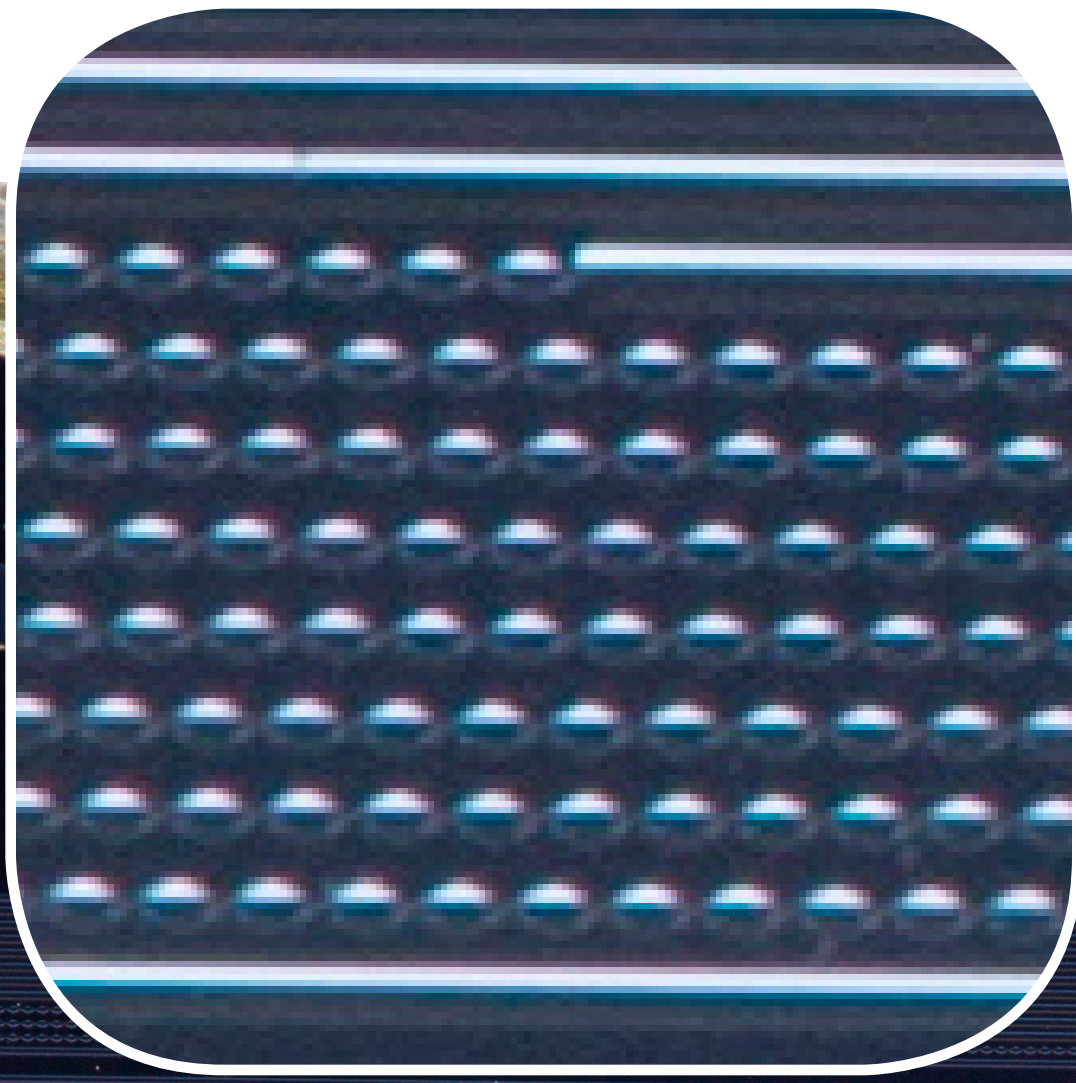


FIG. 5. Lateral beam profiles for a nanofocusing lens, an adiabatically focusing lens, and two kinoform AFLs with three and five segments, respectively.

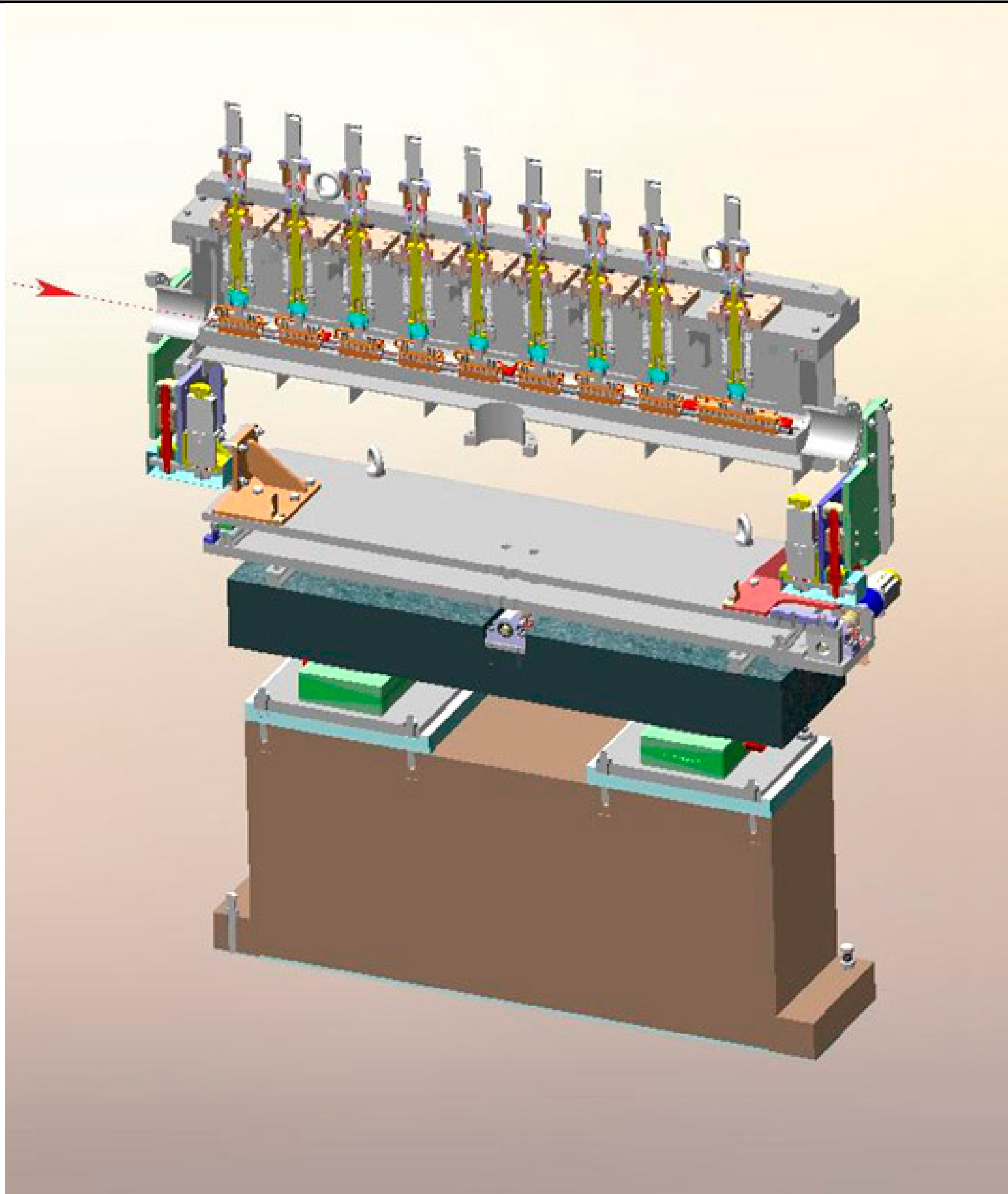
- ▶ absorption limit, use low-Z (Be, Al, C)
- ▶ need phase shift, use high mass density e.g., diamond
- ▶ adapt lens diameter to local beam size
- ▶ aspherical holes to improve quality
- ▶ sub-10 nm possible

CRL Chips

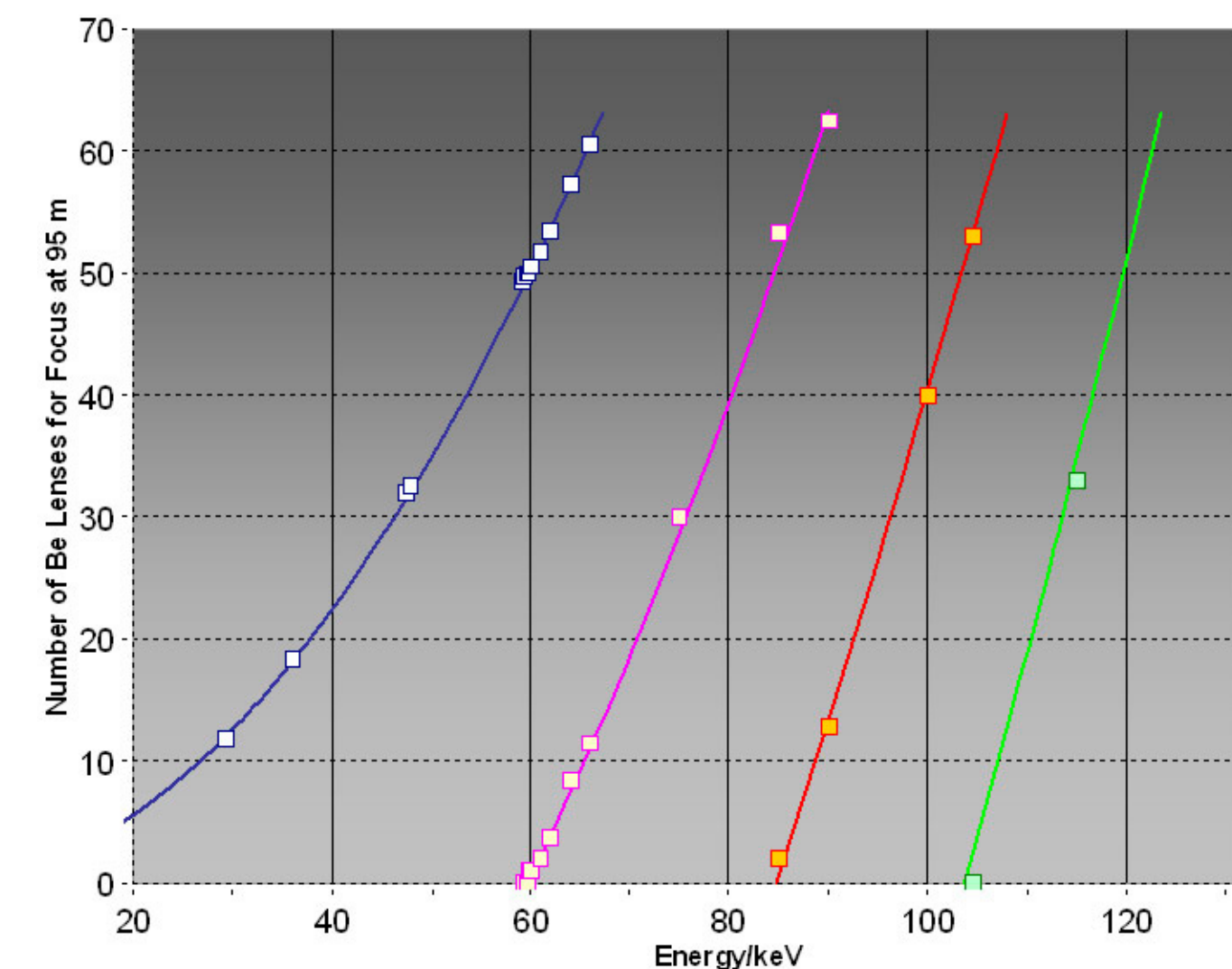


F
10
r

Transfocators



- ▶ zoom capabilities:
cartridges of 2^n lenses
- ▶ choose combination based on
x-ray energy - focal length - beam size
- ▶ developed at ESRF, used at many synchrotrons
- ▶ especially at higher energies, 20 ... 100 ... keV
spot size in micro metre range



Recent Progress

Focusing hard x rays beyond the critical angle of total reflection by adiabatically focusing lenses @ 20 keV

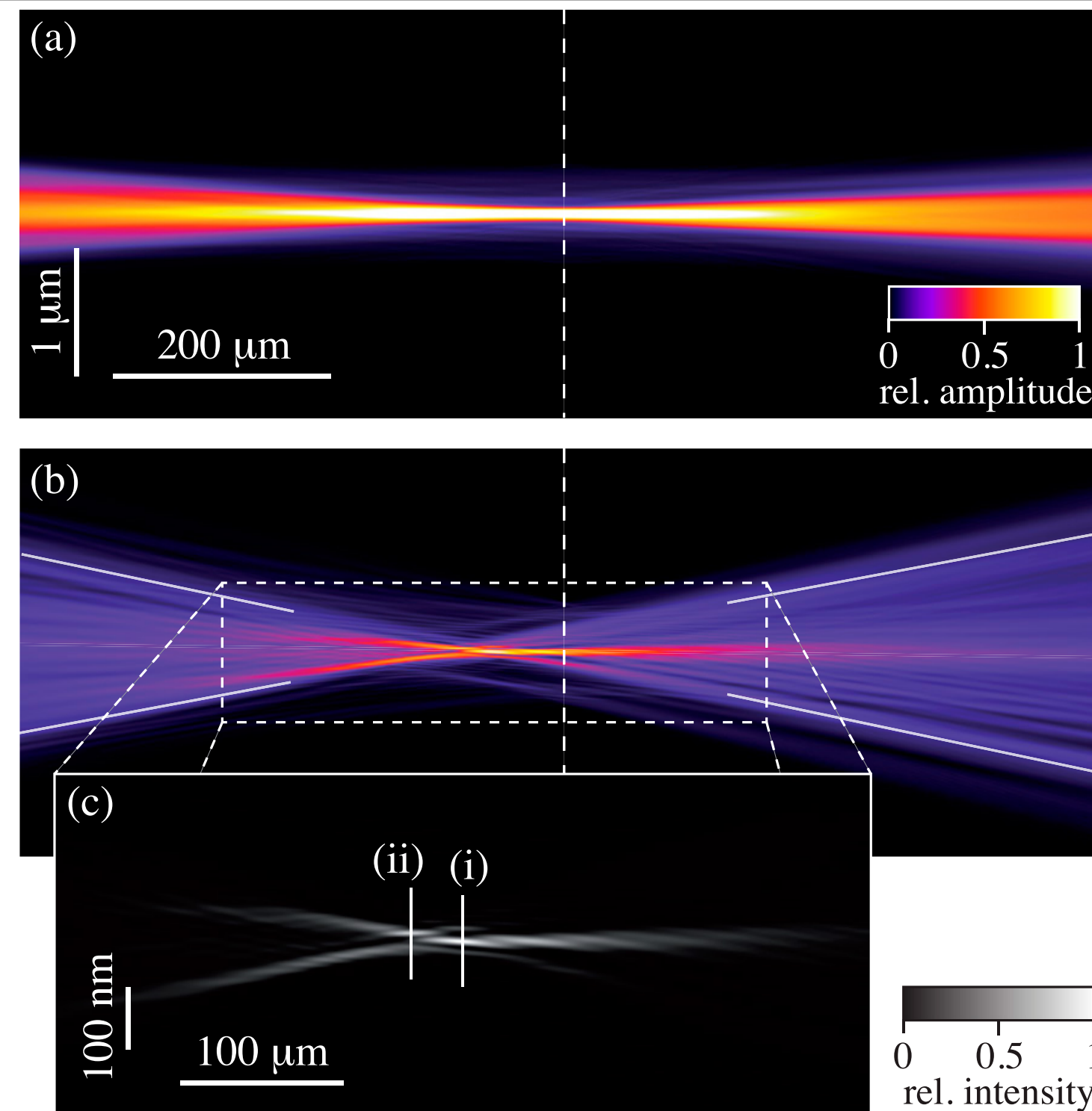
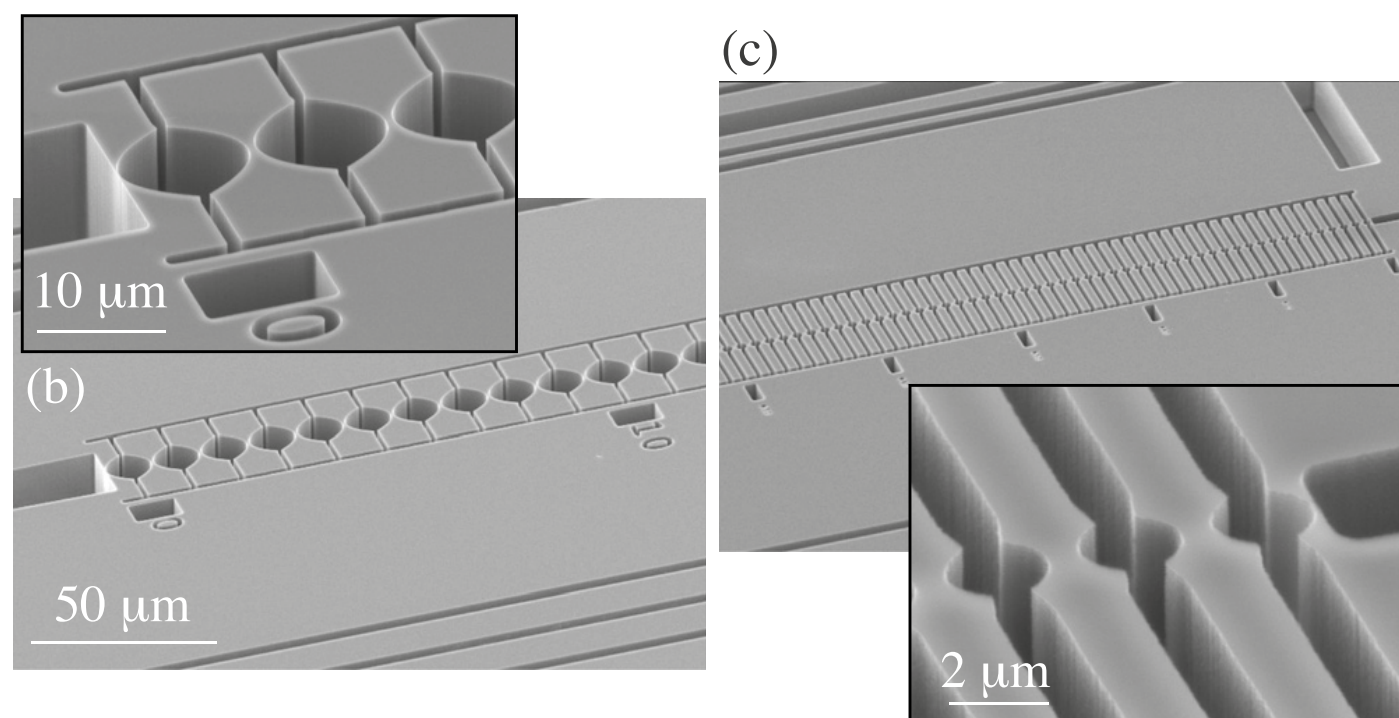
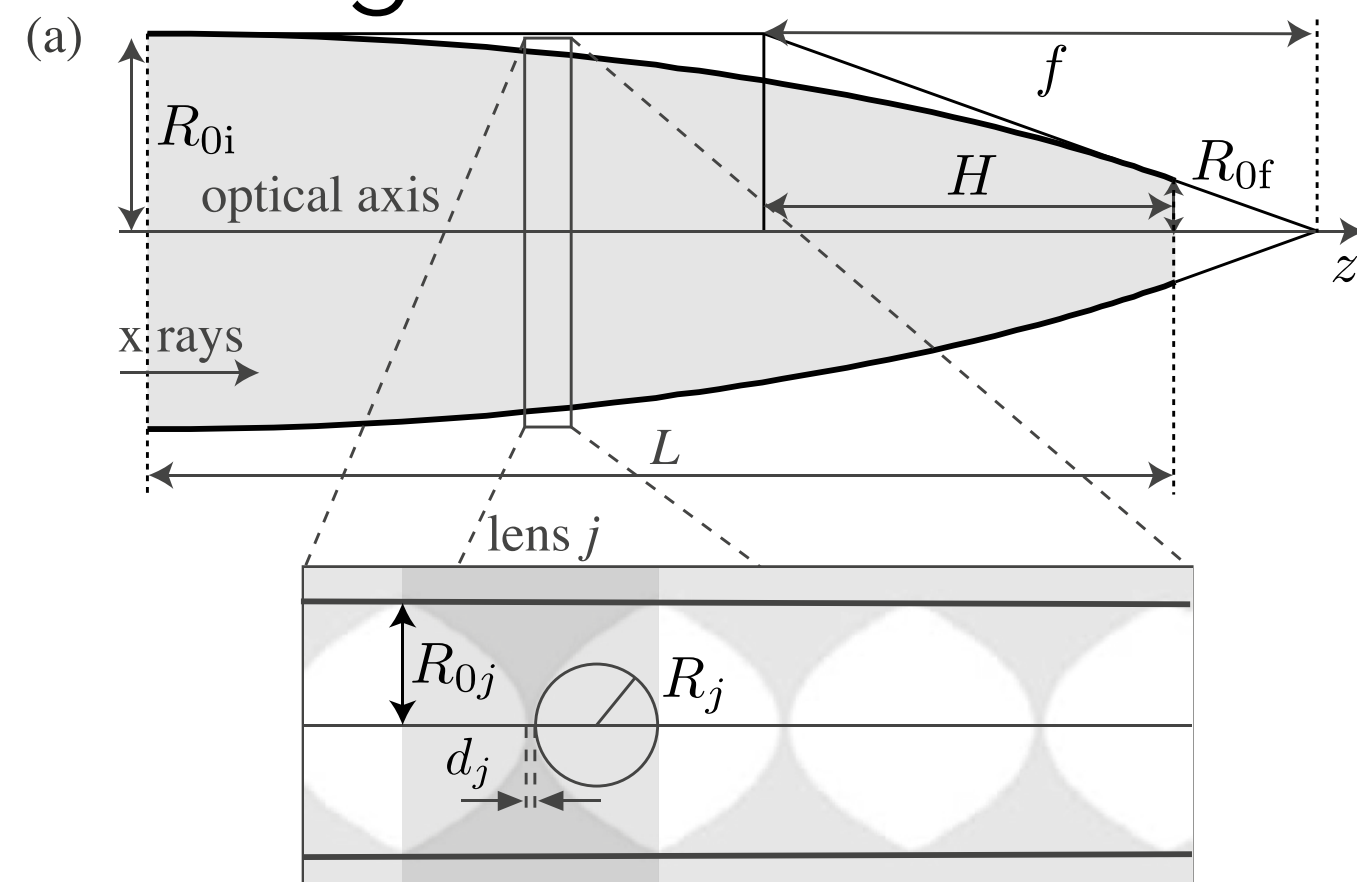


FIG. 3. Caustic of the nanofocused beam: amplitude of the wave field projected onto (a) the vertical and (b) horizontal plane. The dashed line in (a) and (b) depicts the sample plane, in which the ptychogram was recorded. The semi-transparent lines in (b) delineate the numerical aperture. (c) Intensity distribution around the focus [dashed area in (b)] projected onto the horizontal plane. Line (i) in (c) is the section with the highest peak intensity (focus), line (ii) is a section through the laterally smallest speckle.

The horizontal focus that is generated by the AFL is shown in Figs. 3(b) and 3(c). Ideally, the beam would be similarly gaussian as in Fig. 3(a) but with a significantly higher numerical aperture. From the reconstruction of the caustic, it becomes apparent that the AFL suffers from aberrations, generating a far from ideal focus. The brightest speckle [Fig. 3(c)] can be considered the focus and lies in the plane marked by (i) in Fig. 3(c). The horizontal intensity profile in this plane is shown in Fig. 4(i) and shows a focal spot size of 18.4 nm (FWHM). About 65% of the radiation fall into this

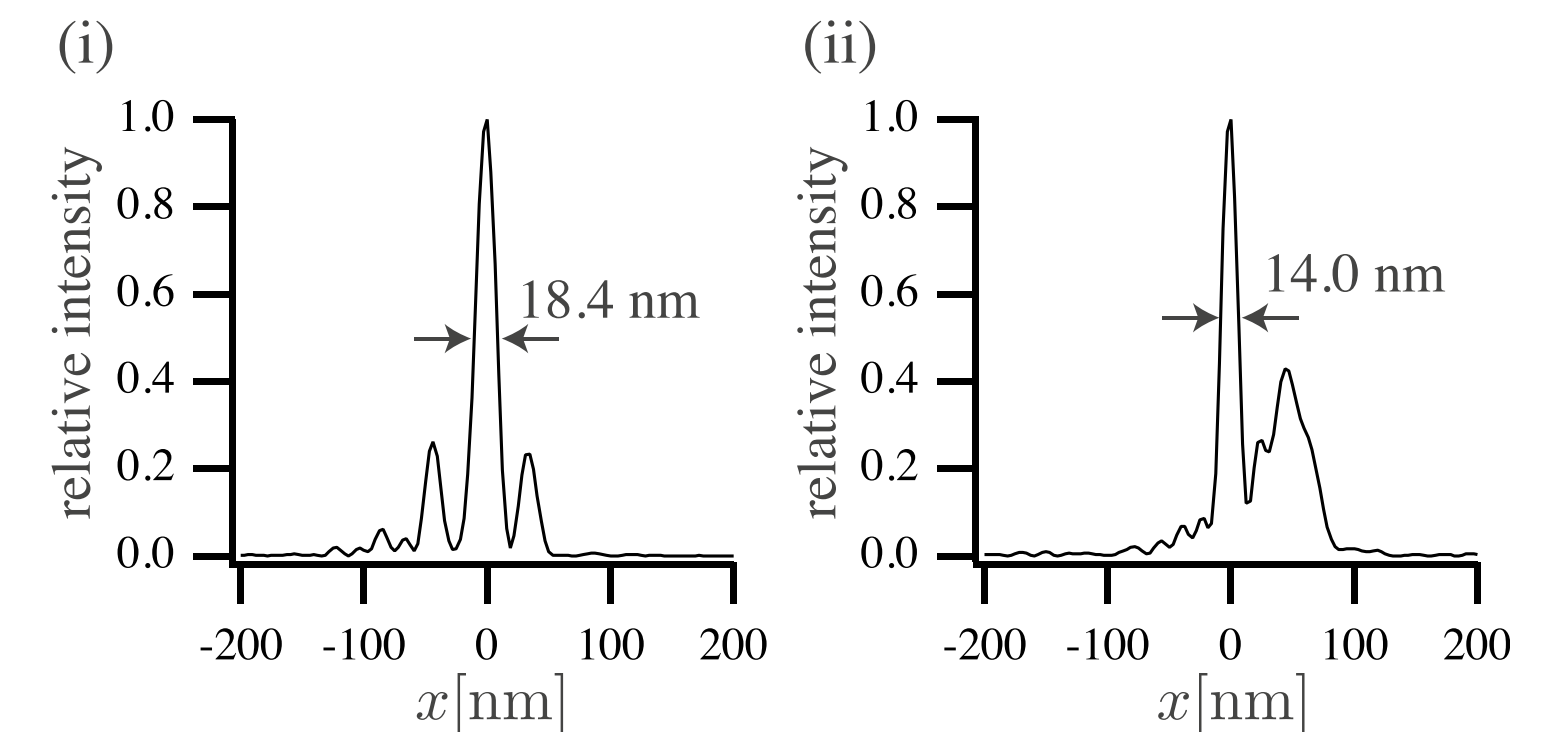


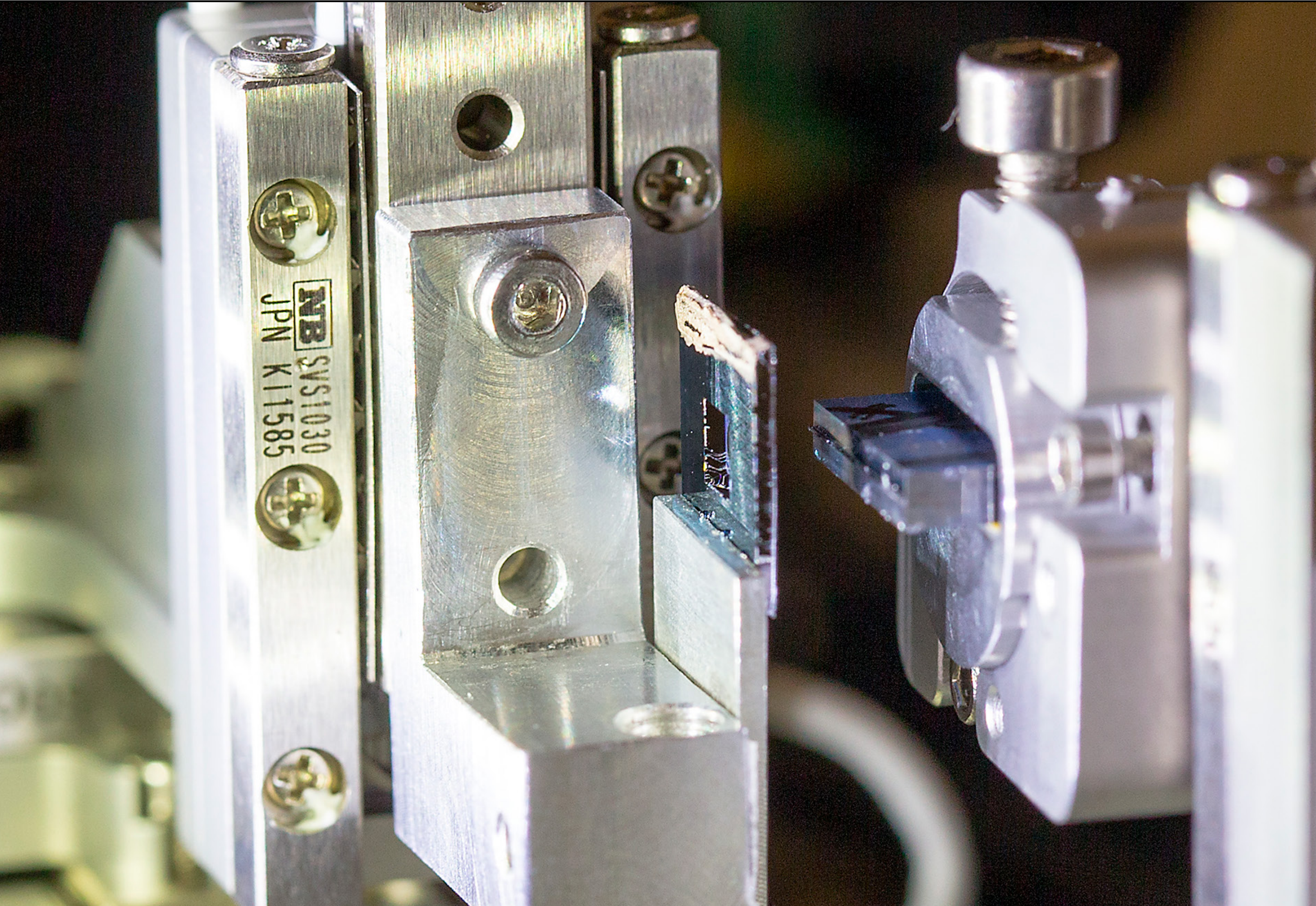
FIG. 4. (i) Horizontal intensity distribution in the focal plane of the AFL [line (i) in Fig. 3(c)]. The central speckle has a lateral size of 18.4 nm (FWHM). (ii) horizontal intensity distribution at the section with the laterally smallest speckle [line (ii) in Fig. 3(c)]. The smallest speckle has a lateral size of 14.0 nm (FWHM).

Waveguides

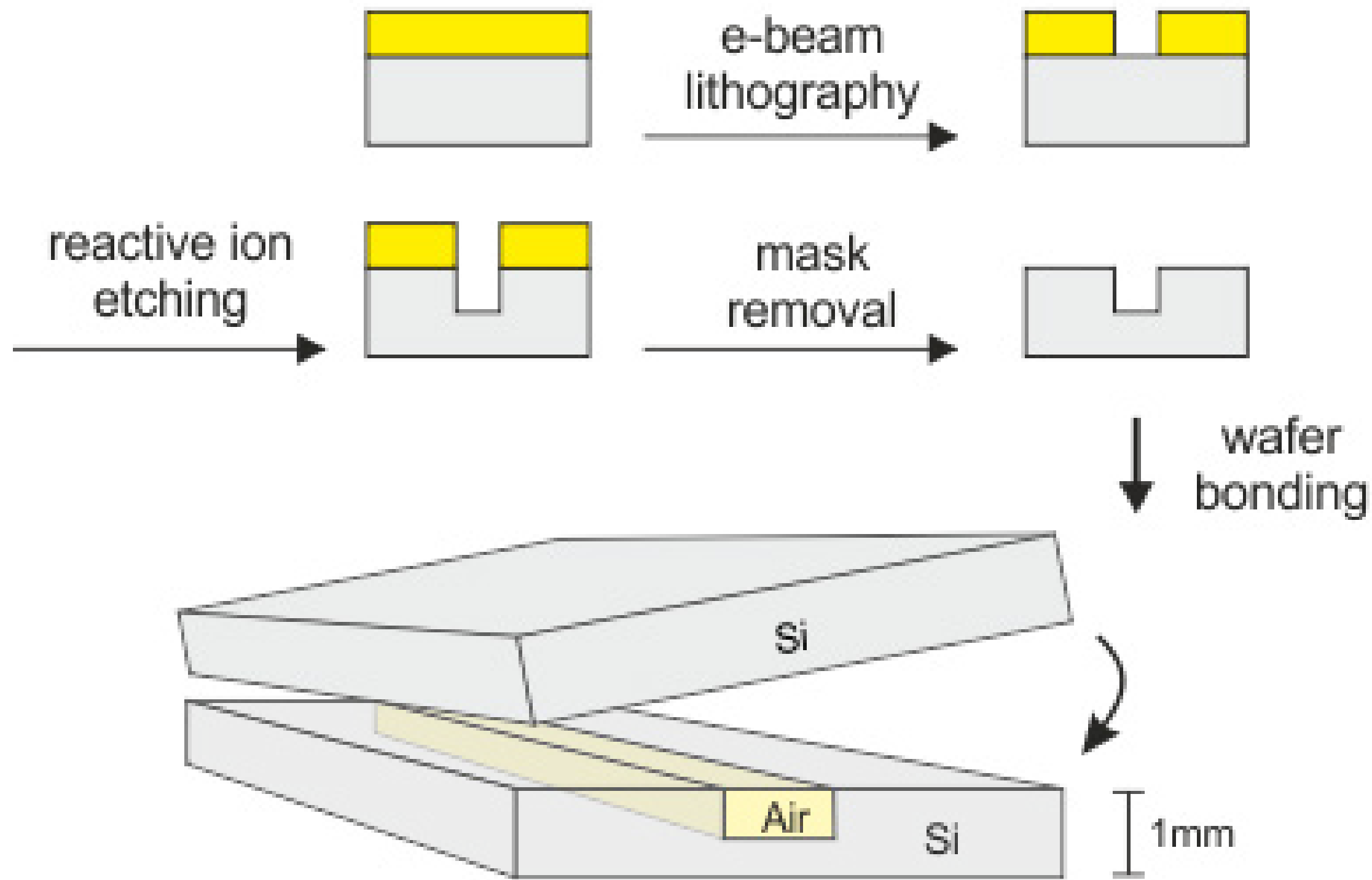


Outline

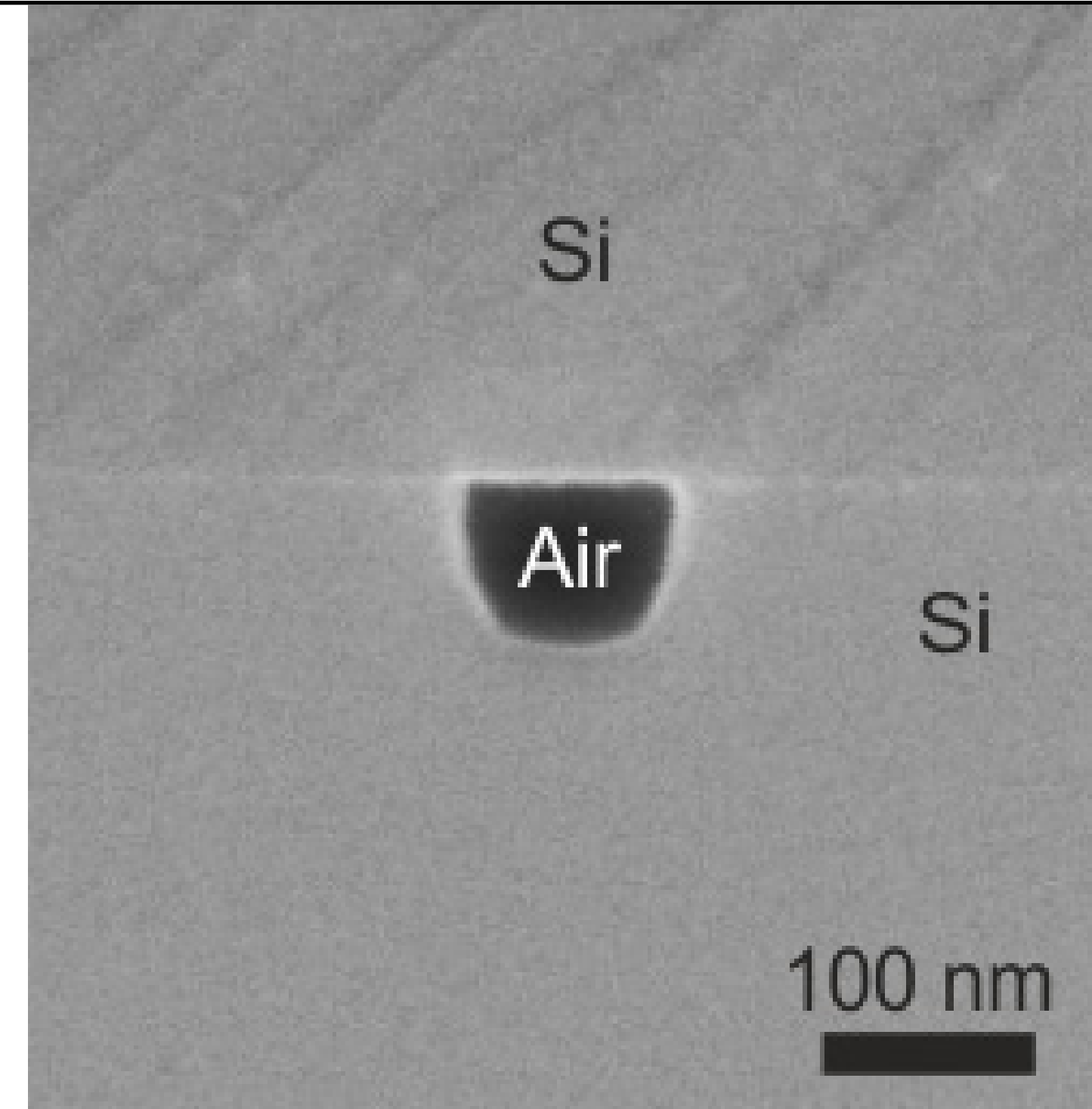
- ▶ Introduction + History
- ▶ Reflective Optics
- ▶ Diffractive Optics
- ▶ Refractive Optics
- ▶ *Waveguides*
- ▶ Discussion



Principle and Geometry



- ▶ rays reflected back and forth, or:
- ▶ wave trapped inside cavity

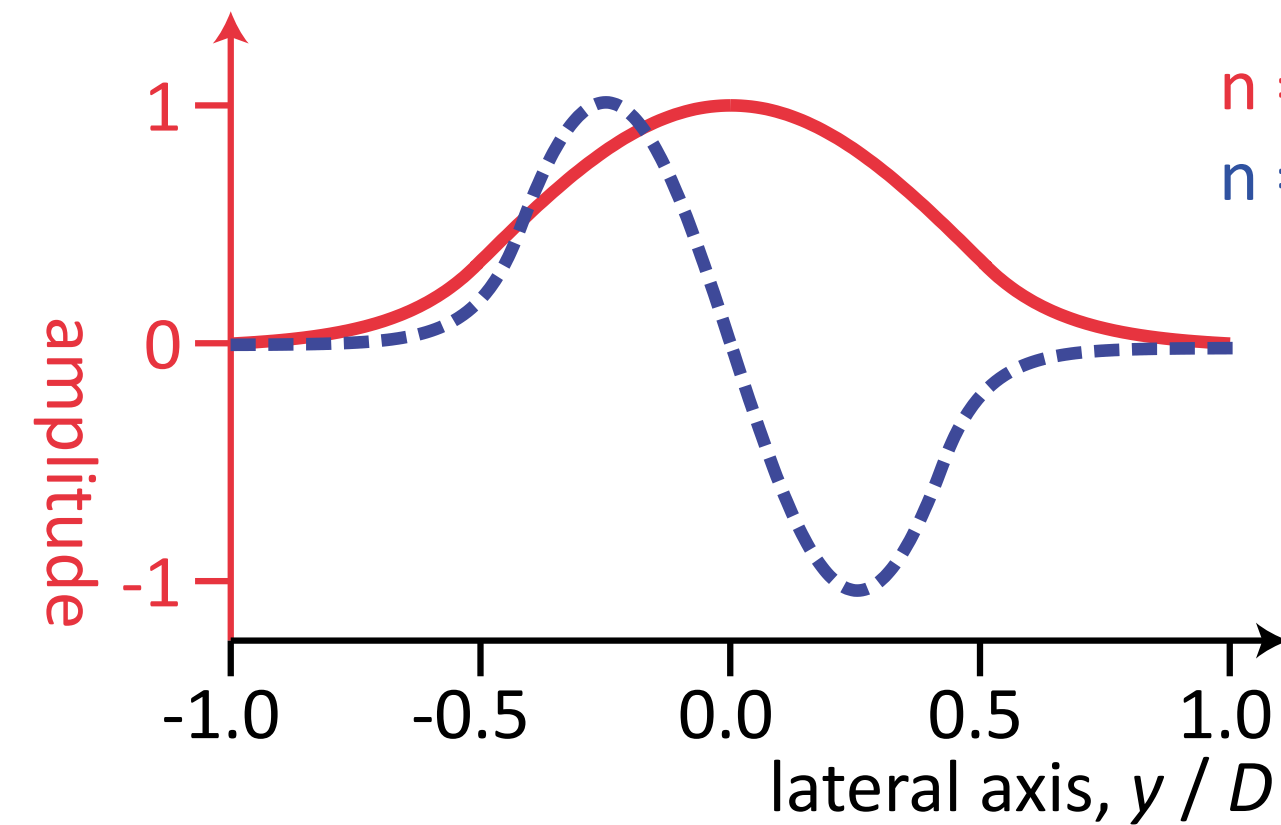


- ▶ channel size: $\sim (20 \text{ nm})^2$
- ▶ channel length: $\sim 1 \text{ mm}$

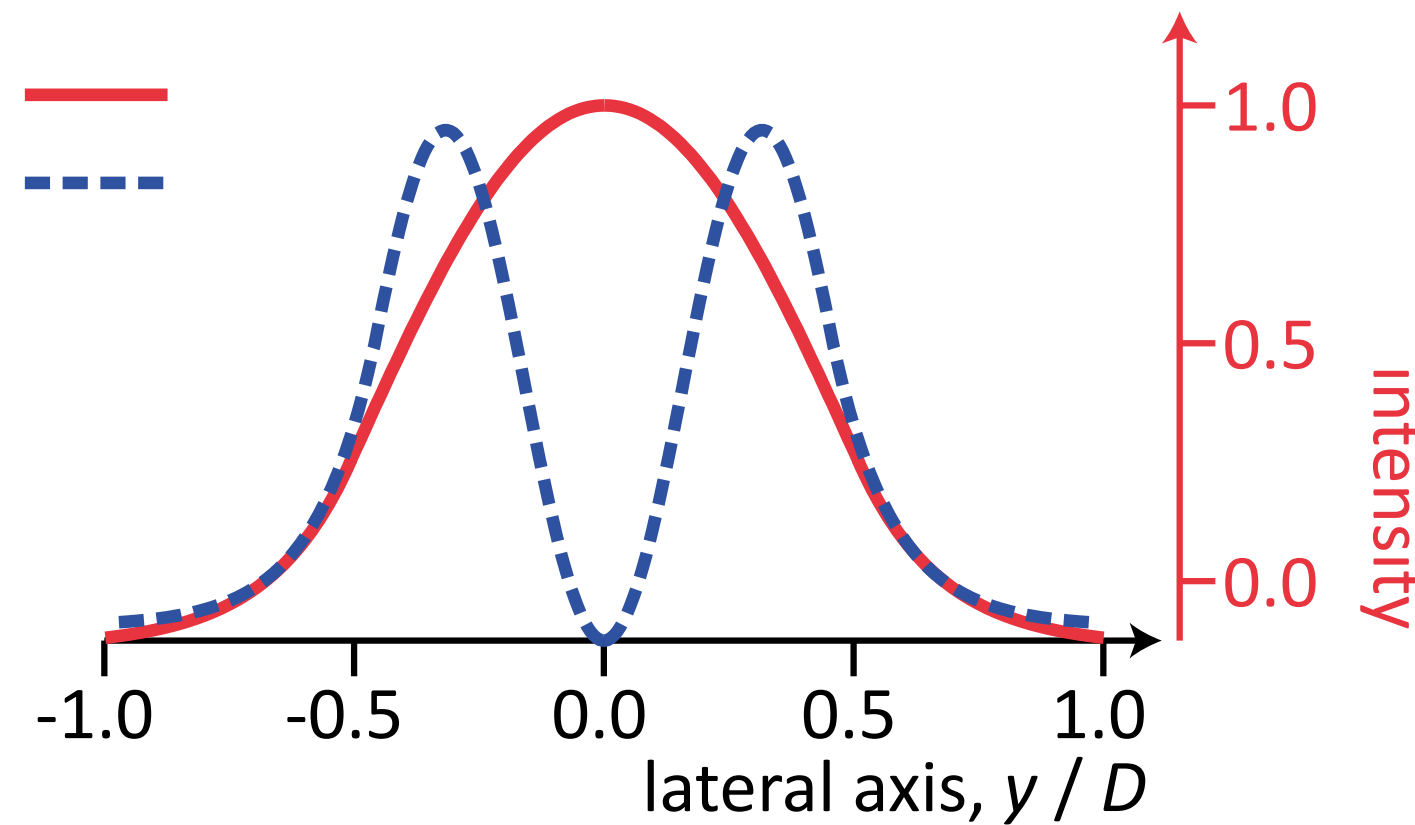
Analytical and Numerical WG Design



(a) Waveguide modes - amplitude



(b) Waveguide modes - intensity

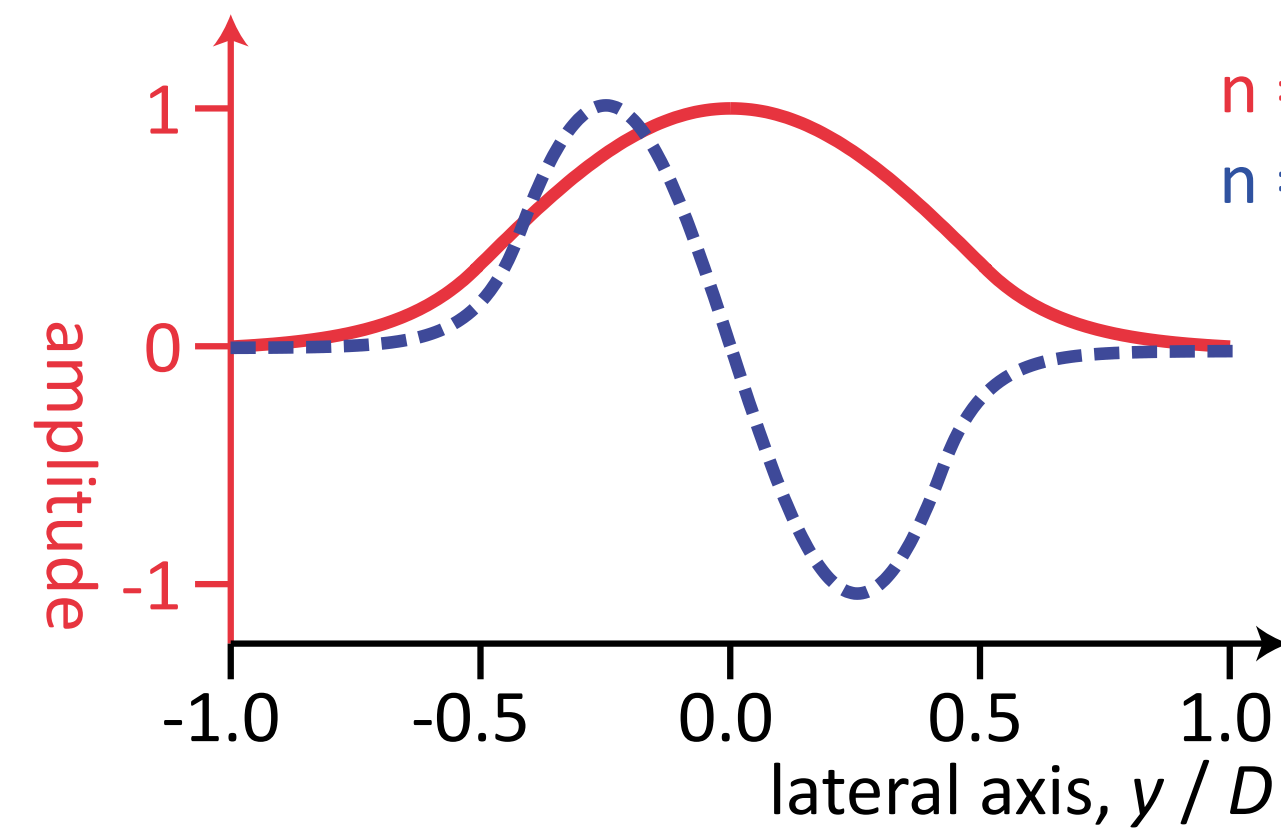


- ▶ first and second guided mode, solving eigenvalue equation in cavity
- ▶ for Si: one mode per 20 nm channel width
- ▶ understand WG fundamentals, including curvature, real structure, multiple components

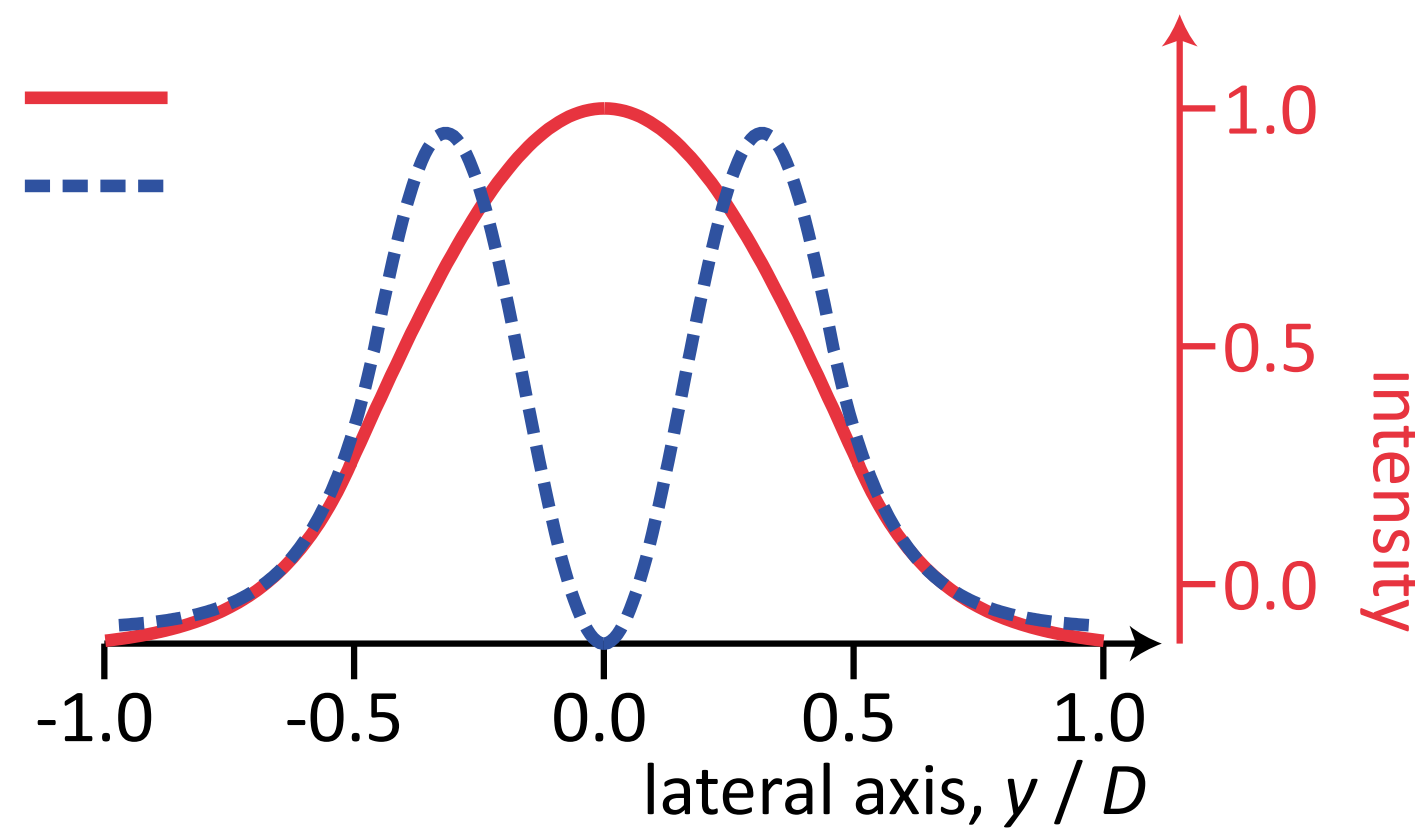
Analytical and Numerical WG Design



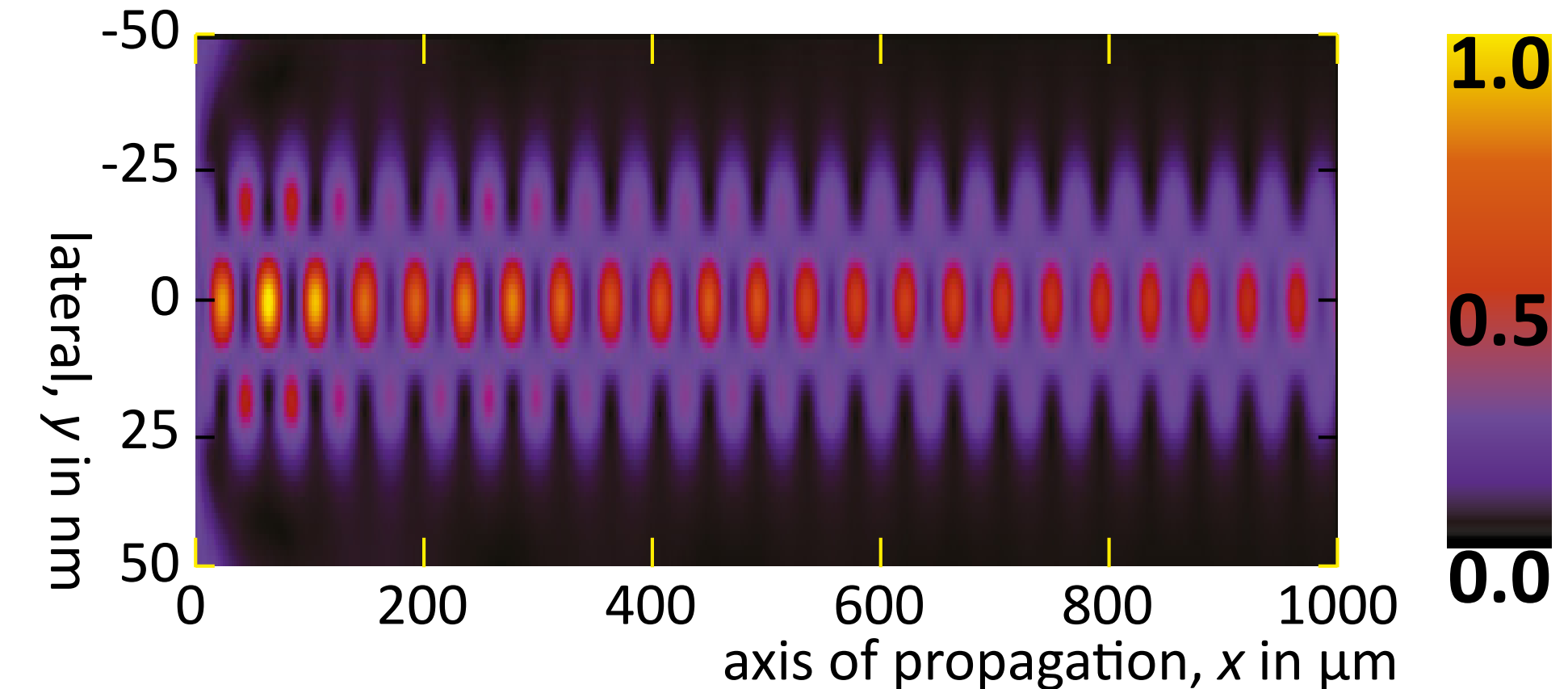
(a) Waveguide modes - amplitude



(b) Waveguide modes - intensity



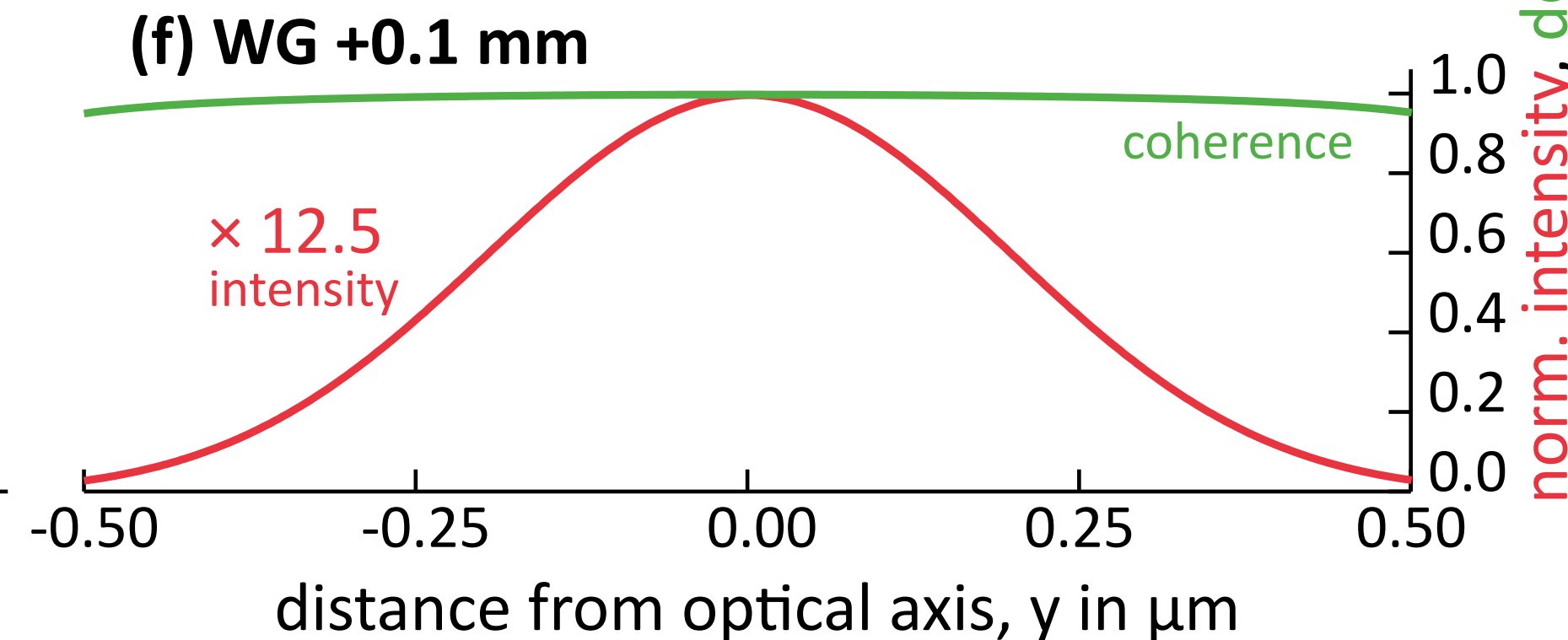
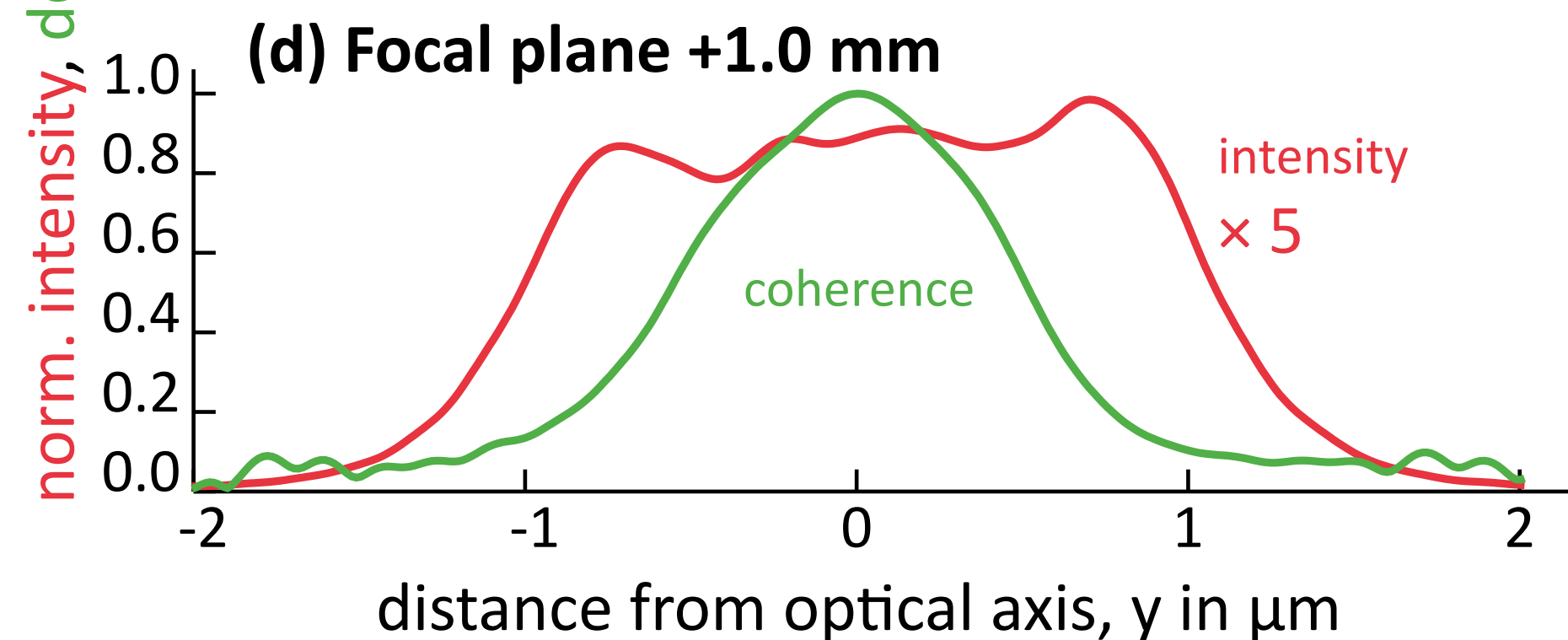
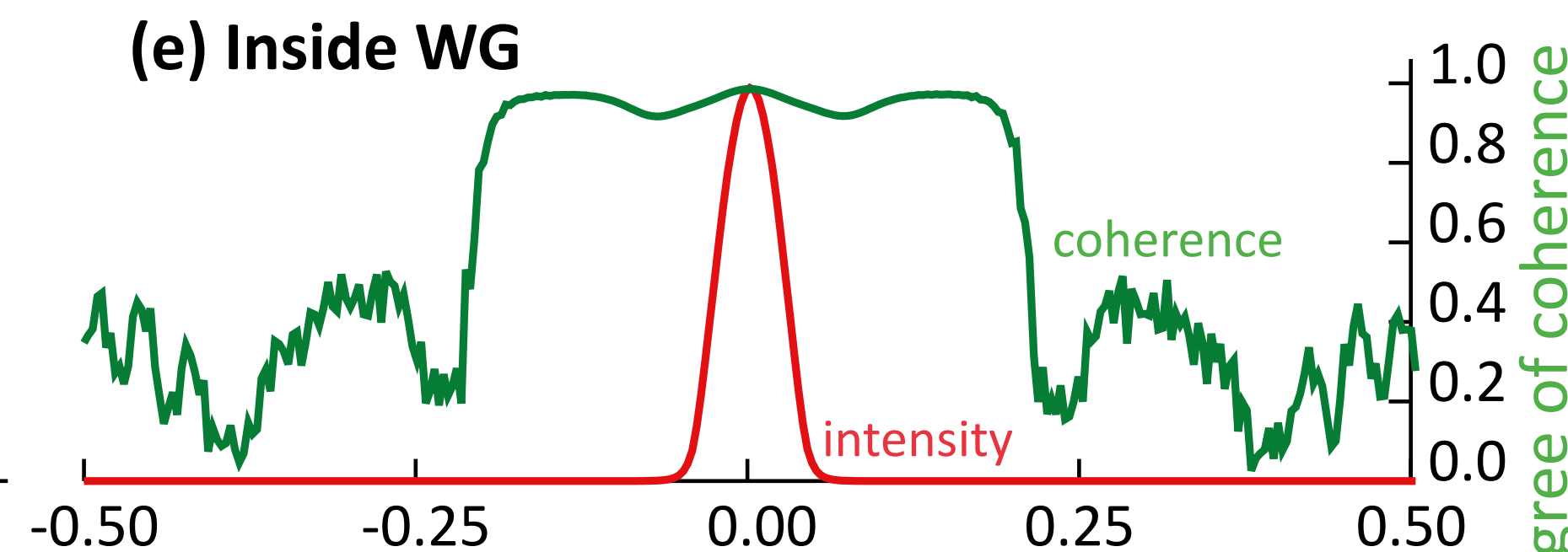
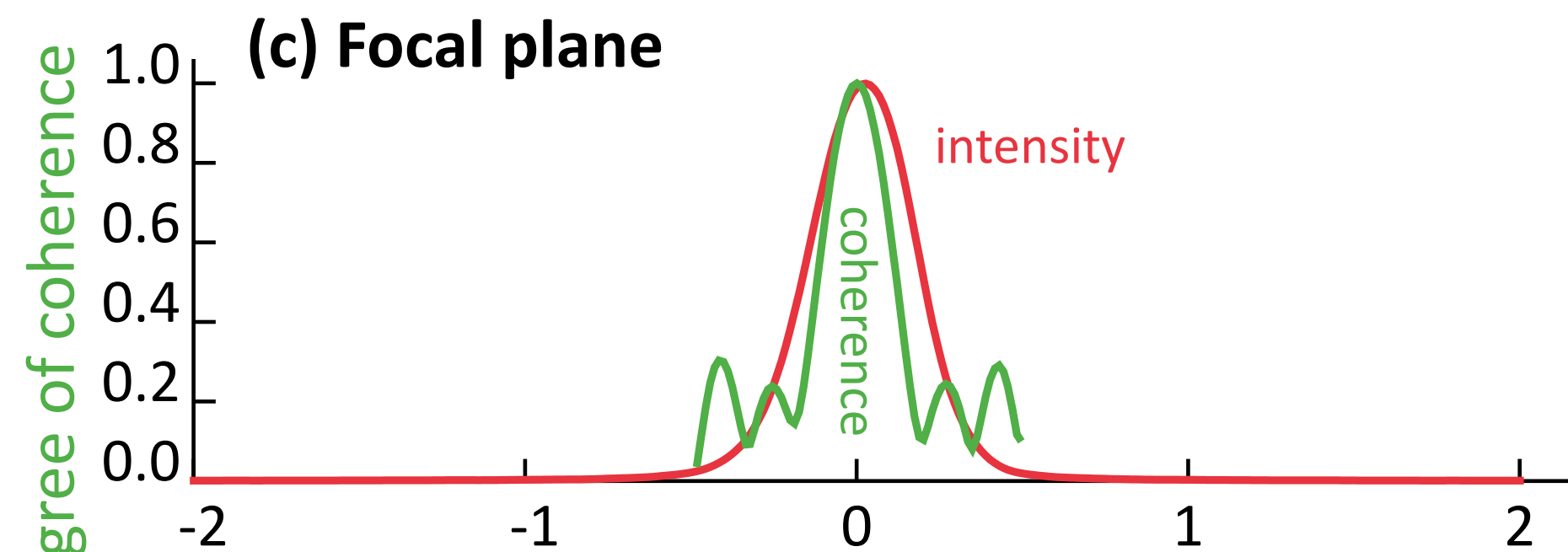
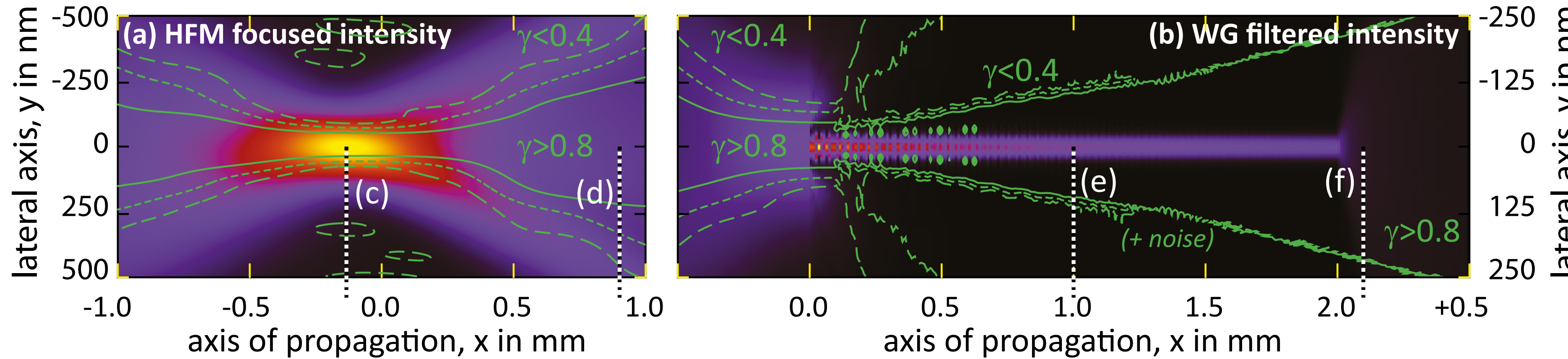
(a) Intensity distribution, $\theta = 0$



- ▶ first and second guided mode, solving eigenvalue equation in cavity
- ▶ for Si: one mode per 20 nm channel width
- ▶ understand WG fundamentals, including curvature, real structure, multiple components

- ▶ simulation inside WG, solving parabolic wave equation
- ▶ mode beating of 1st and 3rd
- ▶ design WGs, including bending, curving and splitting

Coherence Filtering



- ▶ WG is placed in pre-focus, e.g. KB
- ▶ illumination is only of partial coherence
- ▶ WG accepts discrete modes, which are fully coherent
- ▶ further filtering by absorption of higher modes
- ▶ in addition, beam is cleaned from KB stripes

Tapering and Curving

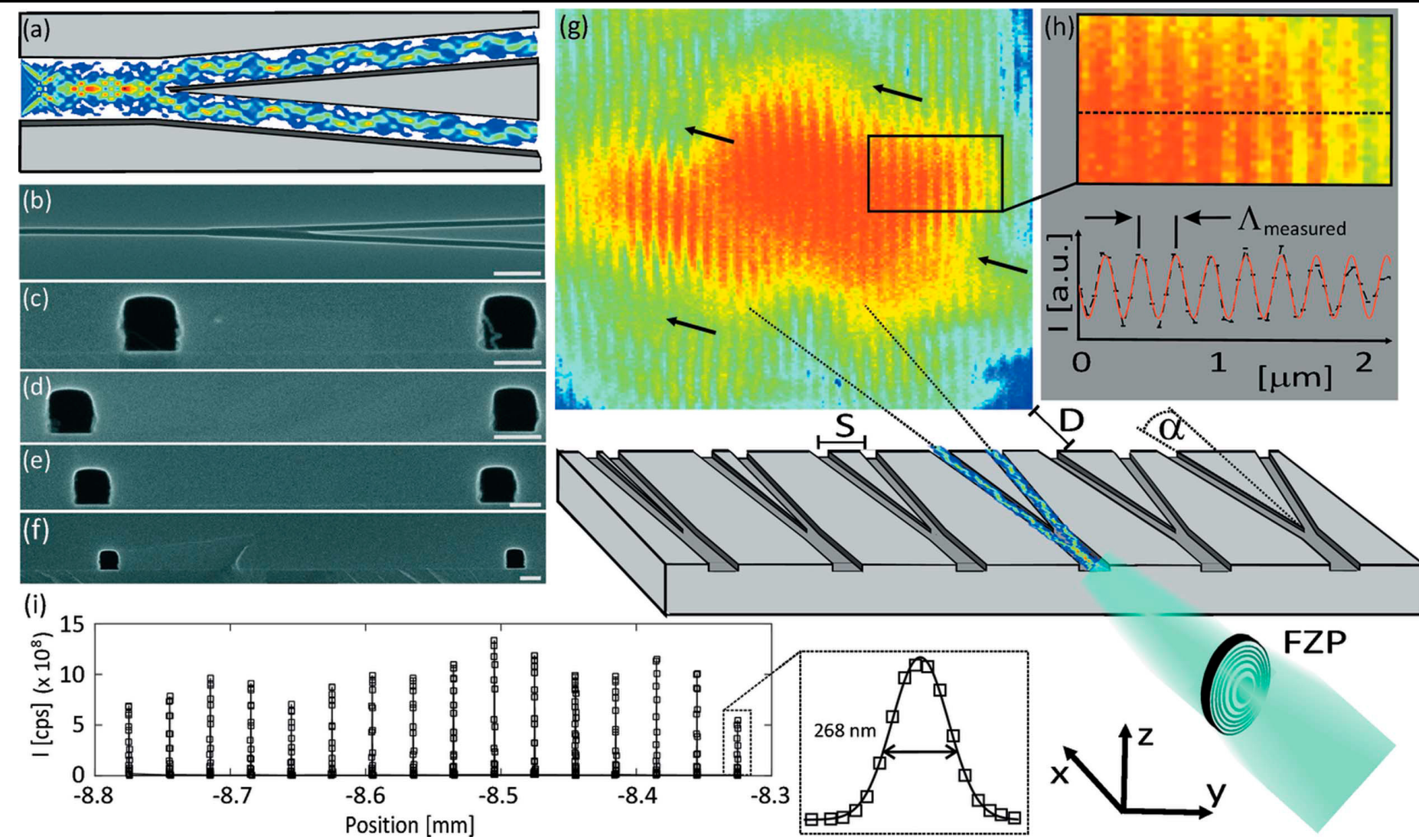


Figure 1
 Experimental geometry. (a) Finite differences simulation of a beamsplitter. (b) Top view SEM image of a splitting structure before wafer bonding. Scale bar denotes 1 μm . (c)–(f) SEM images of the exit side of beamsplitters with different spacings S . Scale bars denote 100 nm. (g) Schematic of the experimental geometry showing the coupling of the focused X-ray beam into the entrance of the beamsplitter, the subsequent guiding in the two channels, the free-space propagation behind the chip, and finally the far-field detector at a distance D . The far-field pattern shows the characteristic double-slit interference pattern, modulated with features of the waveguide modal structure. Arrows mark bifurcations in the interference fringes (fork-shaped structures). Length and angles are not to scale. (h) Enlarged view of the interference pattern with a sinusoidal fit to the intensity oscillations. (i) Scan in the y direction indicating the position of different beamsplitters which have all been defined on the same chip with different geometric parameters, and which can be selected by translating the chip in the FZP focus. Detailed scan profile of a single channel with a width (FWHM) of 282.6 nm giving an upper limit for the beam size in the horizontal direction.

Tapering and Curving

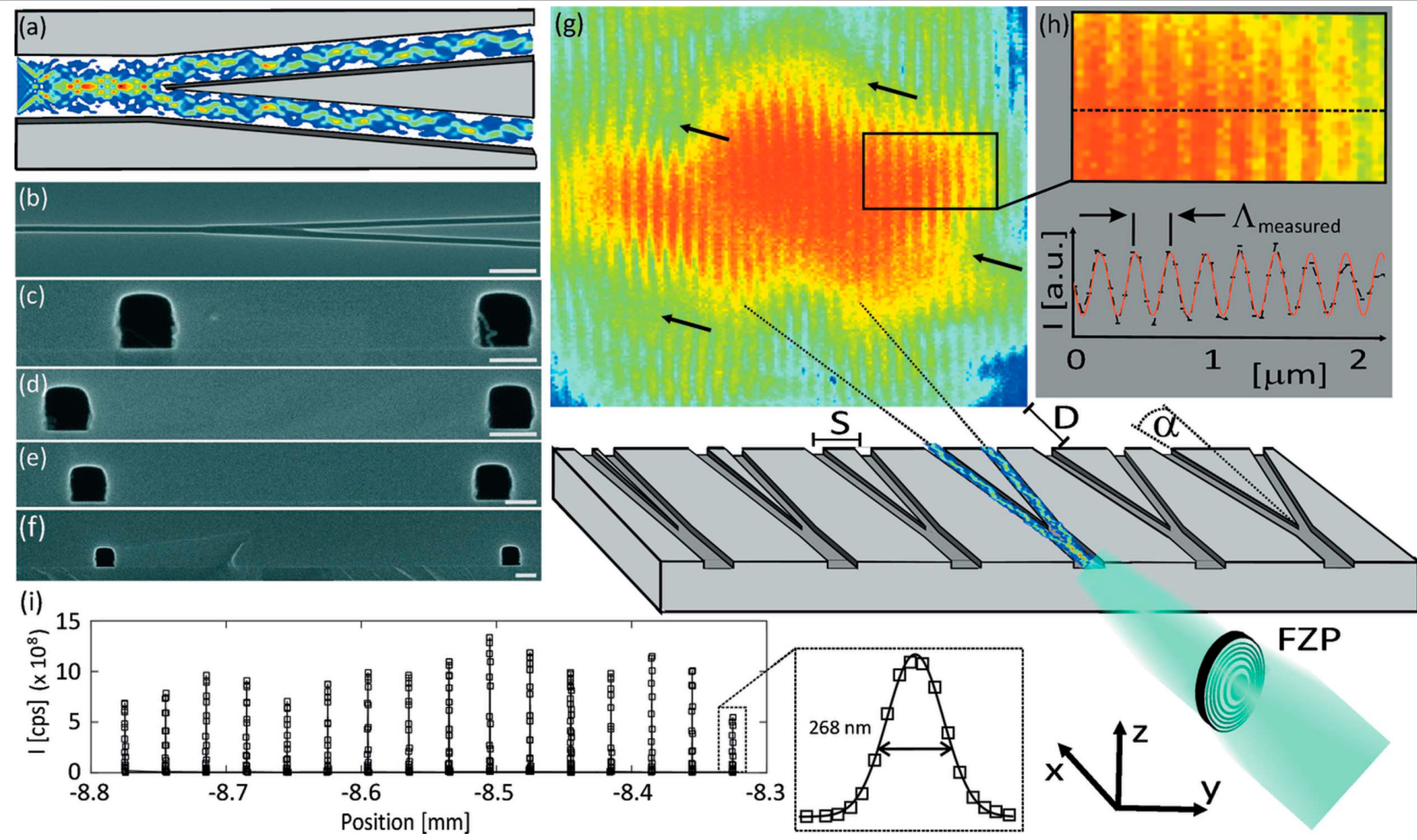
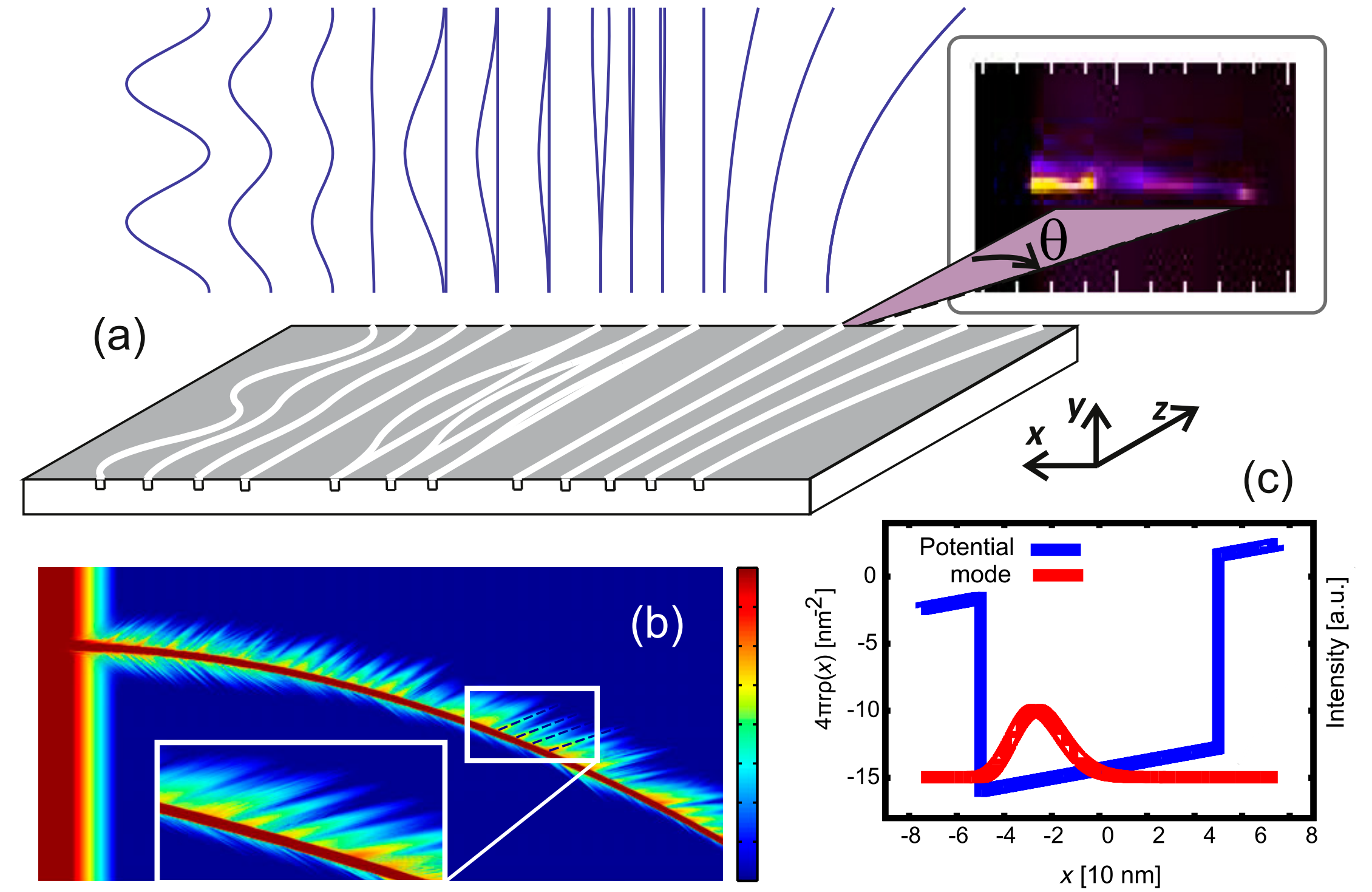
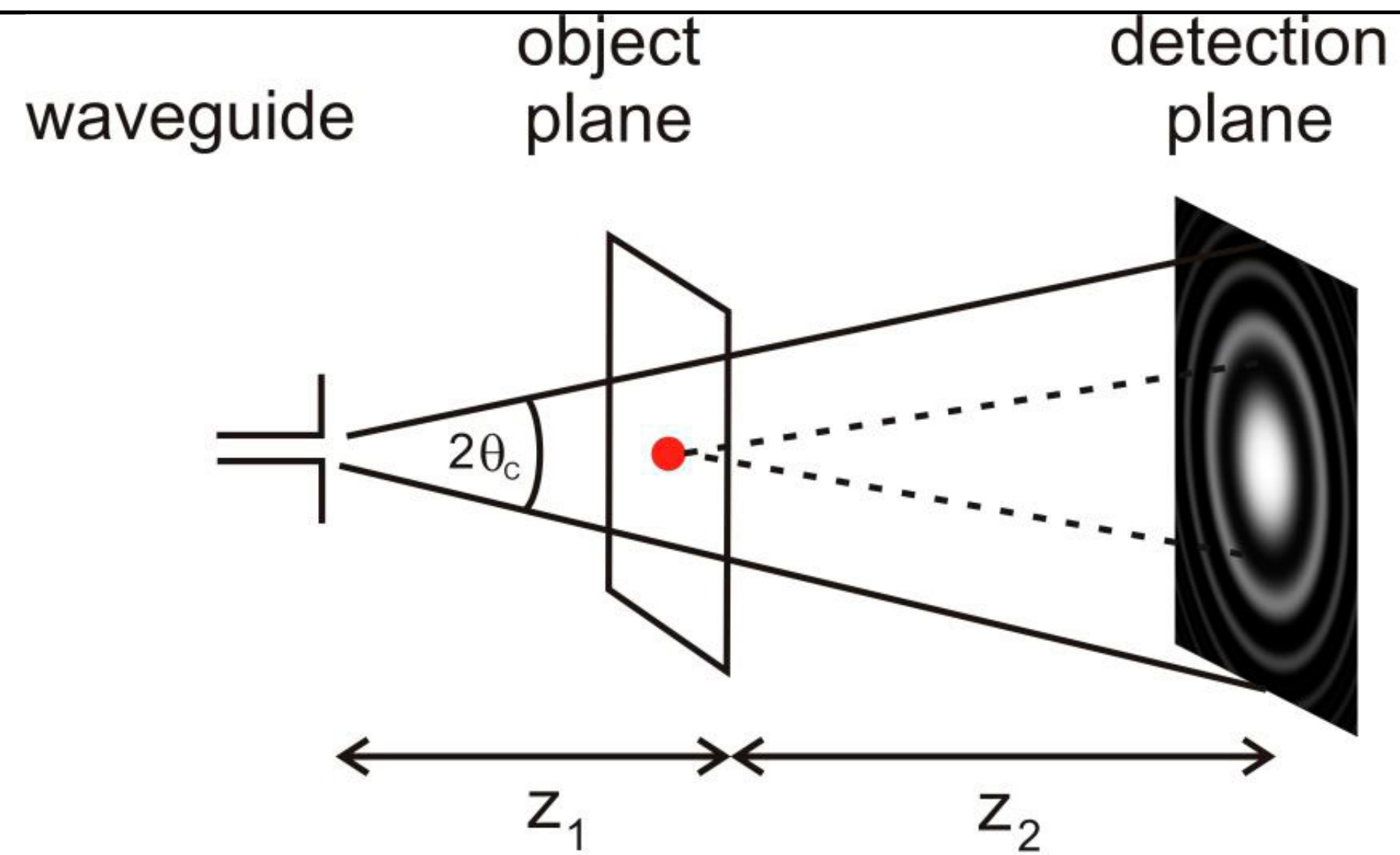


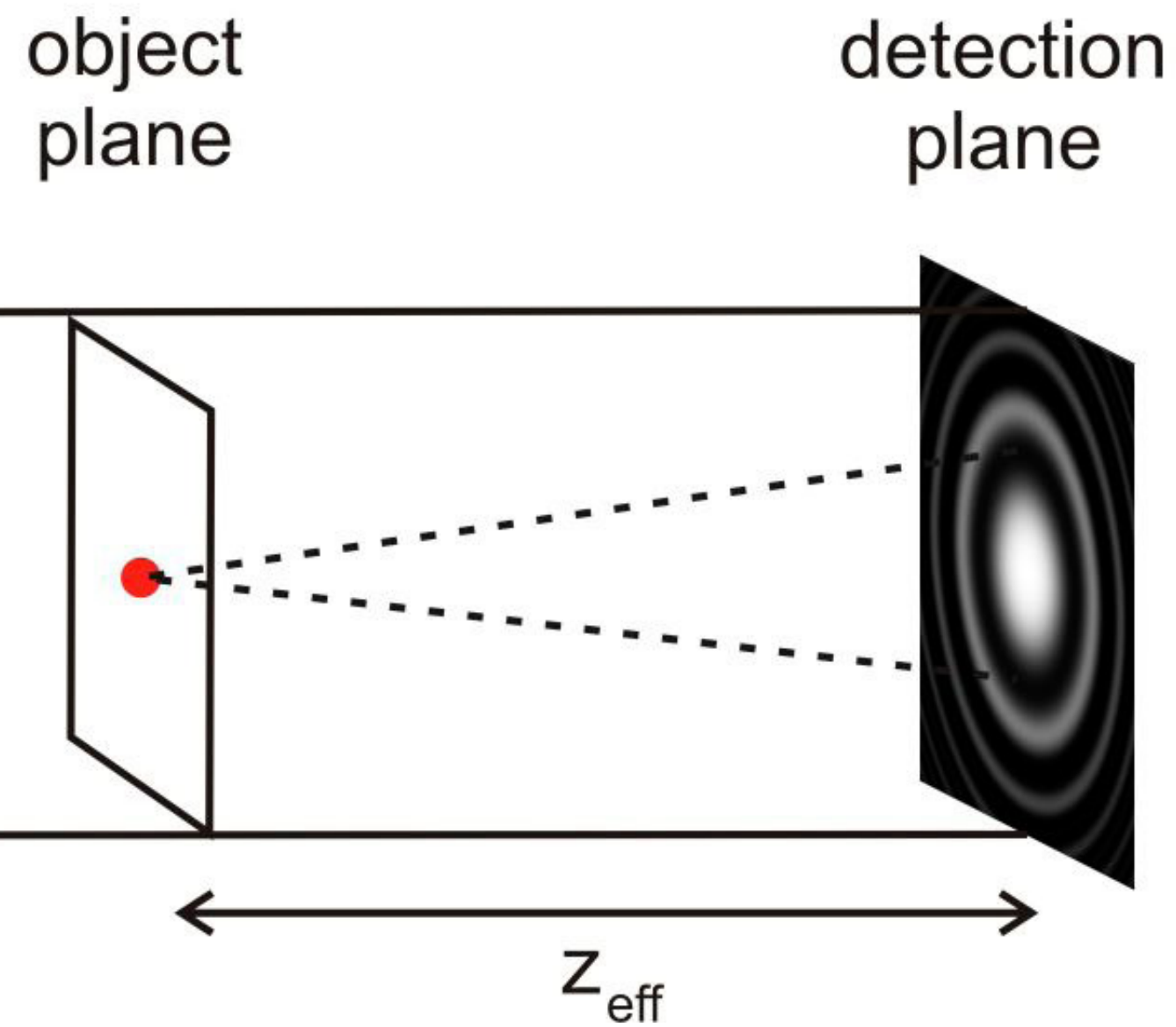
Figure 1
 Experimental geometry. (a) Finite differences simulation of a beamsplitter. (b) Top view SEM image of a splitting structure before wafer bonding. Scale bar denotes 1 μm . (c)–(f) SEM images of the exit side of beamsplitters with different spacings S . Scale bars denote 100 nm. (g) Schematic of the experimental geometry showing the coupling of the focused X-ray beam into the entrance of the beamsplitter, the subsequent guiding in the two channels, the free-space propagation behind the chip, and finally the far-field detector at a distance D . The far-field pattern shows the characteristic double-slit interference pattern, modulated with features of the waveguide modal structure. Arrows mark bifurcations in the interference fringes (fork-shaped structures). Length and angles are not to scale. (h) Enlarged view of the interference pattern with a sinusoidal fit to the intensity oscillations. (i) Scan in the y direction indicating the position of different beamsplitters which have all been defined on the same chip with different geometric parameters, and which can be selected by translating the chip in the FZP focus. Detailed scan profile of a single channel with a width (FWHM) of 282.6 nm giving an upper limit for the beam size in the horizontal direction.



WG Holography



$$M = \frac{z_1 + z_2}{z_1}$$



$$z_{eff} = \frac{z_1 z_2}{z_1 + z_2}$$

WG Holography

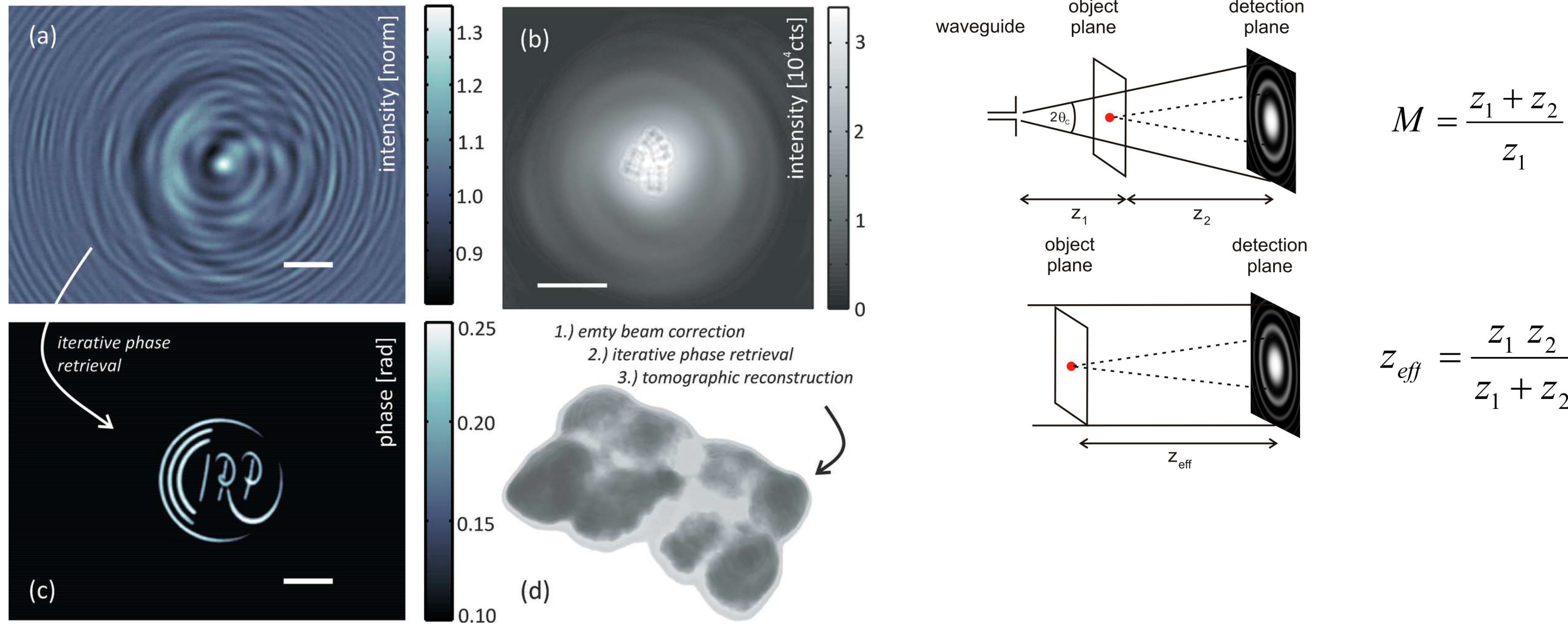


Figure 6
 Holographic imaging with the waveguide probe. Scale bar: $585 \mu\text{m}$ (detector plane). (a) Hologram of a test pattern after division by the empty beam. Scale bar: 6 mm (detector plane). (b) Raw data of a hologram with three *Deinococcus radiodurans* cells, showing the smooth line-shape and tails of the waveguide probe. (c) Phase reconstruction of the hologram shown in (a), with 22.4 nm pixel size. Scale bar: $2 \mu\text{m}$. (d) Rendered three-dimensional density distribution of a *Deinococcus radiodurans* bacteria (Bartels *et al.*, 2012), reconstructed from waveguide-based holographic tomography.

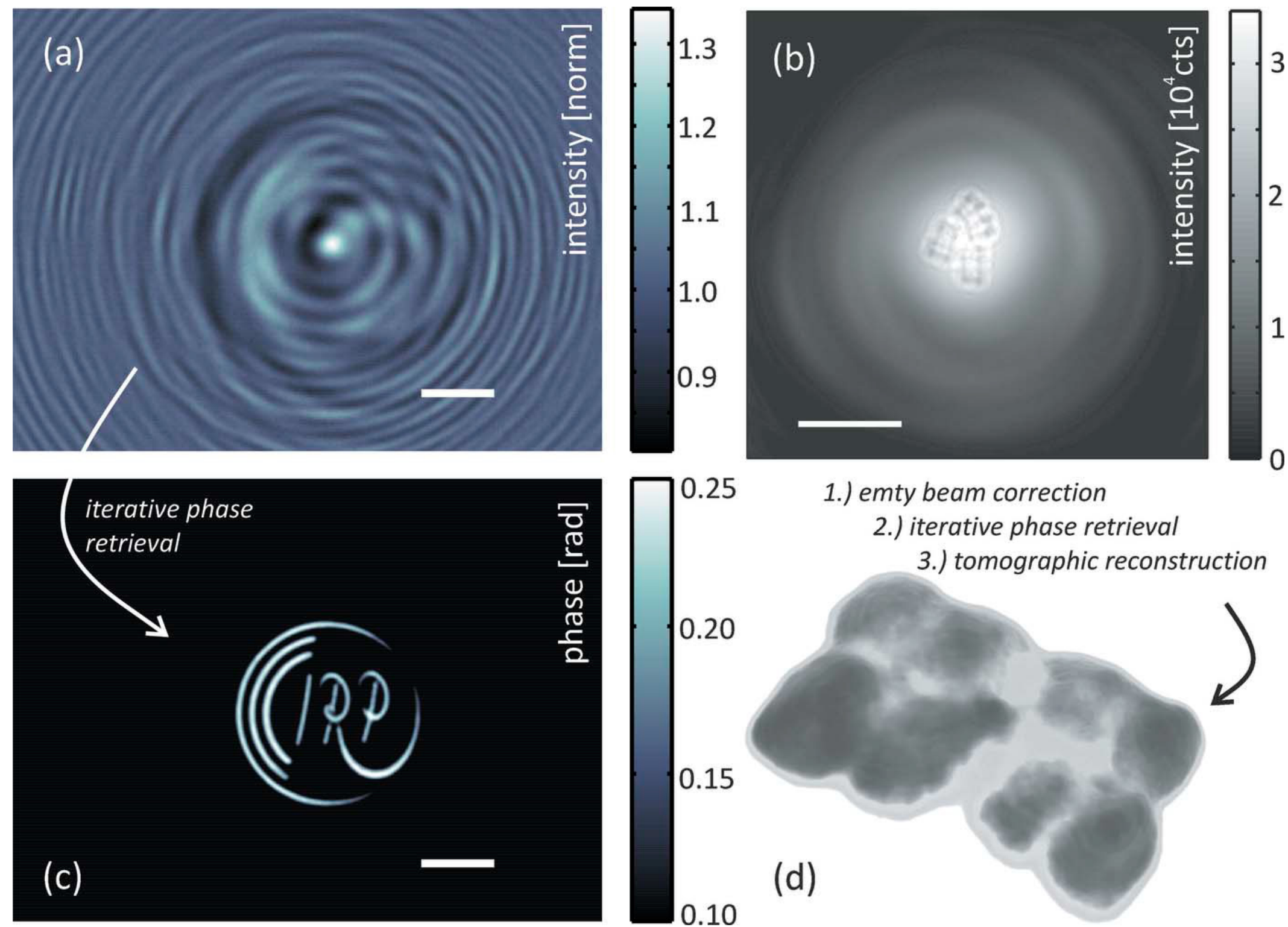
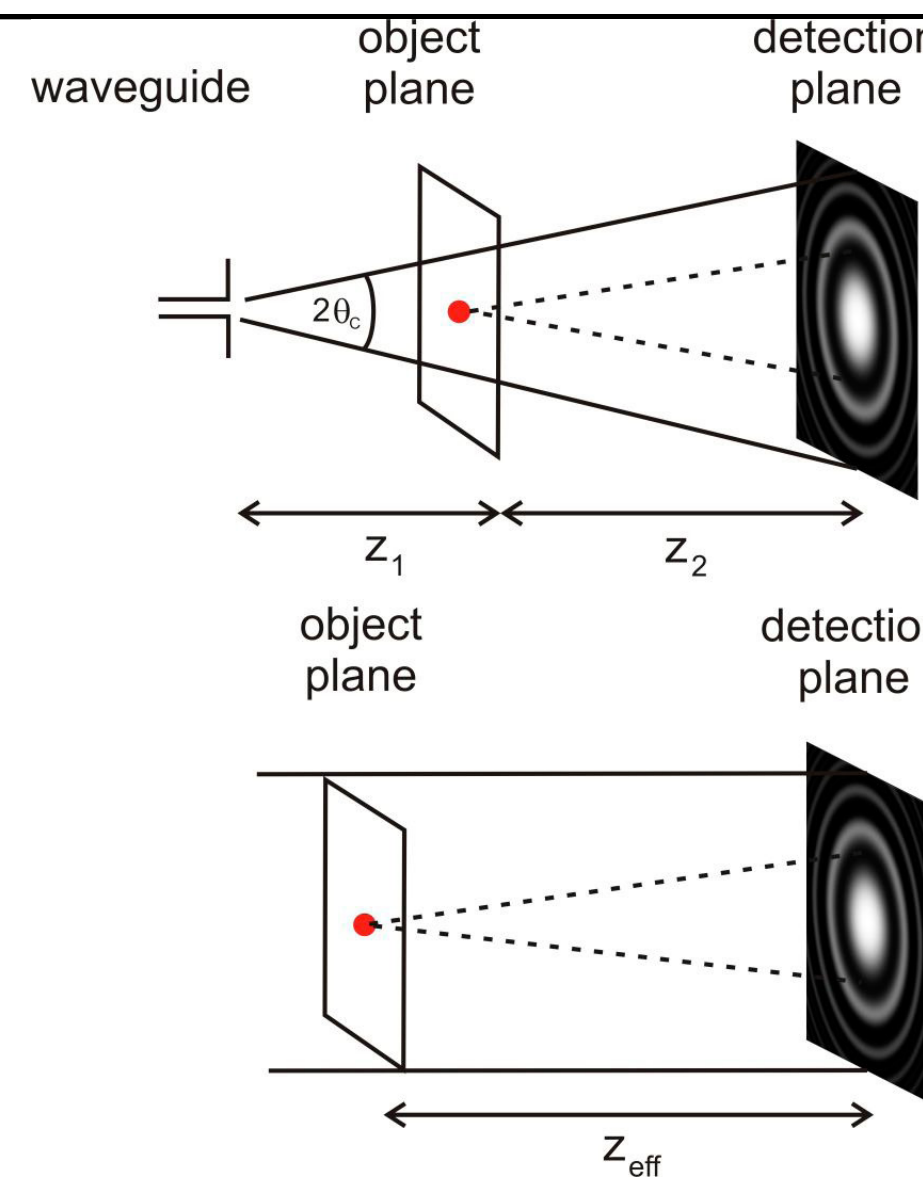


Figure 6 Holographic imaging with the waveguide probe. Scale bar: 585 μm (detector plane). (a) Hologram of a test pattern after division by the empty beam. Scale bar: 6 mm (detector plane). (b) Raw data of a hologram with three *Deinococcus radiodurans* cells, showing the smooth line-shape and tails of the waveguide probe. (c) Phase reconstruction of the hologram shown in (a), with 22.4 nm pixel size. Scale bar: 2 μm . (d) Rendered three-dimensional density distribution of a *Deinococcus radiodurans* bacteria (Bartels *et al.*, 2012), reconstructed from waveguide-based holographic tomography.



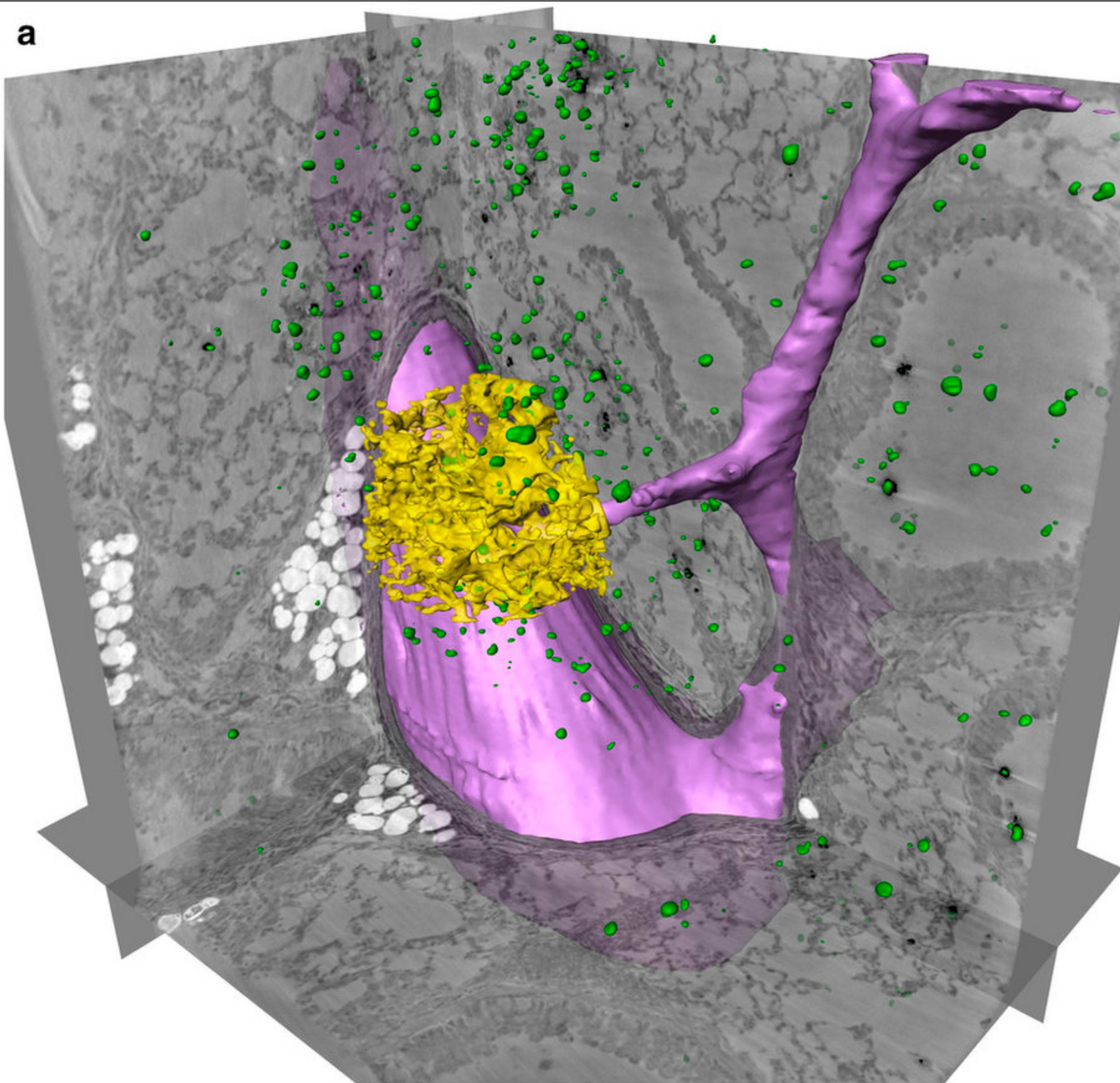
$$M = \frac{z_1 + z_2}{z_1}$$

$$z_{\text{eff}} = \frac{z_1 z_2}{z_1 + z_2}$$

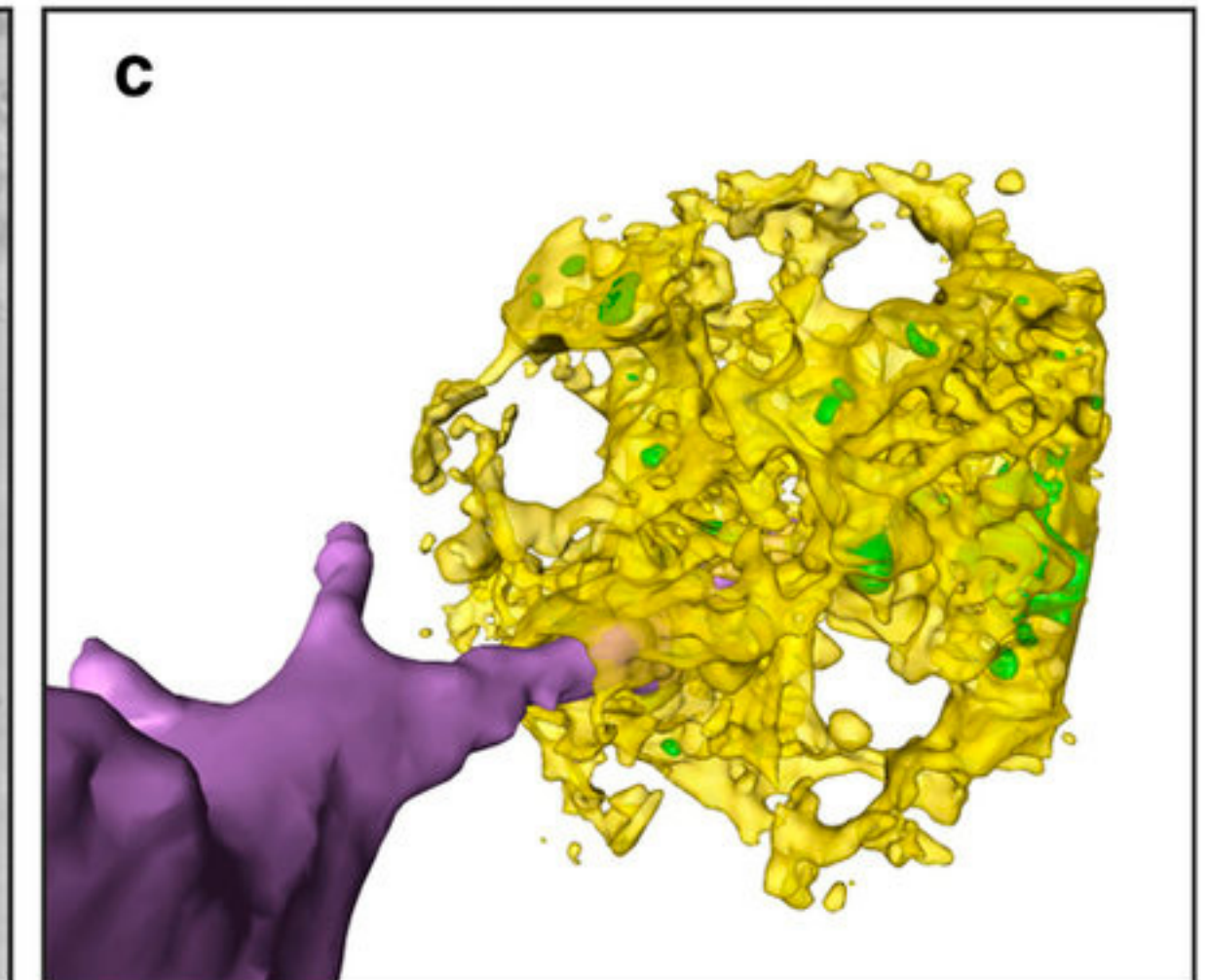
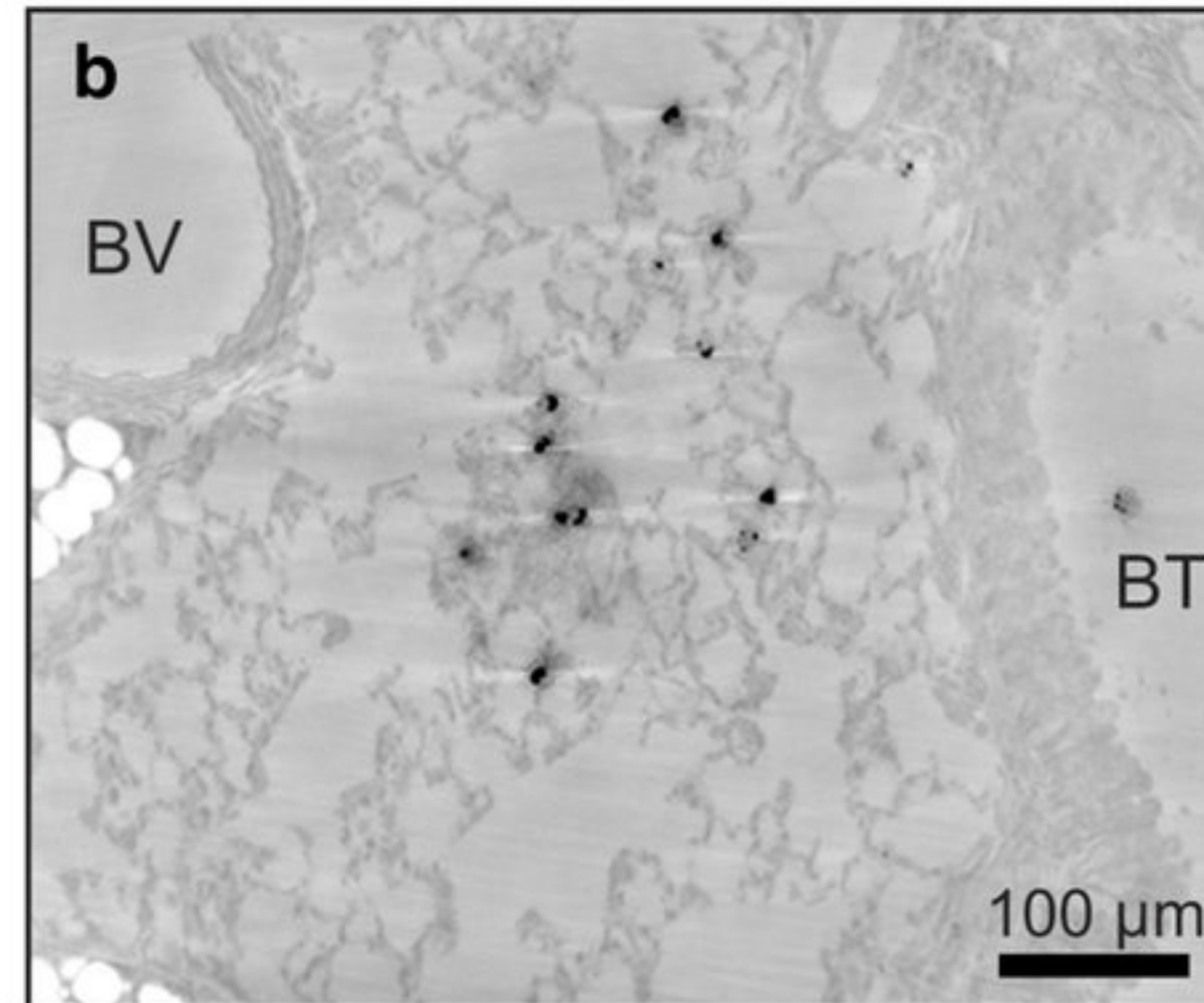
Advantages of WG-Holography

- ▶ full-field method, robust phase-retrieval
- ▶ coherence filtering, KB artefacts filtering
- ▶ geometrical magnification
- ▶ lower dose than ptychography
- ▶ compatible with tomography

WG Holo-Tomography



- ▶ Reconstructed asthmatic lung tissue (mouse)
- ▶ Sub-cellular resolution @ organic field of view
- ▶ Mass density in 3D!

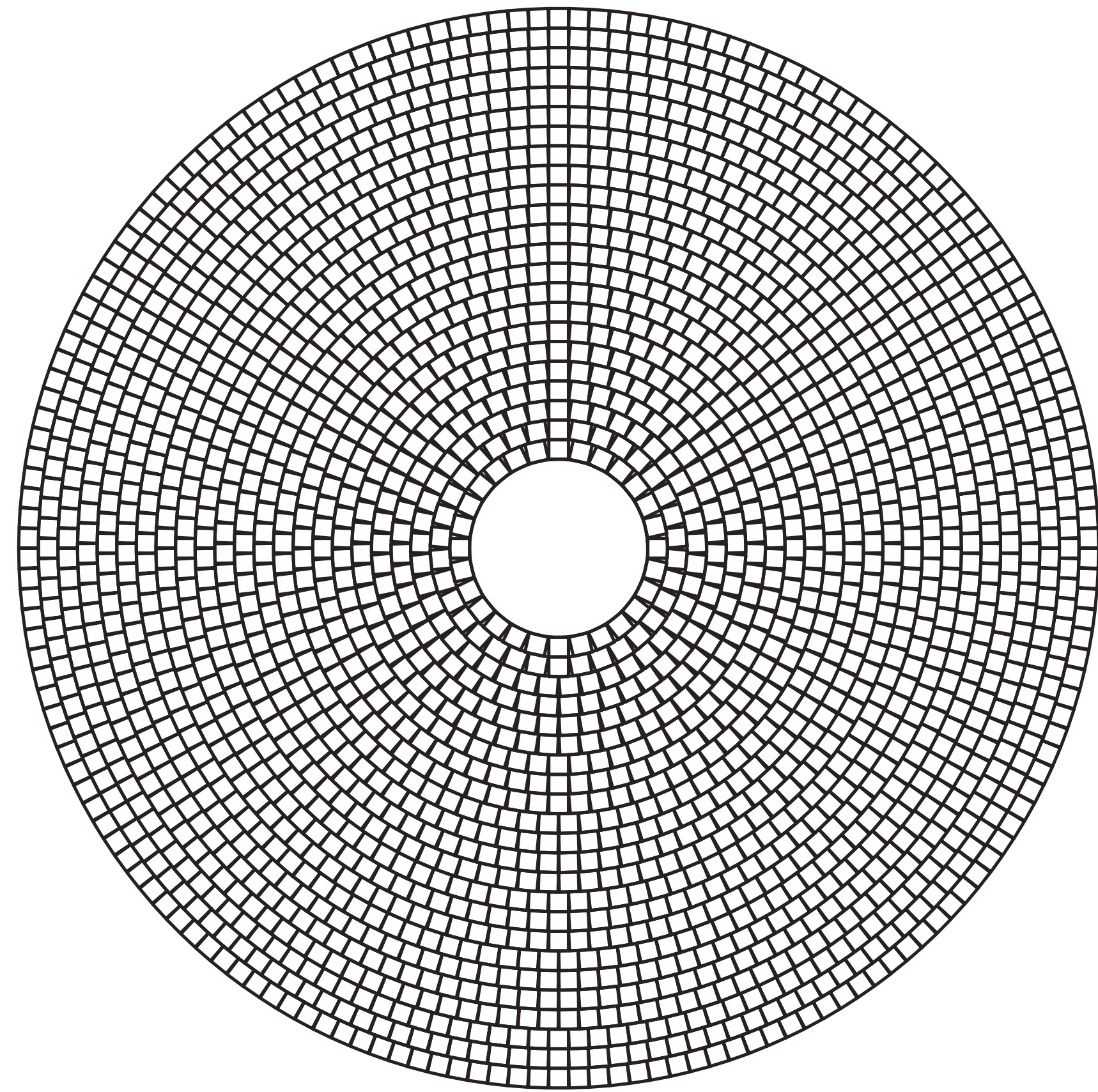




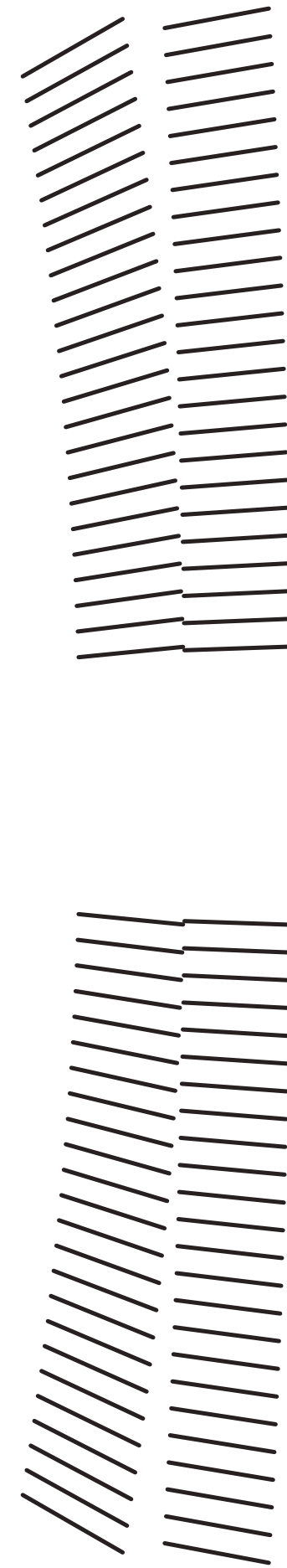
Outline

- ▶ Introduction + History
- ▶ Reflective Optics
- ▶ Diffractive Optics
- ▶ Refractive Optics
- ▶ Waveguides
- ▶ Discussion

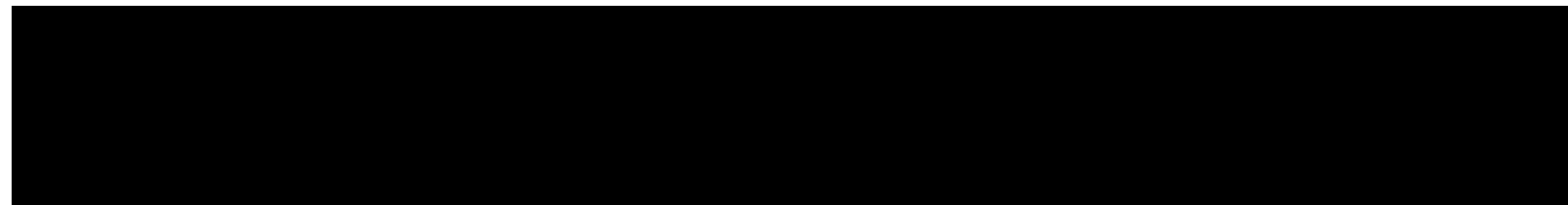
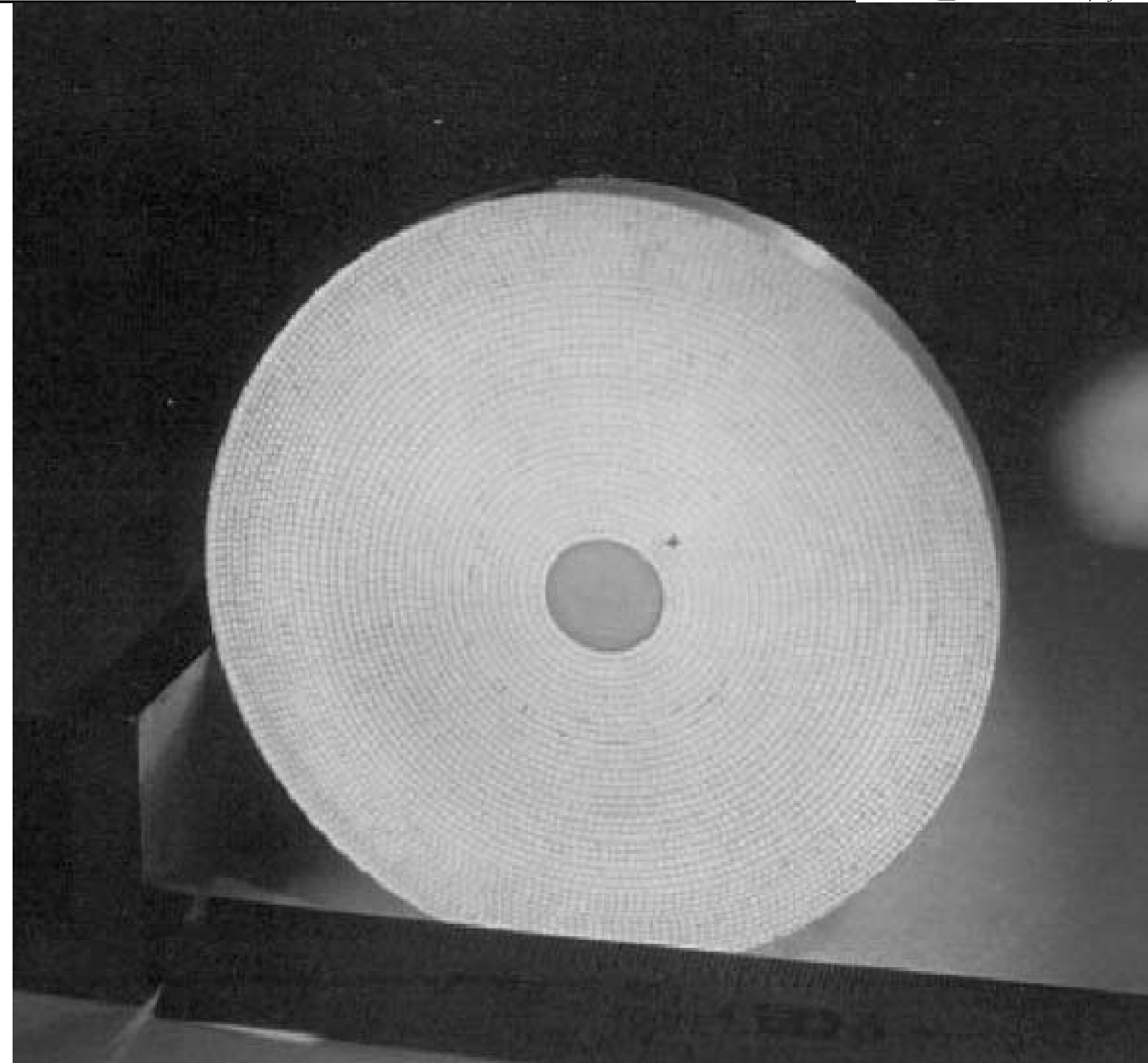
What's that?



(a)



(b)



Lobster Eye, aka Wolter Optic aka Micro Channel Plate

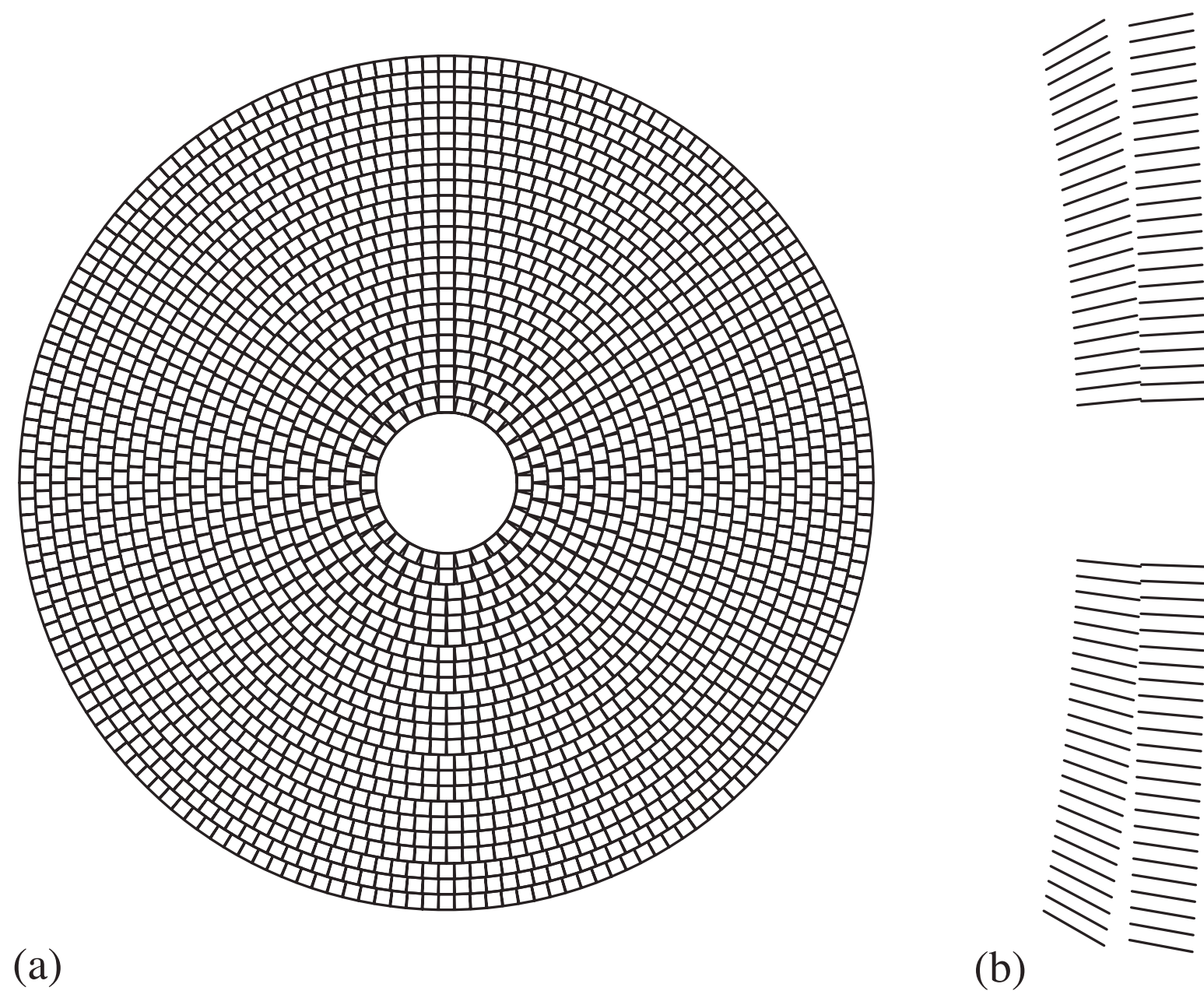


Fig. 1. (a) Packing arrangement around a solid core for a radially packed MCP composed of square multifibres. (b) Cross-section through Wolter pair.

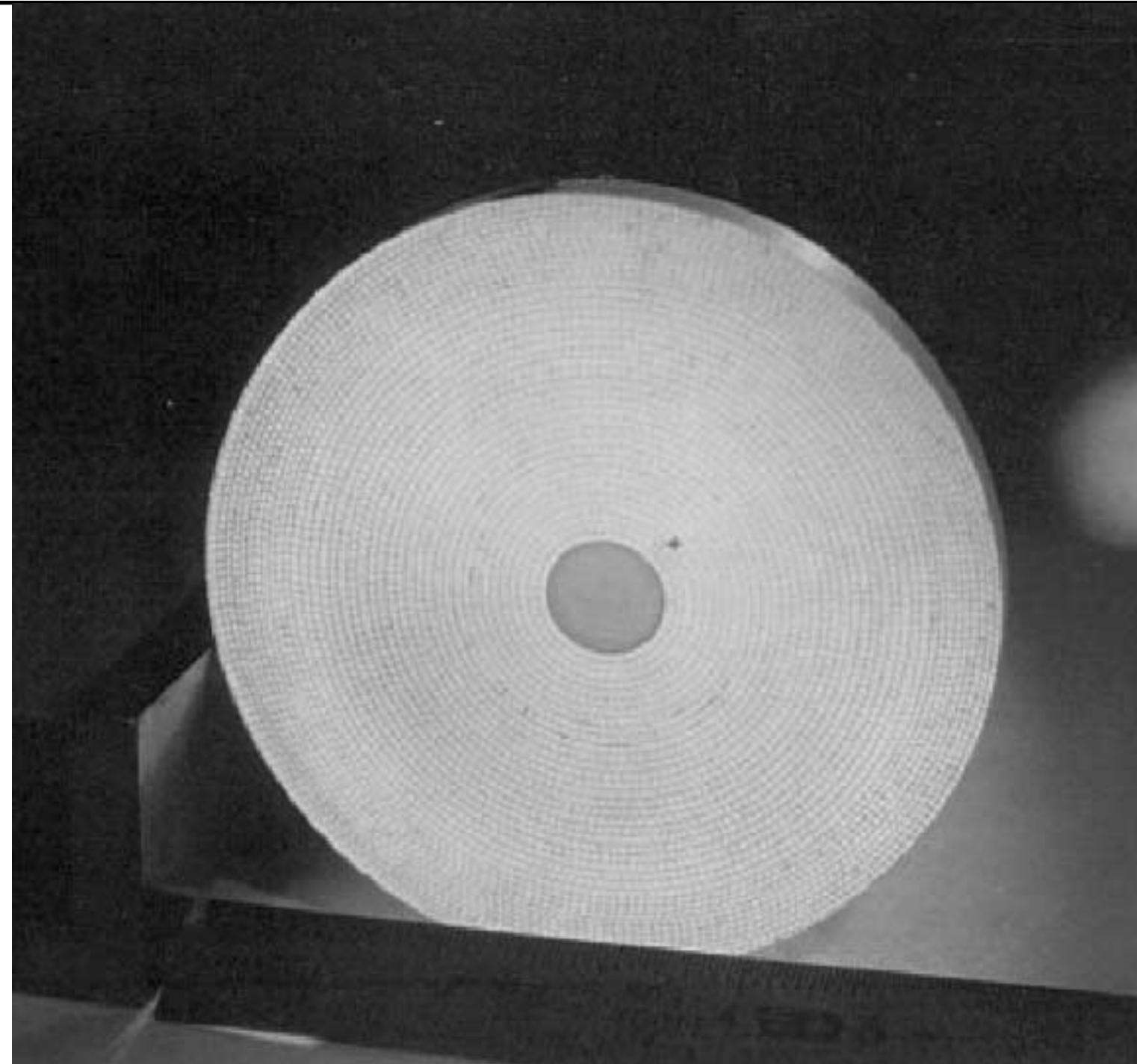


Fig. 2. Prototype radially packed MCP optic [28].

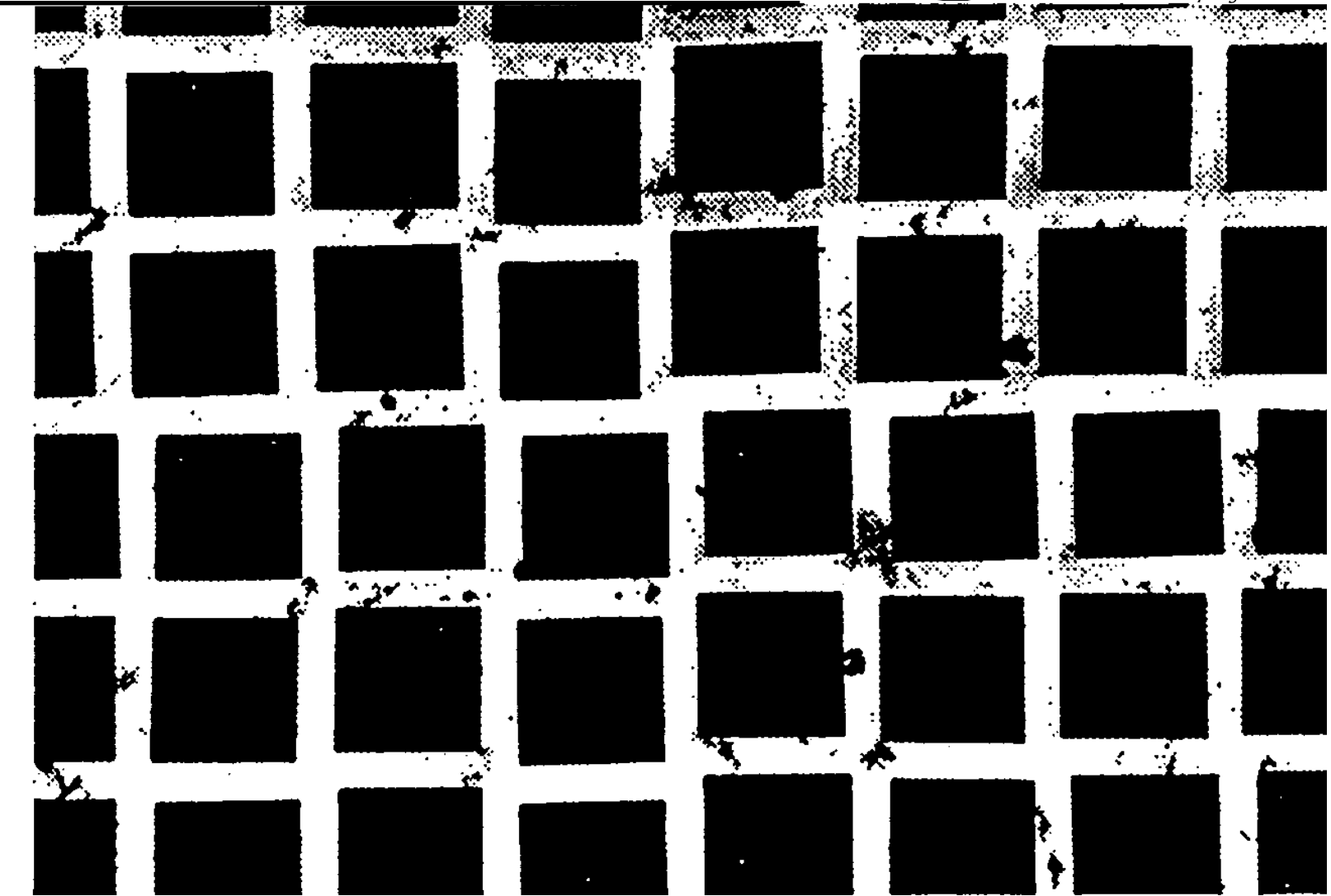


Fig. 2. Optical micrograph of our MCP.

If it looks like a Zone Plate,
it might be a lobster eye :)

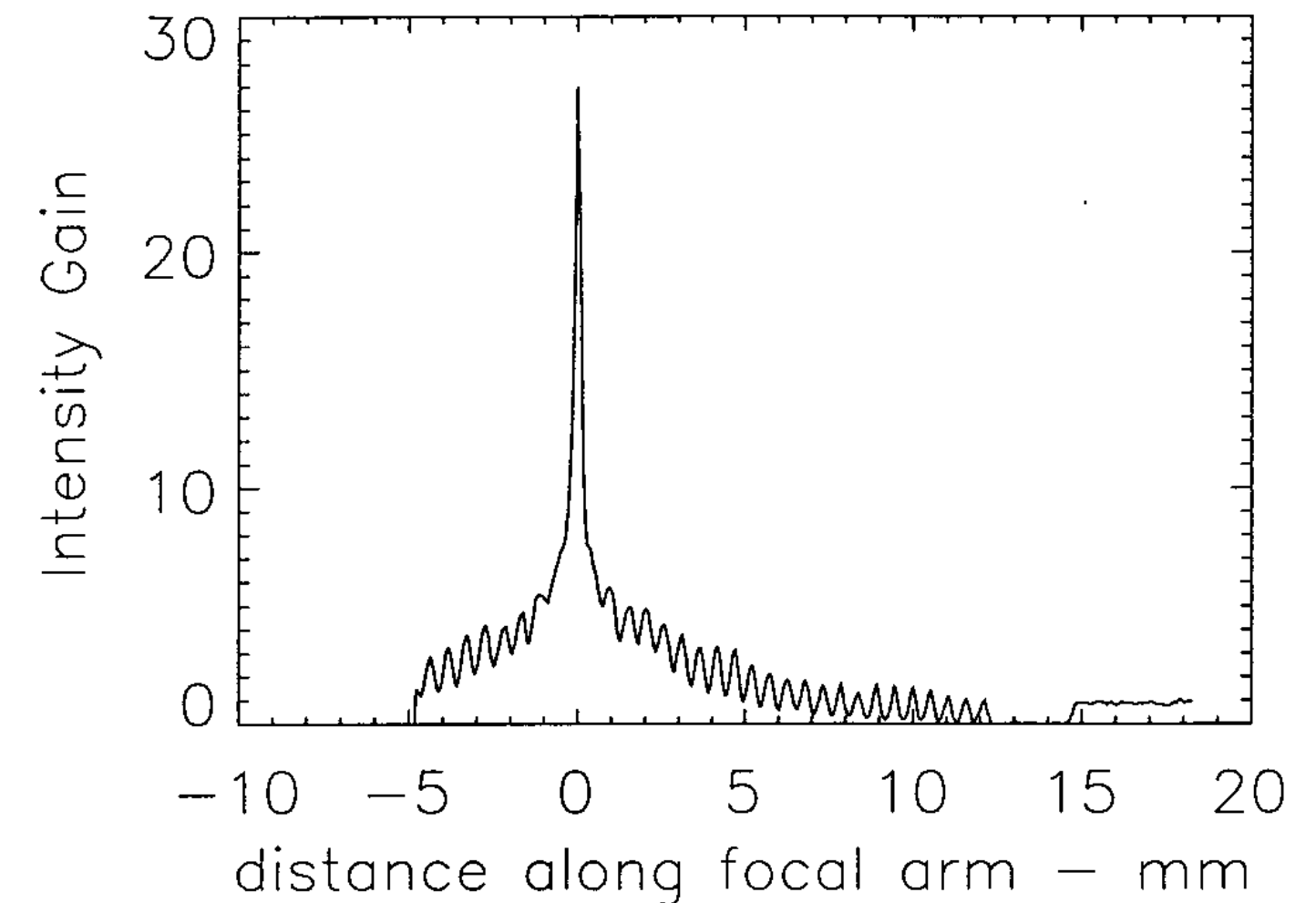


Fig. 6. One-dimensional scan, along a focal arm, of intensity gain vs distance along focal arm - mm. Peele, Siegmund et al, Applied Optics, 1996

Wolter, Grundlagen der Optik, 1956
Price, Tomaselli et al, NIMA, 2002

Summary and Wrap-Up

Mirrors

- ▶ total reflection ≤ 17 keV
- ▶ multilayers ≥ 15 keV

Zone Plates

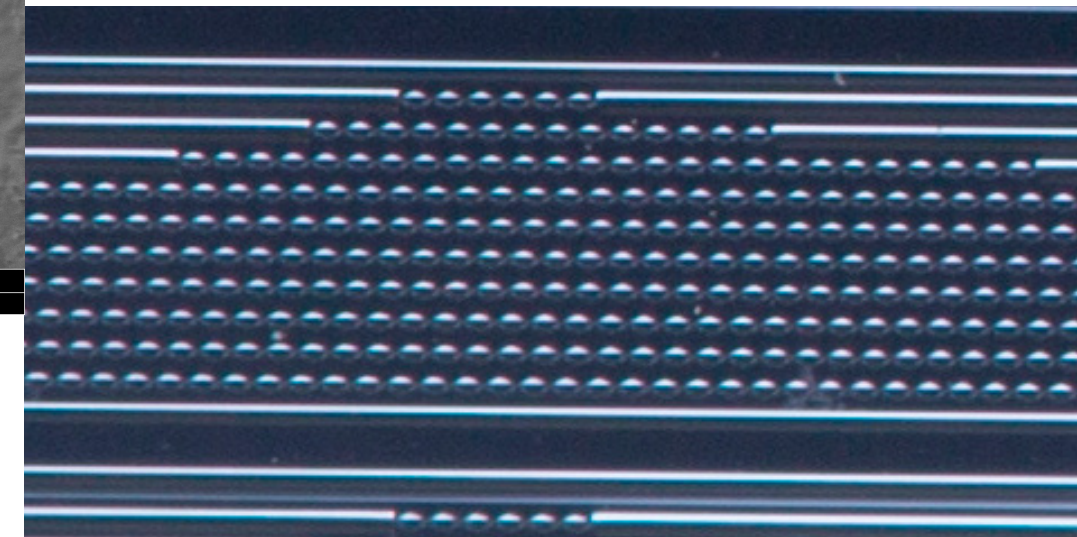
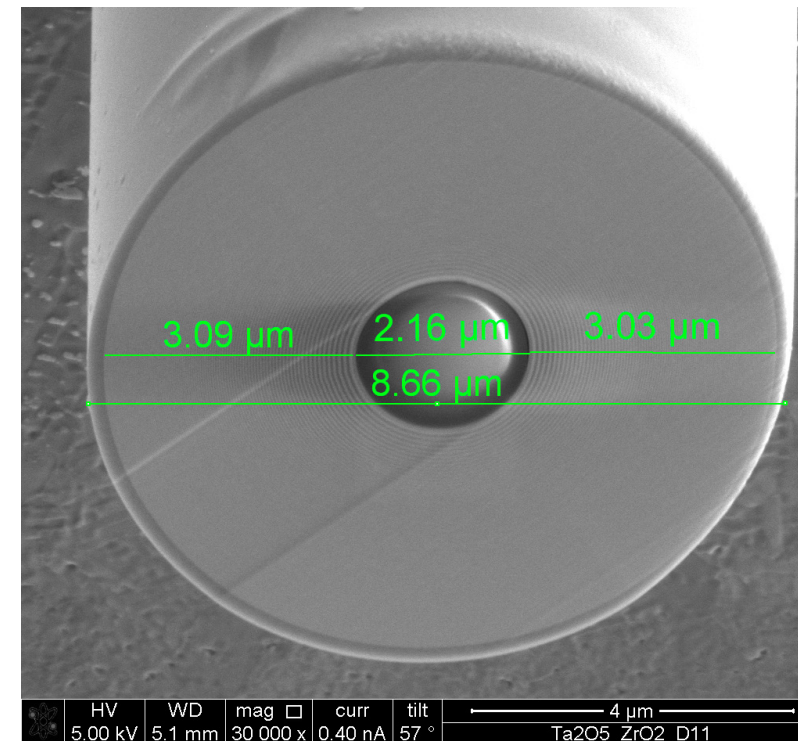
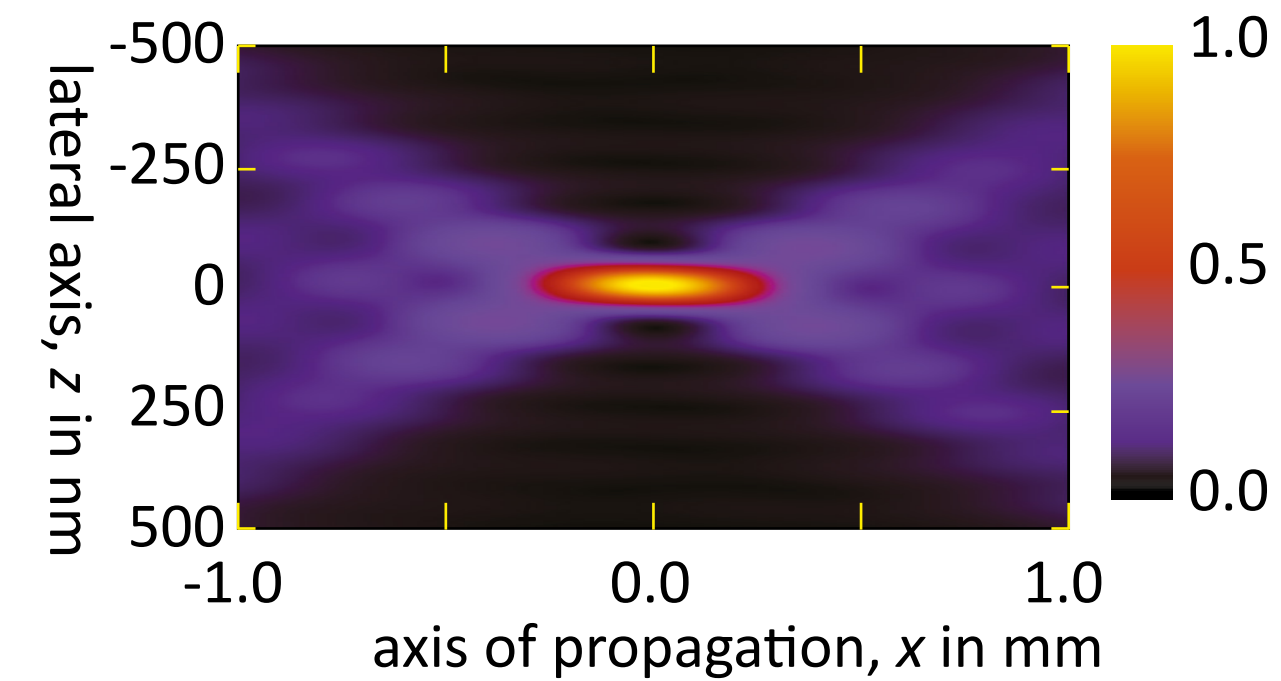
- ▶ Fresnel Zone Plates for soft x-rays
- ▶ Multilayer Laue Lenses, Multilayer Zone Plates for hard x-rays
- ▶ factor of 20 in energy = 20 years of work

Lenses

- ▶ possible, with 100+ lenses

ideal mirror

(a) Intensity distribution



Outline

- ▶ Introduction + History
- ▶ Reflective Optics
- ▶ Diffractive Optics
- ▶ Refractive Optics
- ▶ Waveguides
- ▶ Discussion

Waveguides

- ▶ as coherence filter for holography

